Institute for
Experimental Physics E21

# Annual Report 2003

Annual Report 2003

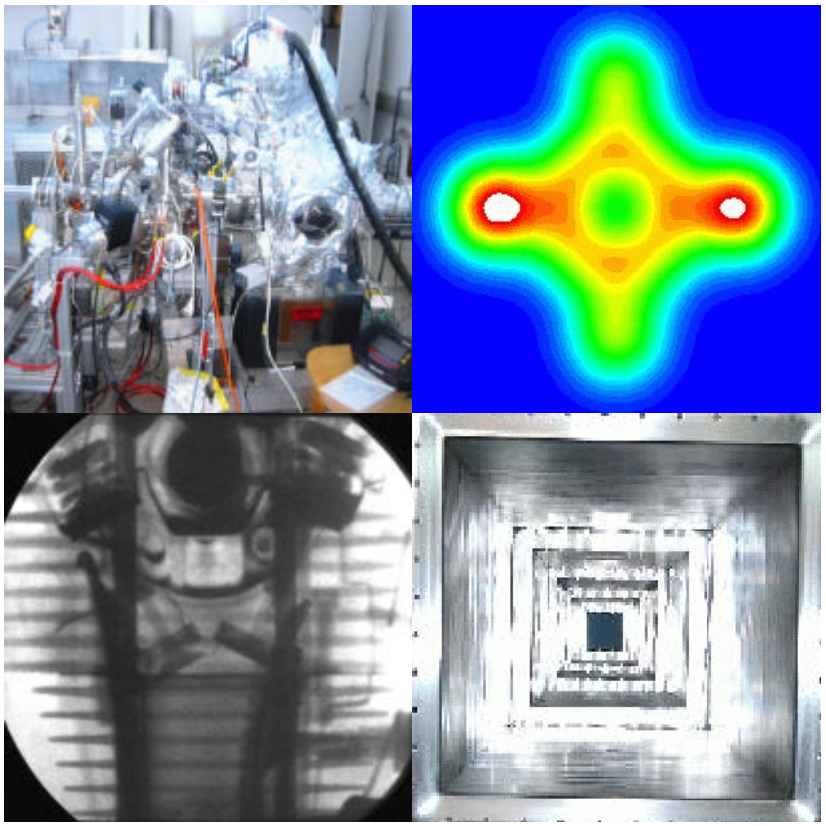

# Annual Report 2003

of the Institute for Experimental Physics E21
Prof. Dr. P. Böni
Technische Universität München

Annual Report 2003
of the Institute for Experimental Physics E21
published: Feb. 2004
Layout by Florian Grünauer
Edited by Florian Grünauer
http://www.physik.tu-muenchen.de/lehrstuehle/E21

Physik-Department E21
Technische Universität München
James-Franck-Strasse
D-85747 Garching, Germany

Phone: +49 89-289-14711
Fax: +49 89-289-14713

# Contents

## Preface

The highlight of the year 2003 was of course the granting of the permission to take the new research reactor FRM-II in Garching into operation. After receiving this good news $D_2O$ and fuel element were transported to Garching. Since June 2003 all essential components are being tested and after a final check we expect that the reactor will become critical early 2004. At the time of criticality at least 19 instruments will be operational.

Because of the lack of neutrons in Garching we have performed the neutron scattering experiments at various facilities in Germany (HMI, GKSS), Switzerland (PSI), UK (ISIS), France (ILL), and the US (NIST). We are very grateful to these institutions that E21 was granted beam time to continue the research. Of course we are extremely eager to conduct the experiments soon in Garching.

One of the most important highlights, besides many publications, is the progress in installing the beam lines of E21 at the FRM-II. We mention in particular the very difficult task to place the numerous shielding blocks for the ANTARES beam line into the proper position in the experimental hall of the FRM-II. We congratulate the ANTARES team for managing this difficult task. All beam lines of E21 will be ready when the neutrons arrive …

On the scientific side we have made significant progress in gaining a better understanding of the temperature dependence of excitations in low dimensional magnets, where we have shown that, unexpectedly, excitations in classical spin chains renormalize upwards. A further highlight was the discovery of a new magnetic mode in Cr. This result was obtained in a US-Japan-E21 collaboration. Another important observation is the appearance of chirality in an exchange biased multilayer system. Using time resolved radiography we succeeded to observe the injection of fuel into a combustion engine.

The research group around the technical director of the FRM-II, Prof. K. Schreckenbach, that belongs scientifically to E21 continues their investigation in fundamental physics with an improved set-up of TRINE searching for a possible violation of the time reversal symmetry in the system of the free neutron decay. With this device Ch. Plonka has finished his experiment at the ILL, which shall provide a further improvement in sensitivity. Already the former limit with TRINE for the D-coefficient was the best obtained till now. It provides an important information for particle physics beyond the standard model in particular for so-called lepto-quark models. Furthermore, the research with positrons in collaboration with the Universität der Bundeswehr in Munich was pursued. The novel type of a slow positron source 'Nepomuc' is now placed at the FRM-II in-pile position and waiting for the nuclear start-up. The instrument for PAES, Positron annihilation induced Auger-Electron Spectroscopy, which was successfully tested with a laboratory positron source is transferred to the FRM-II intense source of slow positrons.

The final license to operate the FRM-II reactor also involved the condition that the TUM should develop, until the end of 2010, a new fuel element allowing the FRM-II to continue its operation with medium enriched uranium (MEU) instead of the present highly enriched uranium (HEU). This work is being performed in the group around Prof. K. Böning. As a first step towards this goal an advanced fuel with a much higher density of uranium than presently available must be developed. At the end of May 2003 an official agreement between the relevant Bavarian (StMWFK) and Federal (BMBF) ministries has been signed to regulate the budgetary question. An international "MEU Working Group" has been established by the TUM which also involves the French fuel element fabricator CERCA and the German reactor planning company Framatome-ANP (formerly Siemens-KWU). Reactor calculations as performed by TUM showed that the density of uranium must be raised from the present 3.0 $gU/cm^3$ (HEU) to about 8.0 $gU/cm^3$ (MEU). At the end of 2003 the production of the MEU starting material has begun and the negotiation of the contracts to fabricate the first test plates and to irradiate them in the French OSIRIS reactor is well advanced.

Although the FRM-II is not yet running, we are happy that neutron scattering is continuously attracting students for diploma works. Most of them enjoyed the freedom to perform the experiments at foreign facilities thus building up new international relations.

In 2003, E21 succeeded to receive grants supporting the scientific exchange between Germany and Russia as well as Germany and France. The biggest success is the acceptance of the neutron optics project and the project on spin turning devices within the framework of the European initiative FP6.

This success is of course darkend by the ongoing non-acceptance of scientific proposals for scientific projects at the FRM-II by the BMBF: The proposals are simply rejected due to the fact that the proposers are affiliated with the Technische Universität München. This is a very new situation in science: It is not the quality that counts, it is the location of the research group. This is a disgrace being hopefully soon resolved by negotiations between the government of Bavaria and BMBF!

By the end of the year 2003, Dr. A. Mirmelstein has left E21 and moved back to Russia. He joined our group soon after my arrival at TUM in 2000 und helped to build up successfully the magnetism group that became mostly engaged in the field of low dimensional and itinerant magnetism. We are very sad to loose Alex, because he was always an extremely friendly and helpful person. We wish Alex a

successful future. We are also sad about the leaving of Dr. M. Bleuel who was responsible for the construction of the spin echo spectrometer RESEDA during the course of his thesis work. He will continue his successful work at the intense pulse neutrons source IPNS at Argonne National Laboratory. We all wish him good luck and are looking forward for a continuing collaboration. Last but not least we had also a change in our secretary's office, where after many years Cornelia Skorski left us and joined E20. We welcome the new secretary Sylvia Jones and wish her a good time in our group.

Garching, in January 2004

Peter Böni Klaus Böning Klaus Schreckenbach

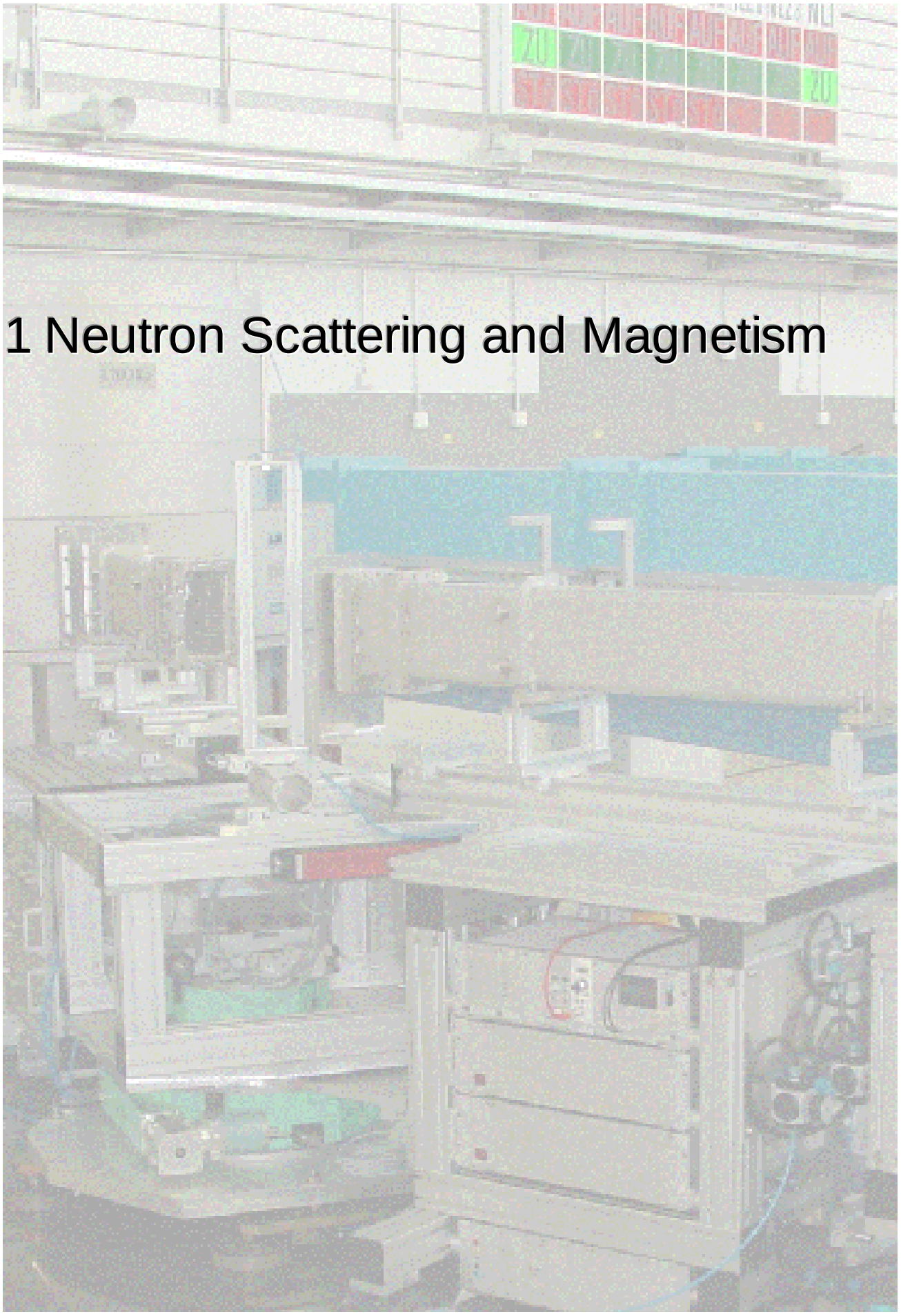

# 1 Neutron Scattering and Magnetism

## 1.1 Asymmetry of low-energy magnetic Excitations in Chromium

P. Böni[1], H. Hiraka[2,3], K. Yamada[3], S. Park[4], S-. H. Lee[4], and G.~Shirane[2]

[1]*Technical University of Munich, Physics Department E21, D-85748 Garching, Germany*
[2]*Physics Department, Brookhaven National Laboratory, Upton, New York 11973*
[3]*Institute for Materials Research, Tohoku University, Sendai, 980-8577, Japan*
[4]*NIST Center for Neutron Research, National Institute of Standards and Technology, Gaithersburg, MD, USA*

*The low-energy excitations of Cr, i.e. the Fincher-Burke (FB) modes, have been investigated in the transversely polarized spin-density-wave phase by inelastic neutron scattering using a single-**Q** crystal with a propagation vector $\mathbf{Q}_{\pm}$ parallel to [0,0,1]. Most remarkably, we find that the spectrum of the FB modes exhibits one exicitation peak at 140 K near **Q** = (0,0,0.98) and two peaks near **Q** = (0,0,1.02), respectively. This is surprising because Cr crystallizes in a centro-symmetric bcc structure (Boeni_Cr_2003.doc).*

Although chromium exhibits a simple bcc structure and consists only of a single element the magnetism is very complicated [1]. Recently, interest has been focused on the unusual spectral features of chromium, namely the low-energy Fincher-Burke (FB) excitations around the commensurate positions [2]. The origin of these modes and their relevance with regard to incommensurable order is still unclear (Fig. 1).

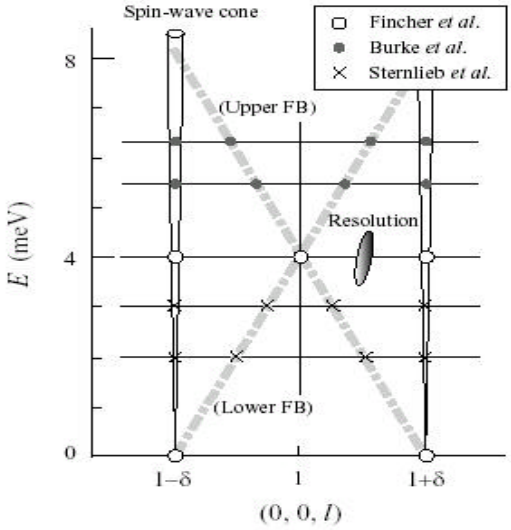


***Fig. 1:*** *Dispersion of magnetic excitations in the TSDW phase of Cr. The vertical cones shows the dispersion of the high-energy excitations emerging from the incommensurate positions $\mathbf{Q}_{\pm}$. The chain lines indicate the FB modes as measured in previous experiments.*

Using a cold neutron triple-axis spectrometer with high-resolution the FB modes were recently investigated in detail using constant-**Q** and constant-energy-transfer scans. It was pointed out that the FB modes neither show a simple linear dispersion nor obey a simple spin-wave picture with respect to intensity. In addition, the intensity contour for $\mathbf{Q}_{-} < \mathbf{Q} < Q_{+}$ indicated that the FB mode is asymmetric with respect to (001) [3]. However, it was not clear if this was due to spurious scattering.

In order to obtain a coherent picture of the low-energy excitations in Cr we have performed a detailed investigation of the FB modes in the TSDW phase using a different single crystal of Cr by means of constant-**Q** scans using thermal- and cold-neutron spectrometers at Tokai and NIST, respectively.

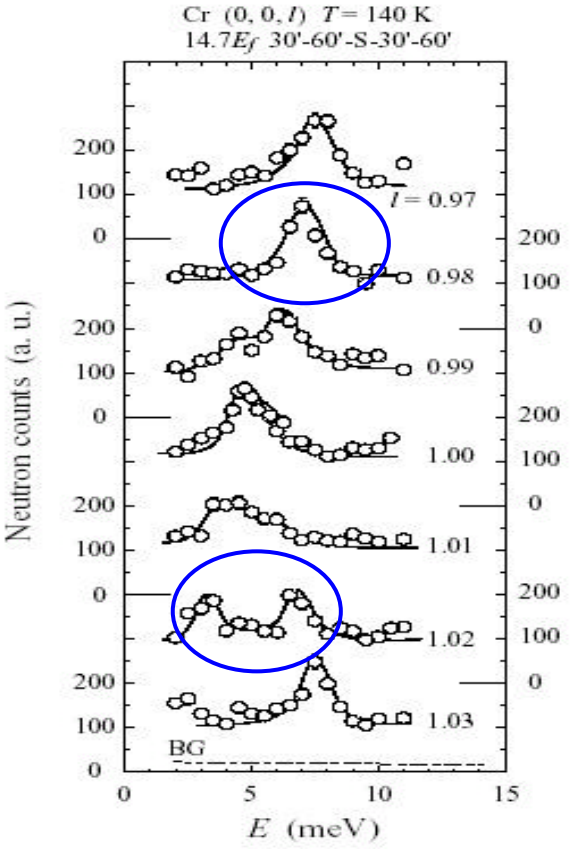


***Fig. 2:*** *Energy spectra measured along [0,0,1] in the TSDW phase. A single peak and a double peak are observed at the symmetric **Q**-positions (0,0,0.98) and (0,0,1.02), respectively. The solid lines are guides to the eyes.*

These results confirm that the observed asymmetry is a real effect and is at variance with the centro-symmetric simple bcc structure of Cr. We have no explanation for this effect yet.

References:

[1] E. Fawcett, Rev. Mod. Phys. **60**, 209 (1988).
[2] H. Hiraka, P. Böni, M. Fujita, Y. Endoh, K. Yamada, and G. Shirane, Phys. Rev. B **67**, 064423 (2003) and references therein.
[3] P. Böni, B. Roessli, E. Clementyev, Ch. Stadler, G. Shirane, and S. A. Werner, Applied Physics A **74** (suppl.), S716 (2002).

## 1.2 Low-energy magnetic Excitations in single-Q Chromium

E. Clementyev[1], P. Böni[1], F. Demmel[2], and G. Shirane[3]

[1]*Technical University of Munich, Physics Department E21, D-85748 Garching, Germany*
[2]*Institute Laue Langevin, F-38042 Grenoble Cedex 9, France*
[3]*Physics Department, Brookhaven National Laboratory, Upton, New York 11973*

*The low-energy magnetic excitations of elementary Cr have been measured by means of inelastic neutron scattering on the triple-axis spectrometer IN3. The [100]/[010] scattering plane was scanned around a few reciprocal lattice positions in the temperature range 170K to 250K. The observed intensity maps indicate that the low-energy excitations in chromium are arranged on a ring in the $Q_h$-$Q_k$ scattering plane around the commensurate positions. In addition, contour maps demonstrate the appearance of magnetic intensity at the silent positions (1,±d,0). The relative contributions of different magnetic modes to the total scattering intensity and their temperature dependencies are discussed.*

The great variety of unusual phenomena exhibited by chromium made it a subject of much interest to experimentalists and theorists alike. This element is one of the most thoroughly studied itinerant antiferromagnets (see [1] and references therein). Recently interest has been focused on the unusual spectral features of chromium, namely the low-energy Fincher-Burke (FB) excitations around the commensurate positions [2]. The origin of these modes and their relevance with regard to incommensurable order is unclear. The response of theory to the challenge posed by these puzzling spectral features has been slow. In the absence of any detailed knowledge about the origin of the FB excitations new experimental information collected in a huge area in the reciprocal space at different temperatures would significantly advance the understanding of the FB mode.

The goal of the present study was twofold. First of all to explore a large region in the reciprocal space and produce contour maps of excitations in Cr at different neutron energy transfers and temperatures. Second to test once again a novel multi detector setup of the TAS IN3 (ILL) equipped by a set of 32 analyser crystals (see [3] for details). Such an array of detectors enables us to take a snapshot of a large area in the reciprocal space by a single scan.

The first measurements of elementary Cr on IN3 have been performed in the year 2002 only at one temperature, namely T=230K [4].

In the year 2003 the INS experiments were carried out at temperatures: T=170K, 230K, and 250K for a fixed final energy of $E_f$ = 31 meV, yielding a resolution of 1.3 meV at zero energy transfer. The $Q$ –resolution was about 0.033 Å$^{-1}$. The crystal was aligned with the [100] and [010] crystallographic directions in the scattering plane. Incommensurate wavevectors of the sample are $\boldsymbol{Q}^{\pm}$ = (1±d,0,0), where $d$ is about 0.04. Constant-$E$ scans were performed around the reciprocal lattice positions $\boldsymbol{Q}$ = (1,0,0), (0,1,0) and (1,1,0) at several energy transfers ranging from 0 meV to 20 meV.

To compensate for a rather large step along the $k$-direction provided by the angular separation of individual analyser crystals (1$^{o}$ degree), each scan was made two or four times with a shift of the whole analyser bloc by 0.5 $^{o}$ or 0.25 $^{o}$. As a result a typical scan covers 4000 to 8000 points in $\boldsymbol{Q}$-space. However only 1000 to 2000 of points were valuable in the case of Cr since the magnetic scattering is located in the vicinity of the points $\boldsymbol{Q}^{\pm}$ and $d$ is rather small.
Typical contour maps of the excitation spectra of Cr measured on IN3 are shown in the previous report (see [4]). Here we present a simple model representing various magnetic contributions. The following contributions are illustrated in Fig.1: the strong peaks on top of the magnetic satellites $\boldsymbol{Q}^{\pm}$, much weaker peaks on top of the silent satellites positions (1,±d,0) and the FB ring of intensity with a center at $\boldsymbol{Q}$ = (1,0,0). The magnetic formfactor of $Cr^{3+}$ was taken into account.

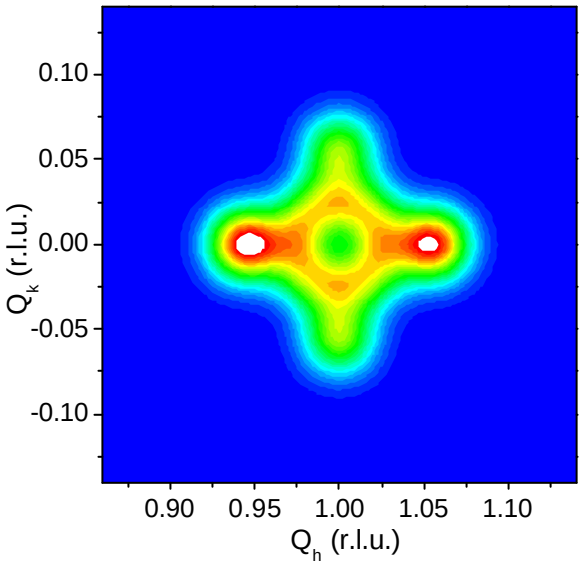


***Fig. 1:*** *Simulated contour map of the excitation spectra of Cr at E = 6 meV used as a model to fit experimental data around* $\boldsymbol{Q}$ *= (1,0,0).*

The values of the integrated intensities of various magnetic contributions are given in Table 1. The FB excitations contribute almost 60% to the total intensity at $E$ = 6 meV. This is not surprising since the FB ring covers a large area in the $Q_h$-$Q_k$ plane while high peaks above the $\boldsymbol{Q}^{\pm}$ are well-localized in the $\boldsymbol{Q}$ space. Within our accuracy the relative contribution of the FB excitations remains constant in the temperature range

170K to 250K. The ratio of the intensities above $\boldsymbol{Q}^{\pm}$ and $(1,\pm d,0)$ is about 5:1. We point out that the inelastic scattering above the allowed and silent satellites positions increases at the same rate with temperature. This rate is much faster than expected from the Bose-Einstein statistics.

| Temperature | 170 K | 230 K | 250 K |
|---|---|---|---|
| FB-excitations | 190±25 | 417±52 | 586±73 |
| Peaks at (1±*d*, 0, 0) | 122±13 | 262±25 | 318±33 |
| Peaks at (1, ±*d*, 0) | 23±7 | 48±10 | 61±15 |
| Total (experim.) | 1 | 2.17±0.2 | 2.9±0.2 |
| <*n+1*> | 1 | 1.29 | 1.38 |

***Table 1:*** *Integrated intensities of different contributions to the intensity map at E = 6 meV (arbitrary units) and the normalized experimental total intensities. <n+1> represents the normalized total intensities expected from Bose-Einstein statistics.*

The main outcome of the present study is the observed ring of intensity $E$ = 6 meV in the $Q_h$ - $Q_k$ scattering plane. The result confirms the recent observation of a dispersive mode perpendicular to the ordering wave vector of the incommensurate structure [5]. The present study provide clear evidence that sizable peaks are located above the silent satellites positions. The TAS IN3 with a novel multi detector setup might allow mapping out the complete $(\boldsymbol{Q},E)$ space of the low-energy excitations in Cr.

References:


[1] E. Fawcett, Rev. Mod. Phys. **60**, 209 (1988).

[2] S. K. Burke, W. G. Stirling, K. R. A. Ziebeck, and J. G. Booth, Phys. Rev. Lett. **51**, 494 (1983).

[3] F.Demmel, The ILL Millenium Symposium & European Users Meeting, Grenoble, 305 (2001).

[4] P. Böni, E. Clementyev, F.Demmel, and G.Shirane, Institute of Experimental Physics E21 Annual report 2002, TUM/Munich, 19-20.

[5] H.Hiraka, Y.Endoh, P. Böni, M.Fujita, K.Yamada, and G.Shirane, Phys. Rev. B **67**, 064423 (2003).

## 1.3 Relaxation of the $Pr^{3+}$ Crystal Field Excitation in heavy Fermion $CeAl_3$

A.Mirmelstein[1], E.Clementyev[1], and P.A.Alekseev[2]

[1]*Technical University of Munich, Physics Department E21, D-85748 Garching, Germany*
[2]*RRC "Kurchatov Institute", 123182 Moscow, Russia*

*Magnetic excitation spectra of $Pr^{3+}$ paramagnetic impurity ions have been measured in a heavy fermion compound $CeAl_3$ and its nonmagnetic reference matrix $LaAl_3$. A significant narrowing of the relaxation width of the crystal field transition has been observed for $Pr^{3+}$ in the cerium-based system. This narrowing takes place in the temperature range much higher than the characteristic Kondo energy scale in $CeAl_3$. The temperature dependence of the line width for $Pr^{3+}$ in $CeAl_3$ is indicative of a sizable redistribution of the conduction electrons due to the formation of a new Kondo ground state.*

$CeAl_3$ is a well known Kondo or heavy fermion (HF) system with the Kondo temperature of about 5K [1]. Along with the f-electrons, the formation of the HF ground state involves also the conduction electrons. It is possible to trace their behaviour by studying the temperature effects in the crystal field (CF) excitation line width. The main source of relaxation of the CF excited states is due to the exchange interaction with the conduction electrons near the Fermi energy. However, for the Ce ions this conduction electron relaxation can hardly be observed and separated from the effects of mixing broadening; a problem to overcome only by investigating the paramagnetic single impurity ion relaxation.

The $Pr^{3+}$ paramagnetic impurity ions were used to study the formation of the new ground state in $CeAl_3$ and to trace the relaxation of the crystal field (CF) states. A strong change of the relaxation of $Pr^{3+}$ in $CeAl_3$ compared to the nonmagnetic reference system $LaAl_3$ has been observed by inelastic neutron spectroscopy at temperatures T<60K [2]. However a limited energy resolution ($\delta$E~0.7 meV) at the position of the inelastic peak (E=4 meV) didn't allow to estimate a self-width of the CF excitation at low temperatures (T<30K) with a good accuracy. That is why it's very difficult to judge about the relaxation width in the most interesting temperature range around the characteristic Kondo energy scale in $CeAl_3$. An improved energy resolution combined with a relatively good statistic are certainly key elements to provide a new insight into the formation of the ground state in $CeAl_3$.

We main goal of the present study was to provide detailed information on the paramagnetic impurity ion relaxation in $CeAl_3$. The time-of-flight spectrometer FOCUS (SINQ/PSI Villigen) was used to measure the magnetic spectral response in $Pr_{0.07}Ce_{0.93}Al_3$ and $Pr_{0.07}La_{0.93}Al_3$ powder samples with a relatively high energy resolution at finite energy transfer (energy range from 2.5 to 4 meV). Due to its focusing option at a specified energy transfer position and its huge counting rate this instrument is well-suited for such a study. The spectra were collected at temperatures 1.5K to 60K. The energy resolution at the positions of the CF peaks was about 0.2 meV which is much better than in the previous study (0.7 meV according to [2]). Typical scans for $Pr_{0.07}Ce_{0.93}Al_3$ are shown in Fig.1. The observed sharp peak corresponds to the CF transition between the ground state and the excited state. The line width of the CF transition in $Pr_{0.07}Ce_{0.93}Al_3$ is clearly enlarged at high temperatures.

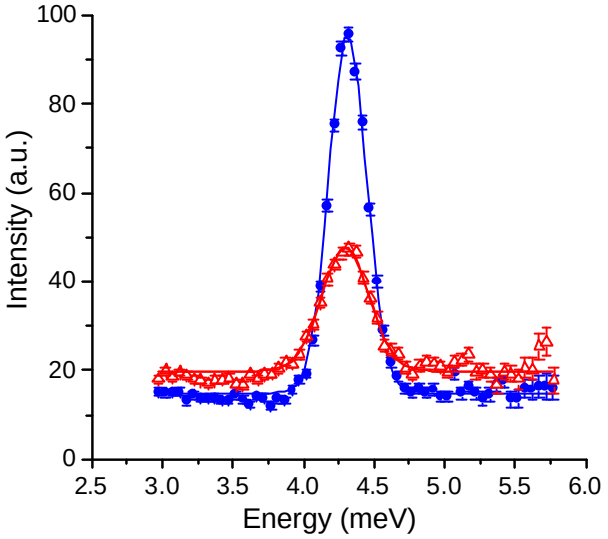


***Fig. 1:*** *Inelastic neutron scattering spectra of $Pr_{0.07}Ce_{0.93}Al_3$ measured at temperatures 1.5K (blue circles) and 45K (red triangles). The solid lines are fits by Gaussians.*

The temperature dependencies of the line width of the CF transitions is shown in Fig.2. The values presented in Fig.2 are fitted peak parameters (Gaussian spectral functions).

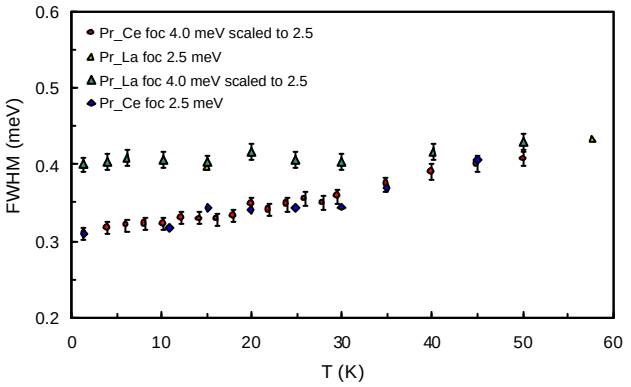


***Fig. 2:*** *Temperature dependencies of the width of the CF transitions for a $Pr^{3+}$ ions in $CeAl_3$ and $LaAl_3$.*

While the width for a $Pr^{3+}$ ions in $LaAl_3$ is almost temperature-independent a significant narrowing of

the relaxation width for a $Pr^{3+}$ ions in $CeAl_3$ takes place at T<40K. This narrowing mainly reflects the reduced interaction with the conduction electrons. This might be the result of a redistribution of the conduction electrons in the density of states in the vicinity of a $Pr^{3+}$ ion which arises from the formation of a new Kondo state. It is worth to note that the characteristic temperature range where the narrowing takes place is much larger than the Kondo temperature ($T_K$ is about 5K in $CeAl_3$).

For a detailed analysis of the relaxation broadening one should extract the values of the intrinsic line width. This work is in progress now.

References:

[1] E.Holland-Moritz and G.H.Lander, in Handbook Phys. & Chem. of Rare Earths, v.19, ch.130 (1994).
[2] P.A.Alekseev, W.Buhrer, V.N.Lazukov, E.V.Nefeodova, I.P.Sadikov, O.D.Chistyakov, M.Zolliker, Physica B **217** (1996).

## 1.4 Crystal Field in $RNi_2$ intermetallic Compounds

E.Clementyev[1], I.Sashin[2], and E.A.Goremychkin[3]

[1]*Technical University of Munich, Physics Department E21, D-85748 Garching, Germany*
[2]*FLNP, Joint Institute for Nuclear Research, 141980 Dubna, Russia*
[3]*Argonne National Laboratory, Argonne, Illinois 60439-4845, USA*

*Inelastic neutron scattering studies of the crystal field (CF) effects have been performed in $RNi_2$ intermetallic compounds for R=Er, Tb and Pr. The complete CF splitting schemes for these ions could be determined on the basis of the observed CF transitions. The number of the CF levels is indicative of a symmetry lowering in the Tb and Er-based systems.*

The Rare-earth-nickel compounds have been intensively studied as promising magnetic refrigeration materials. A very large magnetocaloric effect was observed in a few members of the $RNi_2$ series in which the crystal field (CF) anisotropy plays a fundamental role [1]. Reliable information on the CF splitting is of high demand for a few compounds of this series. In particular conflicting splitting schemes have been obtained for $TbNi_2$ [2,3], there is no well-established set of the CF parameters for $ErNi_2$ and most probably for $PrNi_2$. Moreover in the preliminary triple-axis (TASP/SINQ) measurements of the CF splitting of $Tb^{3+}$ in $YNi_2$ matrix one extra CF level has been observed in addition to the CF levels provided by the cubic local symmetry in $RNi_2$ [4]. A strong exchange coupling between the magnetic rare earth ions and relatively high ordering temperatures (for example, $T_c$=37.5K in $TbNi_2$) lead to rather broad CF transitions in the magnetic spectral response of pure $RNi_2$ compounds (see [2,3]).

The main idea of the present study was to measure the CF excitations in diluted $RNi_2$ compounds with suppressed exchange coupling. Powder samples with 5% paramagnetic impurity ions (R=Tb, Er, Pr) in the nonmagnetic isostructural compound $YNi_2$ were used in the inelastic neutron scattering experiments on the time-of-flight spectrometer FOCUS (SINQ).

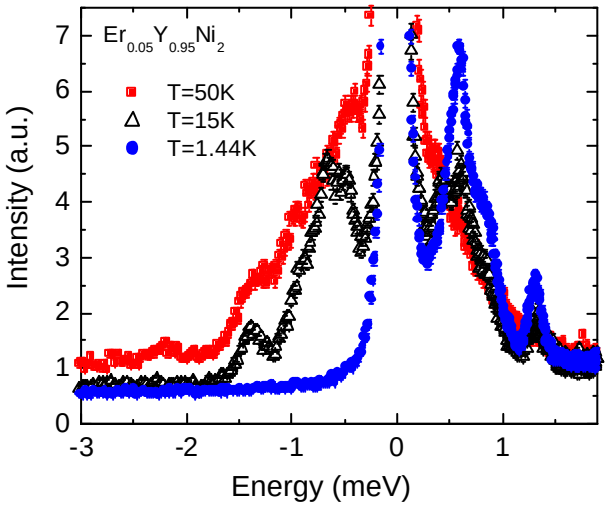


***Fig. 1:*** *Inelastic neutron scattering spectra of $Er_{0.05}Y_{0.95}Ni_2$ measured on FOCUS with $E_i$=3.27 meV. No background and absorption corrections were made.*

The measurements were performed with two values of the incoming neutron energy, namely $E_i$=3.27 meV (for Er, Tb, Pr–based compounds) and $E_i$=7.13 meV (for Er and Pr). Fig.1 shows the spectra of $Er_{0.05}Y_{0.95}Ni_2$ measured at T=1.44K, 15K and 50K. The magnetic contribution dominates in the energy transfer range shown in the figure. Relatively sharp CF transitions out of the ground state are clearly seen at E=0.6, 0.9 and 1.3 meV. At elevated temperatures transition between the excited states show up in the spectra. The ground state, 3 excited CF levels observed in the FOCUS spectra and two CF states at higher energies (observed in [2,3,4]) give us 6 CF states in total which is more than 5 CF levels allowed by the cubic point symmetry in the case of $Er^{3+}$ in $RNi_2$ matrix.

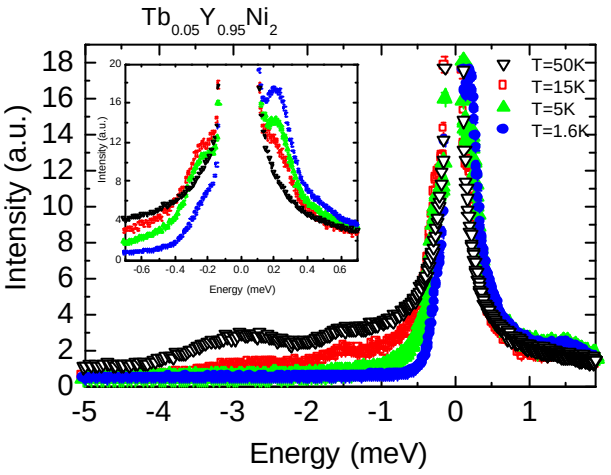


***Fig. 2:*** *Inelastic neutron scattering spectra of $Tb_{0.05}Y_{0.95}Ni_2$ measured on FOCUS with $E_i$=3.27 meV. The insert shows the low energy part of the same spectra.*

In the case of $Tb^{3+}$ paramagnetic impurity a low-energy CF level has been observed at 0.2 meV (see Fig.2). This level along with the CF states at 1.4 meV and 2.8 meV observed on FOCUS and higher CF states known from the references [2-4] are indicative of a unconventional CF splitting for $Tb^{3+}$ in a cubic system. Similar to the case of $Er^{3+}$ the cubic CF Hamiltonian is unable to account for the observed number of CF transitions.

Fig.3 shows the inelastic neutron scattering spectra of $Er_{0.05}Y_{0.95}Ni_2$ and the nonmagnetic reference compound $YNi_2$ measured on FOCUS with $E_i$=7.13

meV. Two CF transitions are seen in the neutron energy loss part of the spectrum at T=1.5K. The energy positions of the excited CF states are 3 meV and 3.7 meV. The same transitions are visible in the neutron energy loss part at elevated temperatures. In addition a peak of magnetic origin is located at E=-5.5 meV. The phonon contribution to the scattering is sizable at high temperatures in the energy transfer range –11 meV to –4 meV (see the spectrum of $YNi_2$).

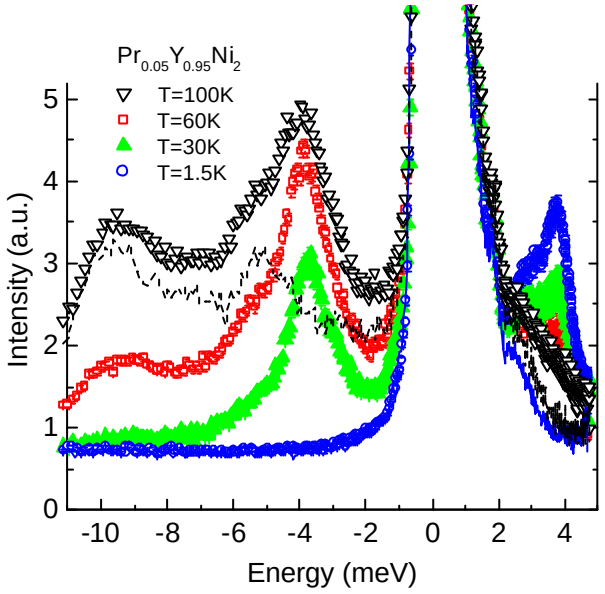


***Fig. 3:*** *Inelastic neutron scattering spectra of* $Pr_{0.05}Y_{0.95}Ni_2$ *measured on FOCUS with* $E_i$*=7.13 meV (symbols). Dashed (black) and solid (blue) lines – the spectra of the nonmagnetic reference compound* $YNi_2$ *measured at T=100K and 1.44K, respectively*

It's worth to mention a huge contribution due to the multiple neutron scattering in the neutron energy loss part (elastic scattering on the sample itself and on the surrounding Al screens). The observed multiple scattering dominates the spectrum of $YNi_2$ up to 4 meV energy transfer. Multiple scattering was not visible in the spectra measured with $E_i$=3.27 since no Bragg scattering from Al is allowed for the corresponding neutron wavelength $\lambda$=5 Å. The neutron energy gain part of the spectra was always clean as expected on a direct geometry time-of-flight spectrometer.

To sum up, detailed informatiom has been obtained on the low-energy CF excitations in $Er_{0.05}Y_{0.95}Ni_2$, $Tb_{0.05}Y_{0.95}Ni_2$ and $Pr_{0.05}Y_{0.95}Ni_2$. The observed CF transitions along with the CF states at higher energies known from previous experiments allow determination of the complete splitting schemes for $Er^{3+}$, $Tb^{3+}$ and $Pr^{3+}$ in $RNi_2$. After that the true sets of the CF parameters will be determined for three members of the $RNi_2$ series. It is obvious from the number of the observed CF states that a cubic symmetry doesn't provide a possibility to fit the observed spectra. We intend to treat the CF effects in $RNi_2$ within the tetragonal CF model. The origin of the symmetry breaking in $RNi_2$ will be discussed in the forthcoming publication.

References:

[1] P.J. von Ranke et al, J. Appl. Phys. **93** (2003) 4055 & Phys. Rev B **63** (2001).
[2] E.Gratz et al, J. Phys. Cond. Matt. **11** (1999)
[3] E.A.Goremychkin et al, J. Magn. Mag. Mat. **81** (1989).
[4] E.Clementyev and I.L.Sashin, unpublished

## 1.5 Interplay of the RKKY and Kondo interactions in $Gd_{1-x}(Ce,La)_xNi$

E.Clementyev[1] and G.Lapertot[2]

[1]*Technical University of Munich, Physics Department E21, D-85748 Garching, Germany*
[2]*DRFMC/SPSMS, CEA/Grenoble, F-38054 Grenoble Cedex, France*

*Magnetic susceptibility measurements of the magnetic ordering temperatures have been performed in $Gd_{1-x}(Ce/La)_xNi$ pseudobinary compounds. A huge difference of the Curie temperatures in Ce and La-based samples is indicative of a strong influence of the cerium 4f electrons on the magnetic ordering in the Gd-sublattice.*

The formation of the ground state in the rare earth based intermetallic systems is a result of a complex interplay of the main interactions, namely the RKKY coupling, the Kondo interaction and the crystal field (CF) potential (see [1] and references therein). The interplay of the first two major players has been extensively studied in many cerium and ytterbium-based systems. The focus of these studies was the magnetic ordering in the Ce (or Yb) sublattice with a substantial degree of delocalization of the 4f electrons. However to the best of our knowledge almost nothing was done on the influence of the partially delocalized cerium 4f electrons on the magnetic ordering of the rare earth ions with well-localized magnetic moments. The main idea of this work was to compare the magnetic ordering in the Gd sublattice diluted either by the nonmagnetic La ions or by the Ce ions with partially delocalized 4f electrons.

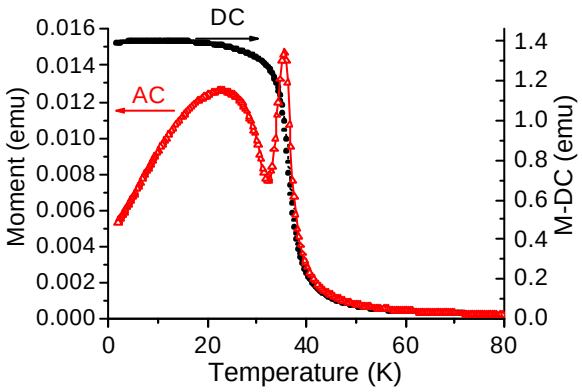


***Fig. 1:*** *The DC magnetization (black circles) and the AC moment (red triangles) of* $Gd_{0.5}Ce_{0.5}Ni$ *measured on the PPMS at H=0.04T (DC signal) and H=5 Oe and frequency 10000Hz (AC signal). The sample mass was 82.1 mg.*

The $Gd_{1-x}(Ce/La)_xNi$ pseudobinary compounds are good candidates to study the role of cerium 4f electrons on the formation of the magnetic or nonmagnetic ground state since Gd has a pure spin magnetic moment and the CF potential doesn't influence the magnetic properties of Gd. GdNi, CeNi and LaNi crystallize in the orthorhombic CrB-type structure and show complete solid solubility. GdNi is a simple ferromagnet with a collinear spin arrangement and the ordering temperature $T_c$ =73K. CeNi is a classical intermediate valence compound with a nonmagnetic ground state. LaNi is nonmagnetic since the Ni ions don't carry any sizable magnetic moment in the RNi series. The 4f electrons of Ce are more delocalized under "chemical pressure" in $Gd_{1-x}Ce_xNi$ than in pure CeNi.

Polycrystalline samples $Gd_{1-x}Ce_xNi$ were synthesized and proved to be single-phase pseudobinary compounds. The measurements of the AC magnetic susceptibility and the DC magnetization have been performed on a standard PPMS (Quantum Design) instrument in the temperature range 1.5K to 300K. Fig.1. shows a typical picture of the DC magnetization & AC response of one of the samples. A sharp peak at T=37K and an upturn of the DC signal correspond to the Curie temperature. The origin of the second peak in the AC susceptibility isn't clear for the moment. The concentration dependencies of the Curie temperature in $Gd_{1-x}Ce_xNi$ and in the reference system $Gd_{1-x}La_xNi$ (taken from [2]) are shown in Fig.2.

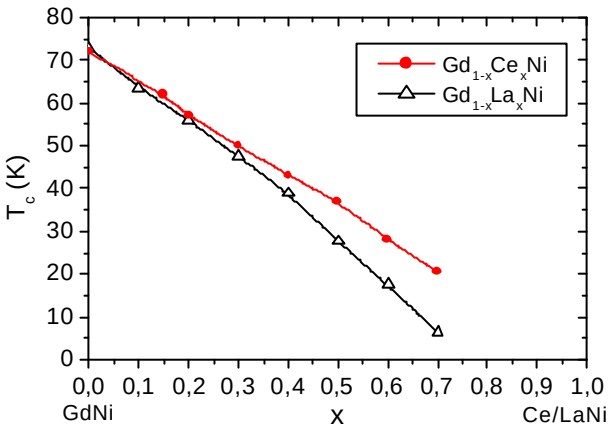


***Fig. 2:*** *Concentration dependencies of the ordering temperatures from the AC susceptibility: red circles* - $Gd_{1-x}Ce_xNi$*; triangles* - $Gd_{1-x}La_xNi$ (from [2]). Lines are guided to the eye.

The ordering temperatures in the Ce-based samples start to deviate from the La-based ones at 80% Gd concentration. At much lower Gd concentrations the difference of the Curie temperatures is huge, i.e. 20.5K and 6.5K in $Gd_{0.3}Ce_{0.7}Ni$ and $Gd_{0.3}La_{0.7}Ni$, respectively. This effect is caused by the 4f electrons of cerium. The role of interionic distances will be clarified in the forthcoming studies.

References:

[1] A.C.Hewson, The Kondo Problem to Heavy Fermions, Cambridge University Press (1997).
[2] E.Gratz et al, J. Mag.Mag.Mat. 54-57, 459 (1986)

## 1.6 Magnetic Structure of $Ca_{2+x}Y_{2-x}Cu_5O_{10}$

V.Kargl, A. Mirmelstein, P. Böni

*Technische Universität München, Physik-Department E21, D-85748 Garching*

The edge-sharing spin-chain compound $Ca_{2+x}Y_{2-x}Cu_5O_{10}$ allows charge doping into its $CuO_2$-chains provoking a dimensional crossover of magnetic ordering. Characterized as 3D antiferromagnet in the low doping region ($0 < x < 1.2$), long-range order vanishes around the critical concentration $x = 1.5$ and reappears in highly doped compounds ($x = 2.15$) [1]. Thus, near the critical doping concentration the macroscopic characterization of the compound series is described by 1D antiferromagnetic spin-1/2 behaviour.

The crystal structure of CaYCuO is monoclinic. However, a reduced orthorhombic Fmmm space group can be used to describe the structure of the parent compound neglecting Ca/Y-modulations along the *c*-axes. Single crystal as well as powder samples of undoped $Ca_2Y_2Cu_5O_{10}$ show that the chain direction runs along *a* and the Cu-spins are aligned parallel to the *b* direction [2,3]. The spin intrachain as well as interchain coupling along *b* is ferromagnetic whereas the chains are staggered antiferromagnetically along *c*.

Investigating the magnetic structure of CaYCuO is crucial to understand the spin dynamics in this material. Thus, we focus our investigations on the doping dependence of the magnetic structure.

Neutron diffraction on the diffractometer DMC, SINQ and on the thermal triple axes spectrometer BT2, NIST, of powder CaYCuO-samples provide results of our investigations. DMC experiments in the doping region $0 < x < 1.2$ cover an experimentally accessible *Q* range of $0 < Q < 4$ Å$^{-1}$ with an incoming wavelength of 2.56 Å. BT2 experiments investigate samples near the critical region ($x = 1, 1.2$) and the highly doped compound $x = 2.15$. Both experiments are carried out with a fixed incident energy of 14.7meV.

Structural modifications resulting from charge doping are expected to be visible in changed ratios of integrated intensities of different magnetic Bragg peaks. Using the ratios (003)/(001) and (023+112)/(001) of the magnetic (001) peak at 0.59 Å, (003) (1.7 Å) and the double peak (023+112) reflection (2.4 Å) provide information about changes up to the critical doping concentration $x = 1.5$ where long range order vanishes (see Fig. 1). We observe that the aforementioned ratios remain constant with doping; thus, we conclude the magnetic structure of $Ca_2Y_2Cu_5O_{10}$ doesn't change with an increasing Ca/Y-ratio up to x =1.2.

Highly doped $Ca_{4.15}Cu_5O_{10}$ features a different magnetic structure which is unknown till now. Its only indication is a new Bragg reflection indexed as (0.5 0 1) [4] as well as the absence of all magnetic Bragg reflections originating from the structure of undoped $Ca_2Y_2Cu_5O_{10}$. The new antiferromagetic peak indicates a doubling of the magnetic unit cell in the *a* direction. Confirming this Bragg peak on BT2, NIST (Fig. 2) is the first step of promising future experiments for a deeper insight into the understanding of structural changes with doping and its microscopic origin.

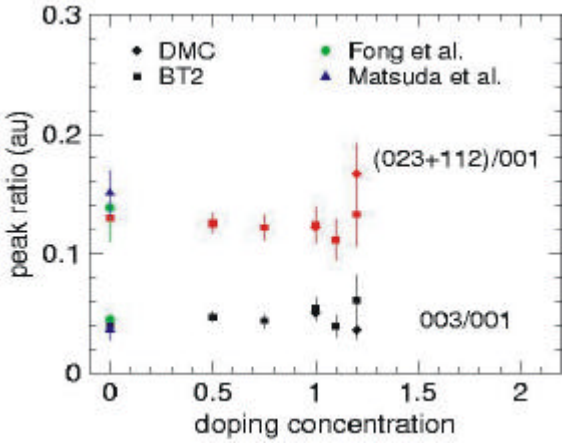


***Fig. 1:*** *Ratios of the integrated intensity of magnetic Bragg peaks.*

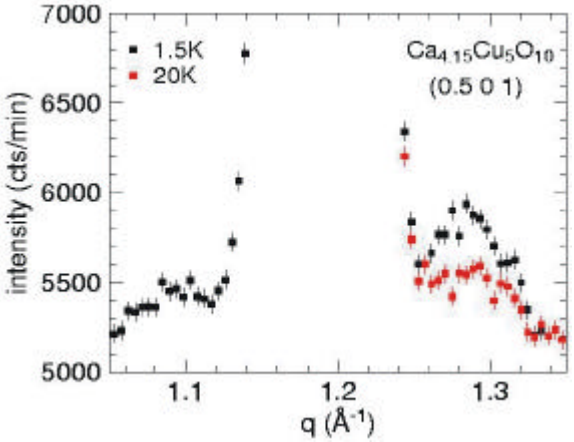


***Fig. 2:*** *Magnetic Bragg peak (0.5 0 1) in $Ca_{4.15}Cu_5O_{10}$*

We kindly acknowledge the support by our local contacts D. Sheptyakov and J. W. Lynn for the DMC and BT2 experiments at the SINQ (PSI) and NCNR (NIST), respectively.

References:

[1] A. Hayashi et al., Phys. Rev. B 58, 2678 (1998)
[2] M. Matsuda et al., J. Phys. Soc. Jn. 68, 269 (1999)
[3] H. F. Fong et al., Phys. Rev. B 59, 6873 (1999)
[4] G. I. Meijer et al., Phys. Rev. B 58, 14452(1998)

## 1.7 Magnetic excitation in $Ca_{2+x}Y_{2-x}Cu_5O_{10}$

V.Kargl, A. Mirmelstein, P. Böni

*Technische Universität München, Physik-Department E21, D-85748 Garching*

Electronically dopable $Ca_{2+x}Y_{2-x}Cu_5O_{10}$ is macroscopically characterized as spin-1/2 Heisenberg chain [1], whose antiferromagnetic (afm) 1D behaviour is suppressed by 3D afm long-range order in the doping region of 0<x<1.2 and x >2 [2,3,4]. Bulk measurements (susceptibility and specific heat) performed with a conventional PPMS at TUM indicate charge ordering in the $CuO_2$-chains [5]. First inelastic neutron measurements were carried out in order to investigate microscopically the only hole dopable spin-1/2 afm Heisenberg chain compound series.

Inelastic neutron measurements of CaYCuO were performed on NG-5 (SPINS) at NIST as well as on TASP at SINQ, PSI. For both experiments const-q scans at the (001) magnetic zone center ($q$ = 0.59 Å) and constant energy scans were carried out; the first sort of scans should reveal the gapped dispersion at q = 0.59 Å whereas constant energy scans confirm scattering free E space below the gap energy and magnetic scattering at the gap energy.

For NG-5 experiments, investigating $Ca_2Y_2Cu_5O_{10}$, $Ca_{2.5}Y_{1.5}Cu_5O_{10}$ and $Ca_3Y_1Cu_5O_{10}$, a fixed final energy of 5 meV with a horizontally focusing analyser (HFA) and the collimation 80'-sample-radial collimator-HFA was chosen to intense the magnetic signal at the expense of a broader $q$ resolution. A Beryllium filter cooled at liquid nitrogen temperature and installed between the sample and the radial collimator accounts for higher λ contamination. For the TASP experiments of $Ca_2Y_2Cu_5O_{10}$, $Ca_{2.5}Y_{1.5}Cu_5O_{10}$ and $Ca_{4.15}Cu_5O_{10}$ a fixed final energy of 5.64 meV/8 meV with a HFA/flat analyser and an open-/open-80'-sample-80'open-collimation were used.

$Ca_2Y_2Cu_5O_{10}$ features at the magnetic zone center (001) a spin gap of 1.8 meV (see Fig. 1) resulting from the easy axes spin anisotropy along the $b$ axes. Surprisingly, instead of a single excitation the sample shows scattering up to 4 meV whose origin is not compatible with the dispersion of an undoped $Ca_2Y_2Cu_5O_{10}$-single crystal [6]. Doping holes into the $CuO_2$-chains leads to a decreasing gap energy in $Ca_{2.5}Y_{1.5}Cu_5O_{10}$, the medium doped $Ca_3Y_1Cu_5O_{10}$ shows constant scattering up to 4 meV. Independent of the doping concentration, all samples show broader excitations instead of a precise gap energy. Highly doped $Ca_{4.15}Cu_5O_{10}$ reveals a magnetic excitation of ~ 2.2 meV at the position of the (001) magnetic Bragg peak (Fig. 2). However, no excitation was found at the corresponding $q$ of (1/2 0 1) which is the only confirmed magnetic Bragg reflection in this sample. Future experiments on $Ca_{2+x}Y_{2-x}Cu_5O_{10}$, in particular on single-crystal $Ca_{4.15}Cu_5O_{10}$, shall help to clarify the magnetic structure as well spin dynamics in the compound series.

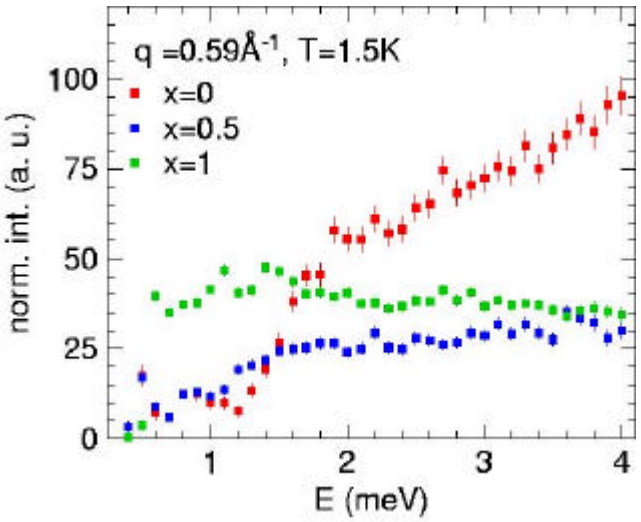


***Fig. 1:*** *Background reduced constant q scans at the (001) magnetic Bragg peak for low doped CaYCuO.*

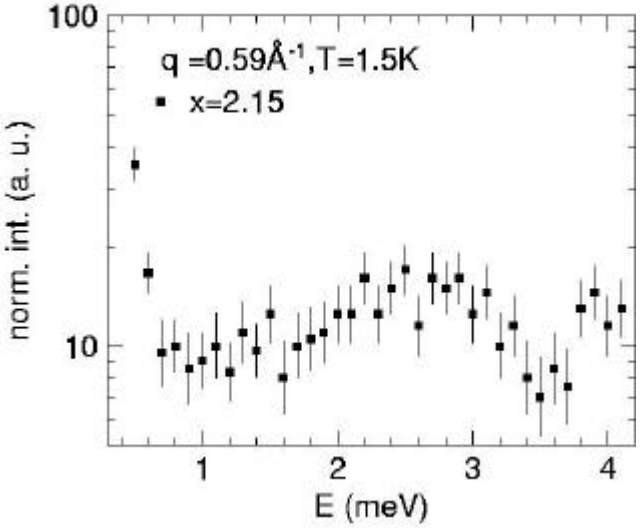


***Fig. 2:*** *Excitation at the (001) position in $Ca_{4.15}Cu_5O_{10}$.*

We kindly acknowledge the support by the TASP and NG-5 instrument responsibles B. Roessli, S. Park and S.-H. Lee of the SINQ (PSI) and NCNR (NIST).

References:

[1] A. Hayashi et al., Phys. Rev. B 58, 2678 (1998)
[2] M. Matsuda et al., J. Phys. Soc. Jn. 68, 269 (1999)
[3] H. F. Fong et al., Phys. Rev. B 59, 6873 (1999)
[4] G. I. Meijer et al., Phys. Rev. B 58, 14452 (1998)
[5] V. Kargl et al., submitted to Physica B
[6] M. Matsuda et al., Phys. Rev. B 63, 180405 (2001)

## 1.8 Doping dependencies of specific heat and magnetic susceptibility in the spin-chain compounds $CA_{2+x}Y_{2-x}CU_5O_{10}$

A. Mirmelstein [1,2], V. Kargl [1], J. Karpinski [3], S. Kazakov [3], P. Böni [1], A. Erb [4]

[1]*Technical University of Munich, Physics Department E21, D-85748 Garching, Germany*
[2]*Institute for Metal Physics, Russian Academy of Sciences, 620219 Ekaterinburg GSP-170, Russia*
[3]*Laboratory for Solid State Physics, ETH Hönggerberg, CH-8093 Zürich, Switzerland*
[4]*W. Meissner Institute, Bavarian Academy of Science, D-85748 Garching, Germany*

*We performed a systematic study of the specific heat and the magnetic susceptibility of the spin-chain compounds $Ca_{2+x}Y_{2-x}Cu_5O_{10}$ (0 £ x £ 2.15) as a function of hole doping induced by the variation of the Ca/Y ratio.*

In order to investigate the doping-induced ground state of quasi-1D copper-oxide systems, we performed systematic measurements of the specific heat and magnetic susceptibility of the edge-sharing spin-chain compound $Ca_{2+x}Y_{2-x}Cu_5O_{10}$ (CaYCO), which consists only of linear chains and allows a variable doping level by the variation of the Ca/Y ratio [1]. The magnetic phase diagram of CaYCO exhibits a crossover from 3D AF order at $x = 0$ to spin-chain-like behaviour at an intermediate doping. At maximal doping in $Ca_{4.15}Cu_5O_{10}$ a new spin-coherent state appears again at ~ 12 K [2], however its nature is not understood yet.

Ceramic sample of CaYCuO were prepared as described in [3]. Specific heat and susceptibility measurements were performed using a conventional PPMS (Quantum Design). The results obtained were analyzed in terms of a uniform and an alternating/dimer spin-chain behavior (Figs. 1 and 2). It is found that for highly doped samples $x > 1$ the uniform spin-chain contribution does not depend on doping and corresponds to a spin concentration ~ 0.5 per Cu ion. Such a behavior can only be understood as an ordering of the doped holes in the chains. The second component is washed out near $x = 2$, so that a new coherent state emerges from the pure spin-chain regime.

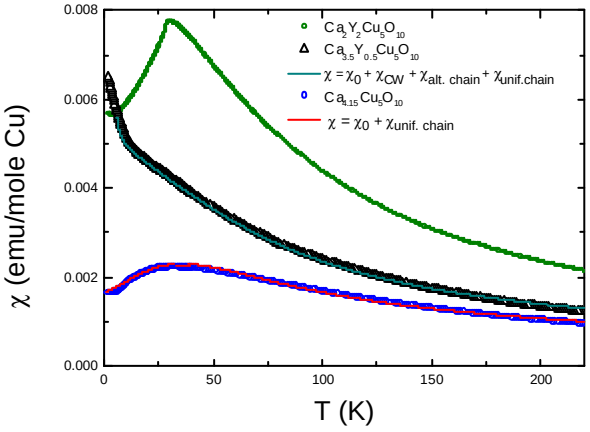


***Fig. 1:*** *The magnetic susceptibility vs. T curves for the CaYCuO samples with x = 0, 1.5, and x = 2.15. Lines are the result of the fit as indicated in the figure.*

Clearly, inelastic neutron scattering experiments are indispensable for microscopic understanding of the phase diagram of CaYCuO. Such experiments are in progress.

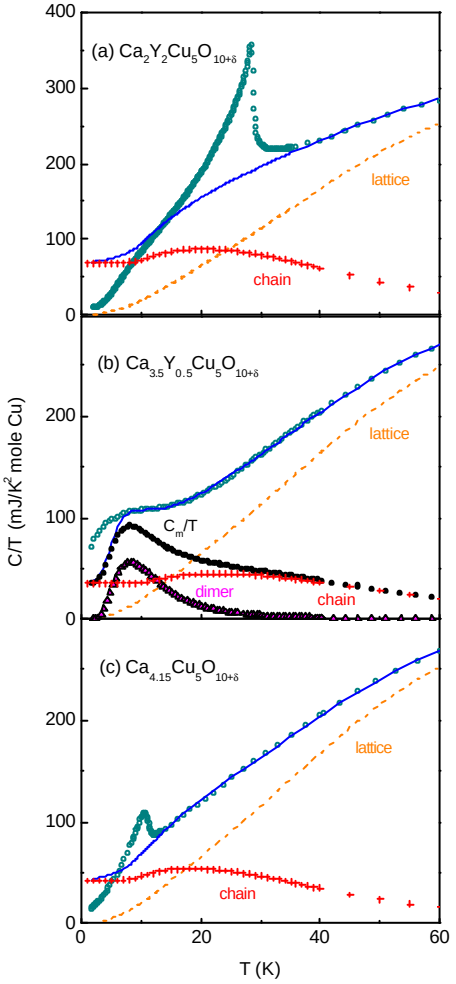


***Fig. 2:*** *C/T vs. T curves (open circles) for the CaYCO samples with (a) x = 0, (b) x = 1.5, and (c) x = 2.15. The solid blue lines are the sum of the lattice, spin-chain, and dimer terms, which are shown separately. $C_m/T$ in (b) is the sum of both magnetic contributions.*

References:

[1]. A. Hayashi et al., Phys. Rev. Lett. **58,** 2678 (1998)
[2]. G. I. Meijer et al., Europhys. Lett. **42** (1998) 339.
[3]. V. Kargl et al., Physica B, in press.

## 1.9 Polarized Neutron Reflectivity Investigations on FeCoV/Ti Spin-valves

M. Senthil Kumar[1], Shah Valloppilly[2], Christian Schanzer[2], Peter Böni[2], Thomas Krist[3], Michael Horisberger[4]

[1]*Department of Physics, Indian Institute of Technology Bombay, Mumbai 400 076, India*
[2]*Physik Department E21 der Technische Universität München, James-Franck Strasse, D85747 Garching, Germany*
[3]*BENSC, Hahn-Meitner-Institut, Glienicker Strasse 100, 14109, Berlin, Germany*
[4]*Laboratory for Neutron Scattering, ETHZ & PSI, CH-5232 Villigen PSI, Switzerland*

*Spin-valve multilayers (MLs) consisting of magnetically hard and soft FeCoV layers separated by Ti spacer layers were investigated for their interface and magnetic properties. Polarized neutron reflectivity (PNR) was performed on selected samples at magnetic saturation, and the spin dependent reflectivities were analysed by modeling the magnetic states of the soft and hard FeCoV layers. Existence of two magnetic phases of FeCoV, i.e, in the bulk and at the interface are detected and the extent of these two regions and their magnetic moments for various Ti thicknesses were estimated from PNR and are utilized to understand the magnetization reversal of these multilayers.*

FeCoV/Ti bilayers investigated previously for their interesting applications as spin-selecting devices in neutron optics [1] have also been investigated now as 'spin-valves'. In this report, we present our investigations to understand the influence of Ti spacer layer on their magnetization reversal. From the x-ray reflectivity (XRR) we found out that the present MLs have rather rough interfaces and the magnetization reversal is influenced by the Ti spacer layer thickness. Therefore, we investigated these MLs by PNR since XRR as well as DC magnetization cannot reveal the magnetic nature of the interfaces.

The MLs [Ti (***t*** nm)/FeCoV (10 nm) /Ti (***t*** nm) /FeCoV (3 nm)]$_{20}$ MLs [***t*** = 3, 5, 8, 10, 12 and 15 nm] were sputter deposited by dc magnetron sputtering at PSI, Switzerland. Specular XRR as a function of momentum transfer perpendicular to the film plane ($q_z$), as shown is Fig. 1, quantifies the interface roughness and chemical periodicity.

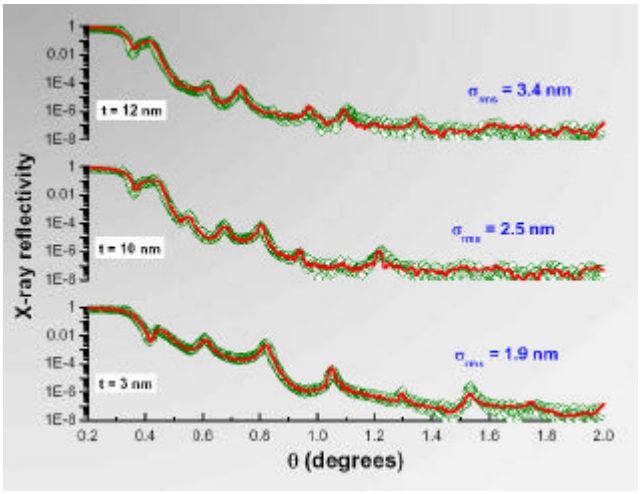


***Fig.1:*** *XRR of some selected samples. Symbols represent the experimental data and the lines represent the calculated XRR.*

Magnetization reversal (Fig. 2) falls in three categories depending on the Ti spacer thickness. At low ***t*** (~ 3 - 5 nm), the magnetization reversal takes place by a coherent rotation of all the layer magnetizations and the soft magnetic layer (3 nm FeCoV) seems to have identical switching field as the hard magnetic layer (10 nm FeCoV). When ***t*** is ~ 8-12 nm, we observe two clear magnetization reversals corresponding to the switching of soft and hard FeCoV layers. When ***t*** becomes ~ 15 nm, the magnetization reversal becomes less sharp and the overall coercivity of both hard and soft layers decreased.

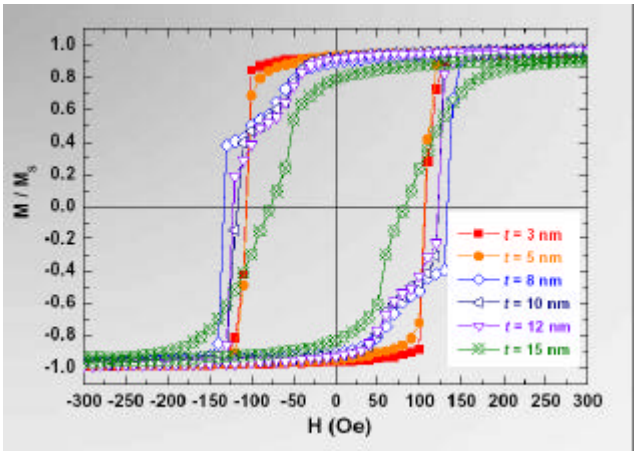


***Fig.2:*** *M-H loops of the Fe CoV/Ti MLs for various Ti spacer thicknesses showing the three different types of magnetization reversals.*

PNR measurements were made at the V14 reflectometer, at BENSC, HMI, Berlin in the angle dispersive mode. The MLs were subjected to an external magnetic field of 700 Oe.

In Fig. 3 are shown the NSF reflectivities ($R^{++}$ and $R^{--}$) for three typical samples viz. ***t*** = 3, 10 and 15 nm, very close their magnetic saturation. $R^{++}$ and $R^{--}$ probe the components of the magnetization parallel to the polarization direction of the neutrons. A recursive matrix calculation using the code *'Simulreflec'* [2] we quantified the layer magnetization in the MLs.

The ML periodicities determined from XRR and PNR match very well. The magnetic FeCoV layer was decomposed in to two phases; one phase corresponding to bulk FeCoV layer with a large magnetic moment and the another phase at the two interfaces with a reduced magnetic moment. For example, for ***t*** = 3nm, the interface region extends over 0.5 nm at each interface with a moment of 0.8 $\mu_B$. Similarly, for ***t*** = 10 and 15 nm, we find the bulk and interface regions assume 2 and 1 $\mu_B$ and 1.7 and

1.3$\mu_B$ respectively. The average widths of the interface regions are 1 and 0.9 nm respectively.

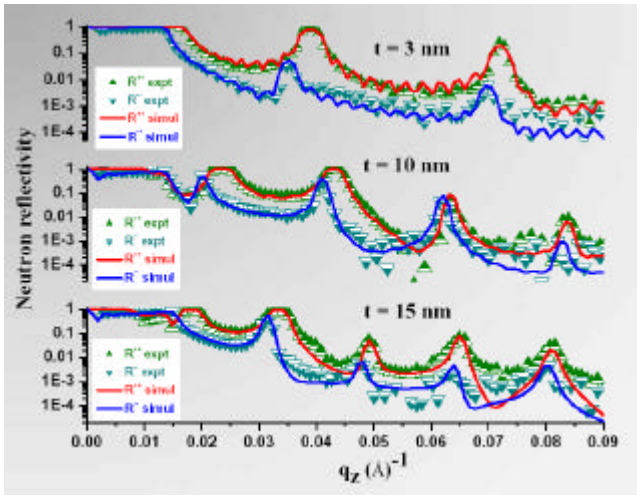


***Fig.3:*** *PNR on selected samples showing the NSF reflectivities at 700 Oe. The lines show the computed reflectivity curves for the NSF case.*

This trend has been verified for the intermediate ***t*** as well. The contributions from bulk and the interfaces estimated from PNR are plotted in Fig. 4.

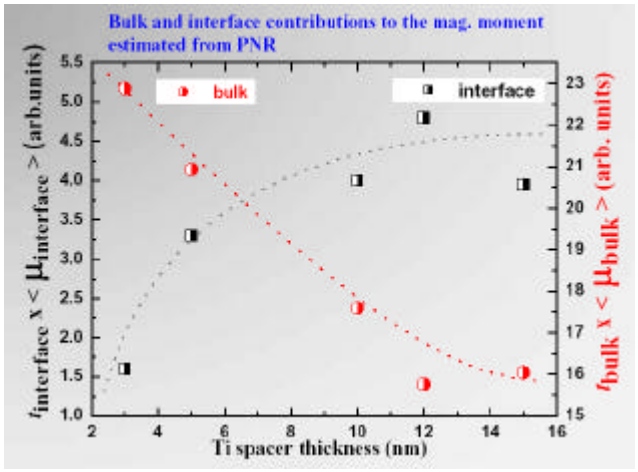


***Fig.4:*** *Bulk and interface contributions to the magnetization extracted from PNR for various Ti spacer thicknesses.*

The reduced magnetic moments at the interface regions originate from magnetic inhomogeneities like non-collinear magnetic structures, magnetic dead layers or interface alloying. With increasing 'magnetic roughness', dipolar fields created at the interface influence the magnetization reversal [3]. Moreover, the reduction of stress anisotropy with increasing thickness results in the formation of domains with random anisotropy axes and can reduce the component of magnetic moments [C. Schanzer *et al.*, in this report], at the interface as well as in bulk, along the field axis at moderate fields. The magnetic dead layers in similar films are much smaller (~ 0.21 and 0.33 nm) than the observed FeCoV/Ti interface layers [4]. Therefore, in the present study we believe that this interface region is most likely due to interface alloying. The results in detail are available in our forthcoming publication [5]. However, the analysis of SF reflectivities and polarization analysis the off-specular reflectivities are essential to separate the chemical and magnetic roughness [6] and this work is in progress.

References:

[1] P. Böni, D. Clemens, M. Senthil Kumar and C. Pappas., Physica B 267-268 (1999) 320.
[2] *SimulReflec*., Frédéric Ott, Laboratoire Léon Brillouin CEA/CNRS.
[3] C. Tiusan, M. Hehn and K. Ounadjela., Eur. Phys. J. B 26 (2002) 431.
[4] M. Senthil Kumar, P. Böni and M. Horisberger., Physica B 325 (2003) 401.
[5] M. Senthil Kumar, V.R. Shah, C.Schanzer, P.Böni, T. Krist and M. Horisberger., Physica B (to appear).
[6] R.W.E. van de Kruijs *et al*., Appl. Phys. A 74 [Suppl.] S 1550 (2002)..

## 1.10 Structural Characterization of FM/AF/FM Trilayers

Shah Valloppilly[1], Christian Schanzer[1], Peter Böni[1], Hans-Benjamin Braun[2] and Michael Horisberger[3]

[1]*Physik Department E21 der Technische Universität München, James-Franck Strasse, D85747 Garching, Germany*
[2]*Institut für Theoretische Physik, Schafmattstr. 32, ETH Hönggerberg HPZ F 10.3, CH-8093 Zürich, Switzerland*
[3]*Laboratory for Neutron Scattering, ETHZ & PSI, CH-5232 Villigen PSI, Switzerland*

*Ferromagnet (FM) / Antiferromagnet (AF) / Ferromagnet (FM) trilayers are synthesized in order to study the spin configurations in the FM and AF as a function of the AF thickness. The texture and chemical composition of the AF NiO, prepared by reactive sputtering of Ni in partial Oxygen atmospheres, have been examined by X-ray reflectivity (XRR) and X-ray diffraction (XRD). The interface roughness, oxide formation etc. have also been determined by XRR when the FM / AF / FM trilayers are formed.*

FM/AF multilayers, well known for their exchange bias properties, have drawn much attention for their industrial applications in GMR heads, MRAMs as well as in the fundamental investigations of their spin structures at the interfaces [1]. When an AFM layer is sandwiched between two FM layers, the interlayer exchange coupling between the FM layers mediated by the AFM layer strongly depends on the interfacial exchange coupling and the AF layer thickness. Theoretically, the existence of a non-collinear magnetic structure in the AF [2] has been proposed and indirect evidence for a spiraling of AF moments within the AF layer and a linear dependence of the magnetization turn-angle between the FM layers on the AF thickness has been obtained [3]. When the AF layer is an oxide, the interface oxidation can also play a significant role in exchange coupling that can be either FM or AF as demonstrated by the soft X-ray resonant magnetic reflectivity [4]. Moreover, texture of the AF oxide that is in contact with the FM is also important as it can lead to spin compensated or uncompensated terminated surfaces that may play the most important role in the interfacial exchange. Therefore, it is very important to characterize the texture, composition and roughness of the AF oxide prior to the making of FM/AF/FM trilayers.

We prepared a series of $NiO_x$ calibration films by reactive dc magnetron sputtering from a Ni target at different total pressures and at different $Ar:O_2$ partial pressures. Their prominent textures are obtained from x-ray diffraction (XRD). Mostly (111) and (200) textures have been found to be developed that represent the spin uncompensated and spin compensated termination of NiO surface, respectively. The thickness, surface roughness and the chemical composition were obtained by x-ray reflectivity [Fig. 1]. The films are found to contain regions of partially oxidized $NiO_X$ at different partial pressures of oxygen and a stoichiometry of ideal NiO was obtained around 16% of $O_2$ in the $Ar:O_2$ admixture at a total pressure of 4 μbar. Below 16%, the films have regions of under and over oxidized Ni and above 16%, they remain close to the ideal NiO.

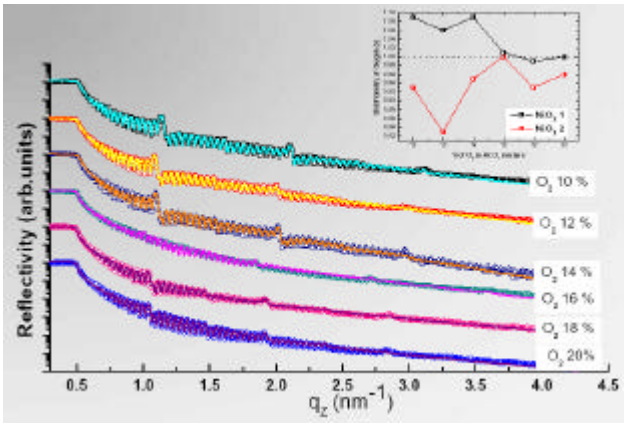


***Fig.1:*** *X-ray reflectivity analysis of the $NiO_X$ single films prepared at different $O_2$ partial pressures. Symbols and lines represent the data and fit. The bumps in XRR originate from periodicity of the two partially oxidised $NiO_X$ (1&2). The inset shows that the stoichiometry reaches the ideal value 1 at 16% of $O_2$.*

FM/AF/FM trilayers, (here, FM = FeCoV and AF = NiO) exhibit very interesting magnetic behaviour as a function of AF spacer thickness and will be discussed by Schanzer *et al.* in this report.

Here, we report the XRR analysis of a FM/AF/FM trilayer [Fig. 2] to demonstrate how the interfaces are formed. FeCoV- oxide formation is detected at both NiO-FeCoV interfaces, but the width of the oxide layer is different. The oxidation at the first interface is large (~ 1 nm) due to the short exposition of the $Ar:O_2$ gas mixture to the first FeCoV layer whereas, that at the second interface is smaller (~0.2 nm) which is only due to a diffusion process. The magnetic nature of these oxide interfaces is unknown so far, however as mentioned before, they could couple ferromagnetic or antiferromagnetic to the adjacent FeCoV layer and can result in the non-collinear spin structures in the AF as well as in the adjacent FM layer. Further investigations in this regard are in progress.

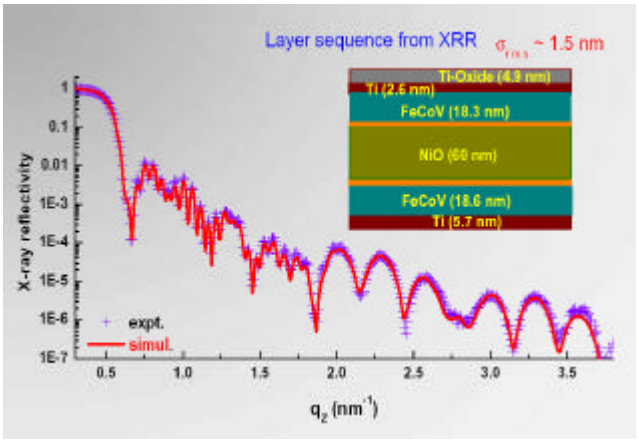


***Fig.2:*** *Characterization of the FM/AF/FM trilayer by XRR. Symbols and line represent the experimental data and the fit. Inset shows the layer structure resulted from the XRR analysis.*

References:

[1] A.E. Berkowitz and Kentaro Takano., J. Magn. Magn. Mater. 200 (1999) 552
[2] Haiwen Xi and Robert M. White., Phys. Rev. B 62 (2000) 3933
[3] F. Y. Yang and C. L. Chien., Phys. Rev. Lett. 85 (2000) 2597
[4] O. Zaharko et al., Phys. Rev. B 66 (2002) 134406

## 1.11 Magnetic Properties of FM/AF/FM Trilayers

C. Schanzer[1], S. Valloppilly[1], P. Böni[1], H.-B. Braun[2], T. Gutberlet[3], M. Gupta[3], M. Horisberger[3]

[1]*Physik Department E21 der Technischen Universität München, James-Franck Strasse, D85747 Garching, Germany*
[2]*Institut für Theoretische Physik, Schaffmattstr. 32, ETH Hönggerberg HPZ F 10.3, 8093 Zürich, Switzerland*
[3]*LNS, ETH Zürich & Paul Scherrer Institut, 5232 Villigen, Switzerland*

Ferromagnetic/antiferromagnetic (FM/AF) interfaces, well known for their exchange bias EB) properties, have attracted much interest because of their relevance in fundamental and applied research[1]. Additionally, in multilayers of FM/AF, interlayer exchange coupling (IEC), mediated through the AF, is observed [2]. The magnetic properties are expected to depend crucially on the spin structure of the AF layer, especially at the interface. We investigated trilayers of FeCoV (FM) / NiO (AF) / FeCoV (FM) where FeCoV layers had a thickness of 20 nm and the NiO thickness was varied from 1 nm up to 100 nm. The multilayers were prepared by DC magnetron sputtering of a $Fe_{50}Co_{48}V_2$ alloy in an Ar atmosphere and of a Ni target in an $Ar:O_2$ atmosphere. The total pressure and the ratio of the $Ar:O_2$ atmosphere was adjusted in order to form proper NiO. The formation of NiO and the structural characterization is discussed by Shah *et al.* in this report. For bulk magnetic properties DC magnetization (DCM) was performed. Polarized neutron reflectivities (PNR) were measured in order to resolve the depth profile of the spin structure. PNR was carried out at the time of flight reflectometer AMOR at SINQ, PSI (Switzerland).

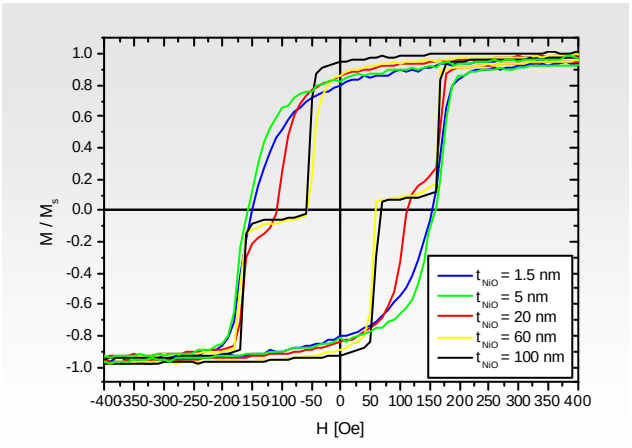


***Fig.1:*** *In plane MH dependence of FeCoV/NiO/FeCoV trilayers with varying NiO thickness: For small NiO thicknesses the magnetization reversal occurs in a single gradual transition. From 20 nm onwards a plateau region forms where the arrangement of spins cancels to zero net magnetic moment.*

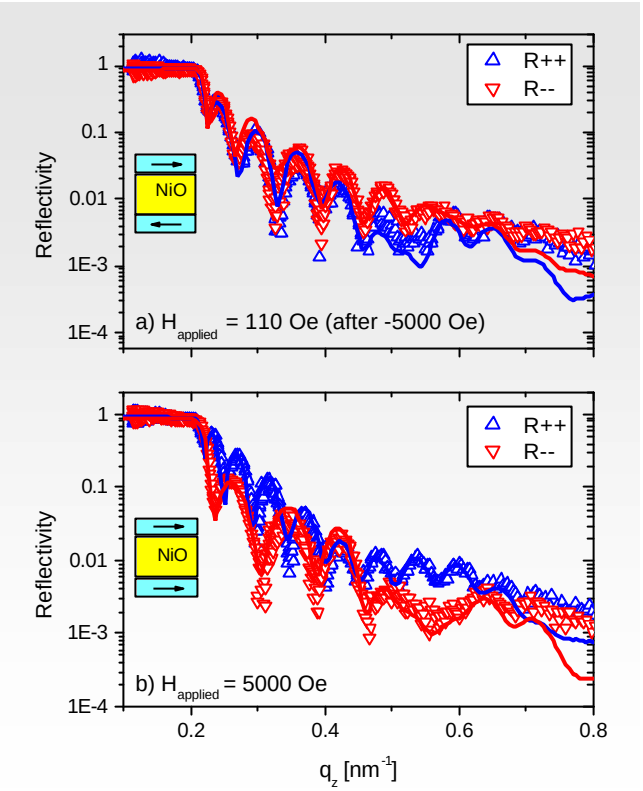


***Fig.2:*** *PNR of FeCoV/NiO (60 nm)/FeCoV: The non spin flip (NSF) reflectivities are recorded at two fields of the hysteresis loop, representing a) the intermediate plateau of about zero net magnetization and b) saturation. The spin structure was modelled (solid lines) to match the experimental data (symbols) and is depicted above.*

The magnetization loops of the trilayers show a dependence on the thickness of the NiO layer (Fig.1). Up to a thickness of 10 nm the magnetization reverses via a single, gradual transition. In trilayers, where the NiO thickness is 20 nm and larger, a region of zero net magnetization forms. The width of this region again depends on the thickness of the NiO layer. PNR was measured on trilayers of different NiO thicknesses and at selected points of the hysteresis loop. Fig. 2 shows the results for NiO of 60 nm. An external field was applied to represent a) the plateau of about zero net magnetization and b) magnetic saturation of the sample in one direction. The spin dependent reflectivities were analysed by modelling the magnetic states of the FeCoV layers [3]. It was found that the adjacent FM layers order antiparallel in a) and parallel in b), as expected for saturation (inset in Fig. 2). The thickness dependence of magnetization reversal and the antiparallel ordering for intermediate fields may be caused from interfacial coupling and the spin structure in the AF [4,5]. In order to understand the mechanism of the magnetization reversal, PNR on

samples at different magnetic history and domain imaging during the magnetization reversal process are in progress.

References:

[1] A.E. Berkowitz and Kentaro Takano., J. Magn. Magn. Mater. 200 (1999) 552
[2] Z.Y. Liu, S. Adenwalla, Phys. Rev. Lett. 91 (2003) 037207
[3] SIMULREFLEC, F. Ott, http://www-llb.cea.fr/prism/programs/simulreflec/simulreflec.html
[4] O. Zaharko et al., Phys. Rev. B 66 (2002) 134406
[5] Haiwen Xi and Robert M. White., Phys. Rev. B 62 (2000) 3933

## 1.12 Spin wave excitations in an isotropic ferromagnet EuS

D. Lamago[1], A.I. Okorokov[2], S.V. Grigoriev[2] , P. Böni[1] , R. Georgii[1] , H. Eckerlebe[2] , P.K. Pranzas[3]

[1]*Technical University of Munich, Physics Department E21, D-85747 Garching*
[2]*Petersburg Nuclear Physics Institute (PNPI),*
[3]*GKSS- Research Center*

*Spin dynamics have been studied in the isotropic ferromagnet EuS by means of small-angle polarized neutron scattering in the temperature range* $14K = T_C = 35K$ *in external magnetic fields H=0-250 mT inclined about* $j = 45°$ *relative to the incident beam. The goal of this research has been to investigate the influence of the dipole-dipole interaction on the critical behaviour of the system at temperatures above the Curie temperature (*$T_C = 16.5K$*).*

Isotropic ferromagnets have been subject of extensive studies. Due to its strongly localized moments and low anisotropy fields, EuS is a very good realization of a Heisenberg ferromagnet. In addition EuS is of particular interest because of the large moment of the $Eu^{+2}$ ions of $7\mu_B$ leading to strong dipolar interactions. Using the asymmetry of the small-angle scattering of polarized neutrons, one can estimate experimentally the contribution of spin wave excitations from the magnetic scattering [1-2].

In order to investigate the influence of the dipole-dipole interaction in the critical region of the system, we performed measurements on the SANS-2 diffractometer at the GKSS-Research center with polarized neutrons ($P_0 = 0.95$) of fixed wavelength $\lambda$ = 5.8Å ($\Delta\lambda/\lambda$=0.1) with an angular divergence of 10 mrad. The sample was mounted inside a cryomagnet inclined by an angle $\varphi$ = 45° relative to the incident beam and providing a field up to 250mT. The scattering intensity was measured in the temperature range from T = 14K to T = 50K. With this experimental set-up one can observe the left-right asymmetry of neutron scattering and thus investigate the critical dynamics due to the spin correlations in the magnetic field and measure with high accuracy the parameters of spin waves in the ferromagnetic phase [3].

Fig.1 shows the temperature dependence of the spin correlation length $R_C$ above the Curie temperature and up to the highest temperature of our experiments. The correlation length increases while approaching the Curie temperature $T_C = 16.5K$ from above. From this measurements one can deduce the change in both the quasi-elastic and inelastic scattering contributions due to the critical spin fluctuations and to the spin-wave excitations.

The spin correlation length decreases with increasing magnetic field as shown in Fig.2. From this decay the value of the critical field exponent $z = 1.54 \pm 0.02$ was evaluated.

The deviation from the theoretical value (z = 2.5) for a pure Heisenberg ferromagnet is attributed to the dipolar interactions.

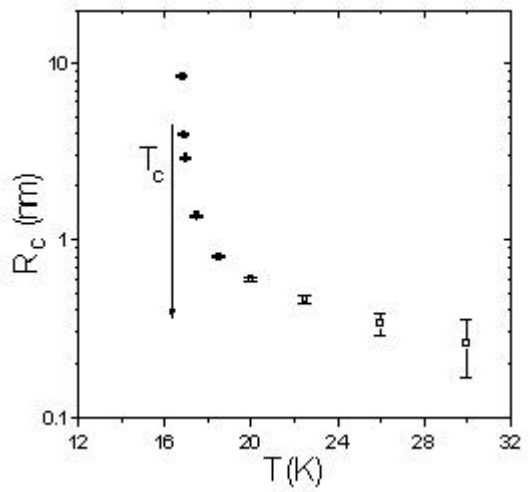


***Fig. 1:*** *Influence of the temperature on the correlation length*

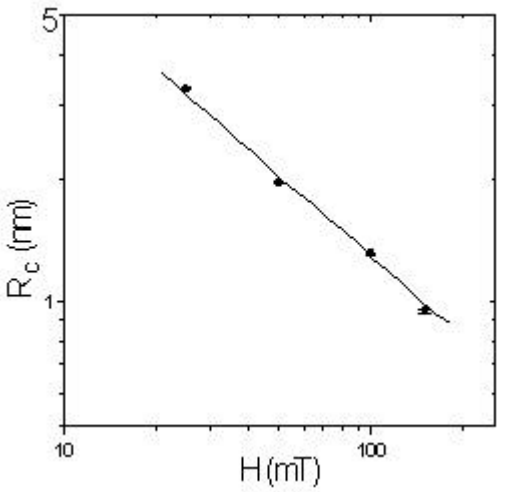


***Fig.2:*** *Magnetic field dependence of the correlation length at the Curie temperature* $(H \propto (1/R_c)^z T_c)$.

References:

[1] A.I. Okorokov, *Physika B*, **276-278**, 204-205(2000).
[2] B.P. Toperverg, V.V. Deriglazov, V.E. Mikhailova, *Physika B*, **183**, 326(1993).
[3] S.V. Maleyev, *Physics Review*, vol.**8**, 323(1987)

## 1.13 Critical exponents in MnSi

R.Georgii[1,2], P.Böni[2], D.Lamago[1,2], S.Stüber[1], S.V.Grigoriev[3], S.V.Maleyev[3], A.I.Okorokov[3], H.Eckerlebe[4], P. K.Pranzas[4], B.Roessli[5], W.E.Fischer[5]

*[1]ZWE FRM-II, TUM, 85747 Garching*
*[2]E21, Physikdepartment, 85747 Garching*
*[3]Petersburg Nuclear Physics Institute, Gatchina, St.Petersburg 188300, Russia*
*[4]GKSS Forschungszentrum, 21502 Geesthacht*
*[5]Laboratory for Neutron Scattering, ETH Zurich &*
*Paul Scherrer Institute, CH-5232 Villigen PSI, Switzerland*

The chiral fluctuations in the weak itinerant magnet MnSi were studied by means of small angle neutron scattering with polarized neutrons (see JB 2002 for details). Due to the lack of a centre of symmetry the magnetic moments are arranged along a left-handed spiral due to the Dzyaloshinskii-Moriya (DM) interaction. The experiments show that the incommensurate magnetic peaks evolve with increasing temperature into diffuse scattering that is mainly concentrated in a ring with the radius $q_0$ = 0.039 Å$^{-1}$ centred at the position of the direct beam q = 0.

For the determination of the critical exponents we started to interpret the data by extracting difference spectra of the two beam polarisations. Therefore, the effect of background scattering is eliminated and only the full anti-symmetric part of the magnetic cross section is considered. The spectra are integrated along a ring of constant q for both polarisations independently (i.e. the integration is performed along a half circle of 180°) and the intensity is plotted against q. The resulting structure is fitted with a Lorentzian peak. The two parameters of this fit, the width and the intensity, are plotted against the temperature as shown in Figure 1. From these two plots the following critical exponents can now be extracted using $T_c$ = (28.7 ± 0.05) K for all fits:

As the imaginary part of the paramagnetic susceptibility is proportional to the neutron magnetic scattering function we can derive the critical parameter $\gamma$ for $T > T_c$ directly from the intensity plot. For MnSi we obtain a value $\gamma = 0.61 \pm 0.01$. As the intensity of the scattering in the ordered phase is proportional to the square of the magnetisation we get the critical parameter $2\beta$ for $T < T_c$ from the intensity plot. For MnSi we obtain $\beta = 0.218 \pm 0.016$. The width of the peak is proportional to the inverse of the correlation length $\kappa$, therefore we obtain $\nu$ from the width of the peak. We find $\nu = 0.541 \pm 0.011$.

These results are so far only preliminary as we intend to remeasure MnSi for obtaining better statistics and also need to include the effects of the finite instrument resolution. But a few conclusions can already be drawn: While the values for $\beta$ and $\nu$ are similar to the values of other magnetic systems [1] the value for $\gamma$ clearly is smaller. Another interesting observation is that for d=2 we get for $\gamma+2\beta-d\nu = -0.036 \pm 0.017$, indicating a two-dimensional magnetic system.

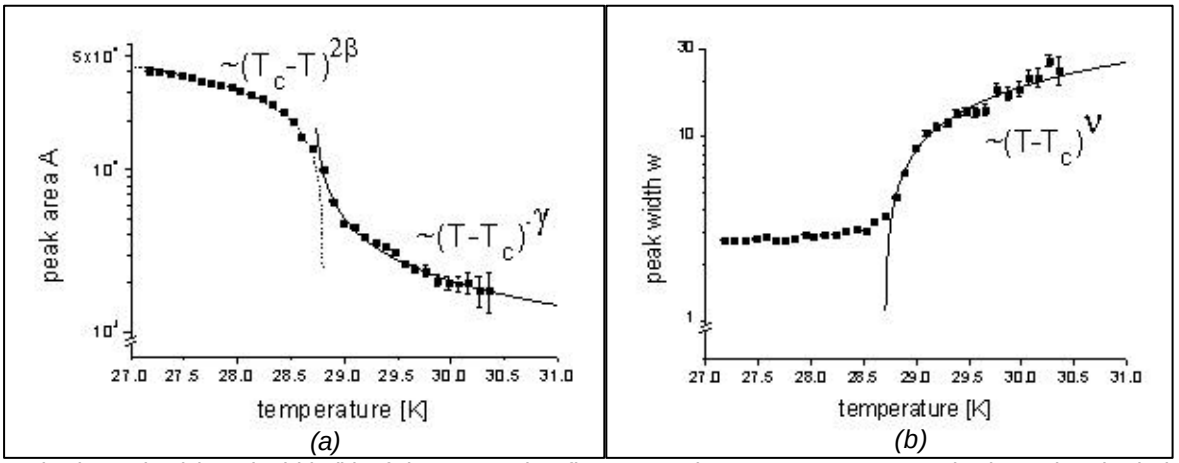


***Figure 1:*** *The intensity (a) and width (b) of the Lorentzian fits versus the temperature. From the intensity plot below $T_c$ the critical exponent $g$ for the magnetisation M and above $T_c$ the critical exponent $b$ for the paramagnetic susceptibility $c$ is obtained. From the width one gets the critical exponent $n$ for $k$, the inverse of the correlation length.*

References:

[1] B.D. Gaulin, M.F. Collins and T.E. Mason, Physica B 156&157 (1989) 244.

## 1.14 Multiple Small Angle Neutron Scattering

T. Hils, R. Gähler

*Technical University of Munich,*
*Physics Department E21, D-85748 Garching, Germany*

Research on polymers, colloid systems, cements, microporous media, are examples of a rising field, where µm correlations play a crucial role. Small angle X-ray and neutron scattering (SAXS and SANS) commonly measures lateral correlation lengths in the 0.01 to 0.1 µm range. To measure µm correlations with neutrons, various specific instruments have been designed, and the technique is commonly known as USANS (ultra small angle neutron scattering)[1]. However these methods are sensitive to scattering only in one dimension and suffer from intrinsic small angle scattering due to structure material in the beam.

Here we propose MSANS (Multi hole SANS), a new USANS option for a standard long baseline SANS instrument on pulsed or steady state neutron sources. It uses the common SANS infrastructure except for the detector, which requires enhanced spatial resolution. The system is sketched in Fig1.

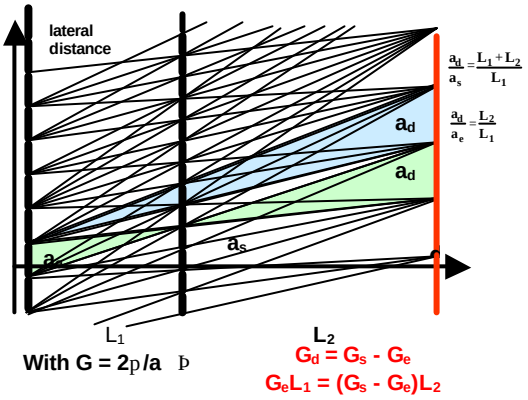


***Fig.1:*** *Condition for the lattice constants $a_e$ and $a_s$ and distances $L_1$ and $L_2$ for 'focussing' in the detector plane d.*

It is based on multi-hole apertures at the entrance ($M_e$) of the collimator and near the sample ($M_s$) with lattice constants $a_e$ and $a_s$ and hole diameters $d_e$ and $d_s$ respectively. With the choice

$$G_{e,s} = \frac{2p}{a_{e,s}}; \qquad G_e \cdot L_1 = (G_s - G_e) L_2; \qquad G_d = G_s - G_e$$

an intensity pattern of well separated peaks with lattice constant $a_d$ in the detector plane is observed ($a_d = 2\pi/G_d$). The equations holds separately for x and z-direction, i.e. the lattice constants in both dimensions can be chosen according to the requirements. The validity of the above equations may be directly seen from Fig. 1.

[1] q-resolution is in the order of $10^{-3}$ to $10^{-5}$ Å$^{-1}$ for USANS.

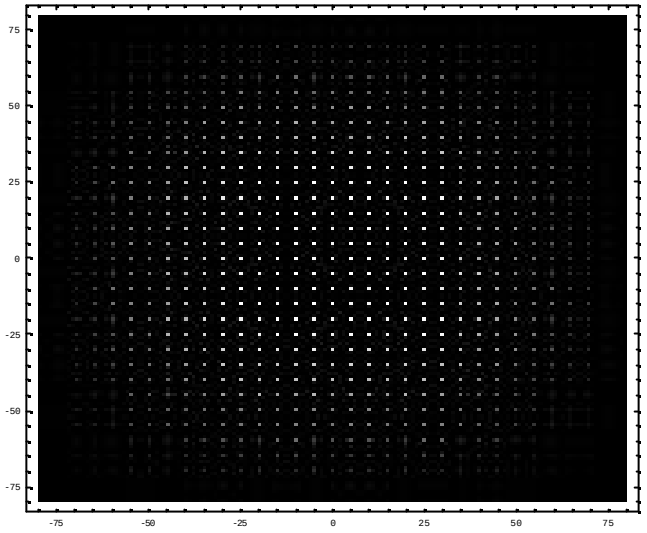


***Fig. 2***

### Upgrading the system with lenses

As an increase of intensity by enlarging the apertures would lead to a broadening of the images at the detector, the simple hole apertures could be replaced by lenses to establish detector-focusing. So the transmission factors and therefore intensity at detector position will be increased. The principle is shown in Fig 3.

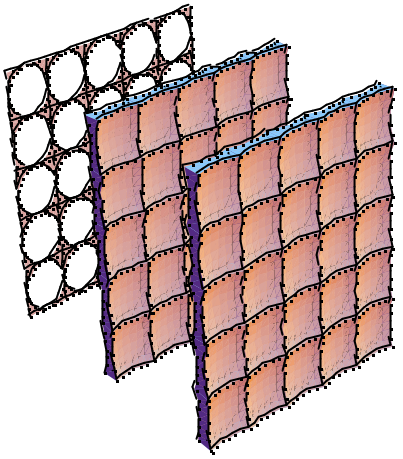

***Fig. 3***

The multi hole mask at the sample now becomes a multi lens mask. The lens mask consists of single lenses made of quartz ($SiO_2$) each with a diameter according to the lattice constant of the sample mask. As the refractive index n of neutrons is smaller than 1 ($n-1 = -5.69*10^{-5}$), concave lenses are needed. The

focal length of 10m, a wavelength of 10 Angstrom lead to lenses with a radius of 1.14 mm. Different kinds of aberration will occur when using lenses.

### Spherical aberration

Spherical aberration is caused by thick lenses due to the strong curvature. In this case a major broadening of the images at the detector of 0.12mm is expected. Substitution of the single lensmask by two separated lensmasks lead to thinner lenses and decreases spherical aberration. An additional hole mask reduces stray-beams. With this configuration an aberration is achieved of only 0.06mm.

### Gravitational correction

Due to large proportions of the system (typ. length = 20-40m) the deflection of neutrons due to gravitation can't be disregarded. With ?=10Å a vertical adjustment at the detector of about 5cm is necessary. Different neutron velocities (?v/v=10%) therefore would lead to severe overlap. This distortion can be corrected by using prisms. To focus beams with different wavelength in one spot at the detector, it is important to get symmetric passage through the prism. This is realised with an apex angle of the prism of 175°, as seen in figure 4.

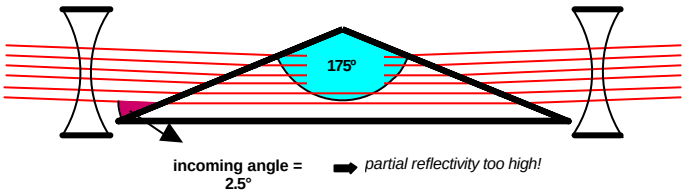


***Fig. 4***

Using one prism leads to an incoming angle of 2.5°, which means that the partial reflectivity at the surface of the prism would be much too high. To decrease this effect, one can use two instead of only one prism with an apex angle of both prisms of 169°. That increases the incoming angle to more than 5° and reduced partial reflectivity. With this correction the broadening of the image at the detector due to gravitation is about ?h=0.2mm and mainly caused by nonsymmetric passage through the prism.

In 2003 detailed calculation were conducted and coating (typ. >10 µm) of prototypes of the multihole-apertures with $^{10}B$ was begun.

## 1.15 MIRA – Very cold neutrons for new methods

R. Georgii[1], N. Arend[2], P. Böni[2], H. Fußstetter[1], D. Lamago[1], G. Langenstück[1], H. Wagensonner[1]

*[1]ZWE, FRM-II, TU München, Lichtenbergstr.1, 85747 Garching*
*[2]E21, Physik-Department, TU München, James-Franckstr., 85747 Garching*

The instrument MIRA (see JB 2002 for a detailed description) in its current configuration provides neutrons in the wavelength range 8 to 15 Å using a mica monochromator. The instrument has been designed for being able to measure a great variety of phenomena with very cold neutrons.

The reflectometer for mesoscopic structures is equipped with a polarised option. Neutrons will be polarised using a switchable transmission multilayer polarizer. Then a field of approximately 50 Gauss provided by permanent magnets will guide the polarised beam to the sample. Here the standard FRM sample environment (cryostats, cryomagnets and ovens) can be used. At last the neutrons are again guided by a magnetic field to the detector. Currently a $^3$He detector is being used. A 2-dimenisenional position sensitive detector with 20 x 20 cm sensitive area and a resolution of about 1 mm has been bought from GKSS and is currently tested a the reactor in Geestacht. It will be available early next year.

The instrument setup for this option has been successfully installed (see figure 1). It is fully operational, with the exception of the analysing possibility, which will be added early next year. The instrument control software exits, but is still on a very basic level. Nevertheless first reflectivity measurements could be performed. A simple evaluation software has been developed and will be available after testing with real data also early next year.

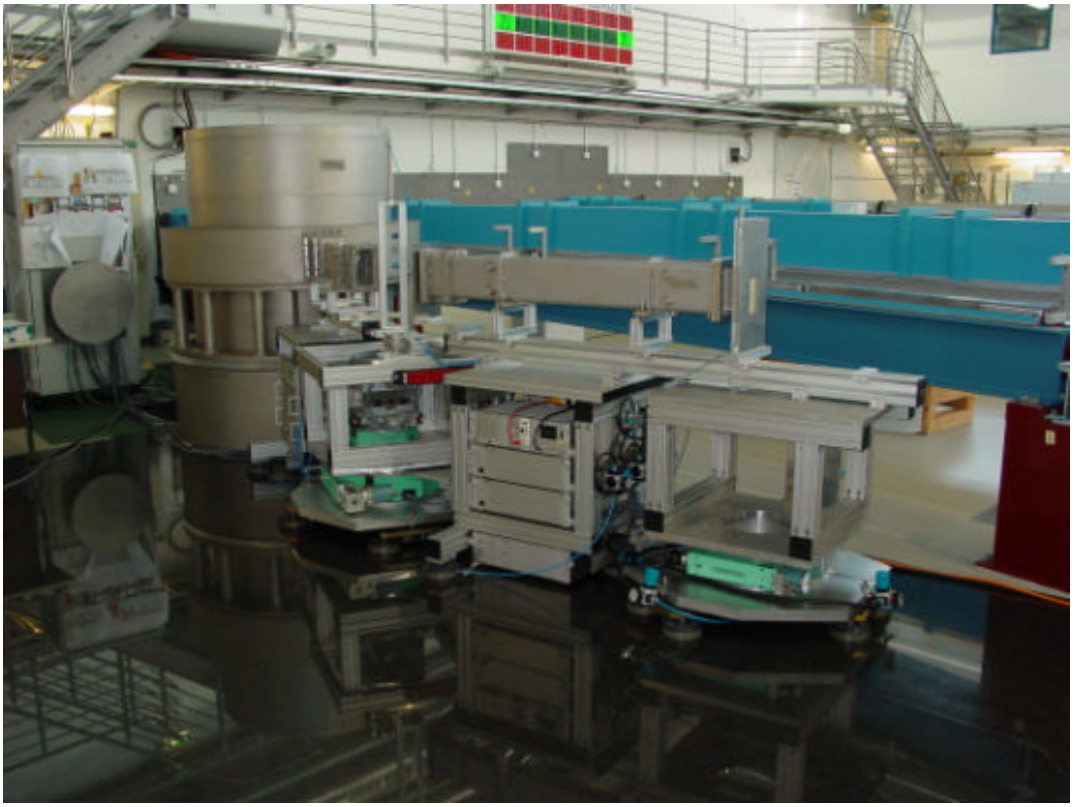

***Fig. 1:*** *The reflectometer option of MIRA without the detector and the magnets for the guide field.*

## 1.16 The multi-level MIEZE Option of the instrument MIRA

N. Arend[1], R. Georgii[2], H. Wagensonner[2], T. Keller[3]

[1] *TU München, Department of Physics, Institute E21, 85748 Garching*
[2] *TU München, FRM-II ZWE, 85747 Garching*
[3] *Max-Planck-Institute for Solid State Research, 70569 Stuttgart*

### NRSE coils for MIRA

For the multi-MIEZE (Modulation of IntEnsity by Zero Effort) [1] option of MIRA, NRSE (Neutron Resonance Spin Echo) flipper coils must be implemented. The standard design of those coils requires the neutron beam to penetrate them and therefore interact with the coil material. MIRA will operate in the cold neutron range, this must be taken into account when choosing materials and the design to avoid strong absorption and scattering.

### Design efforts

The NRSE flipper coils used at other FRM-II instruments (RESEDA and TAS-NRSE) have two properties that make them unfavourable for MIRA: the DC coils are made of a 0.5 mm × 8 mm aluminum band which has an anodised $Al_2O_3$ coating that features a periodic structure. This structure causes significant small angle scattering at higher wavelengths. Furthermore, since the winding density is relatively low, high currents ( 100 A) must be used to achieve the nominal DC field of 0.03 T. In order to get around those drawbacks a new design is planned for the MIRA coils. It is based on a design proposed in [2] and developed at the MPI für Metallforschung in Stuttgart. Thin (0.5 mm) profiles made of a rigid Al alloy (see Fig. 1) are piled on top each other, forming the windings of the DC coil. A considerably higher winding density (and therefore smaller current) as well as improved scattering properties can be achieved.

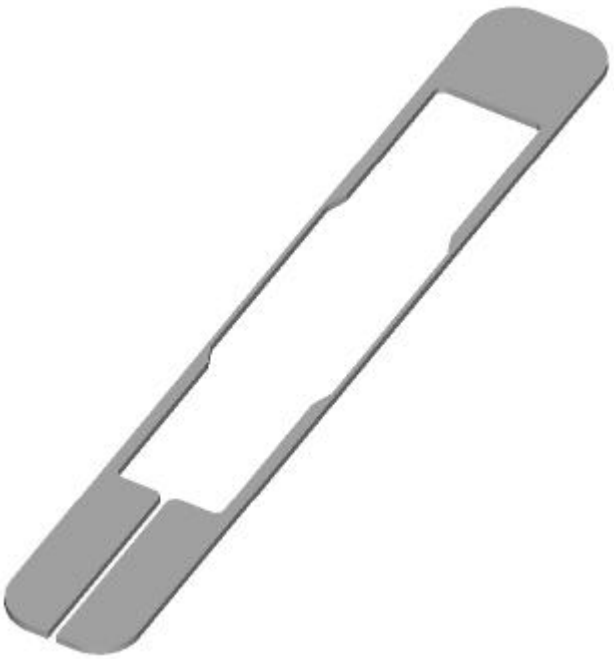

***Fig. 1:*** *Simplified single DC coil winding (cooling channels are omitted).*

Several approaches are being followed concerning electrical insulation (e.g. sputtered glass coating), contacts of the windings, and cooling . The design process
is work in progress, but significant improvements seem possible compared to the original Stuttgart design.

### B-field simulations

In order to test various designs prior to building them, numerical simulations help finding design flaws and optimising the model. Fig. 2 shows a B-field contour plot at the center of a DC coil of 31 cm width (150 windings @ 2 mm profile thickness, 13 A current) based on the sketched pro- file. The mu-metal shielding as well as cooling and other details are neglected. Deep red areas mark high, blue areas lower field magnitudes. This simulation was done using the IES© Faraday© software package.

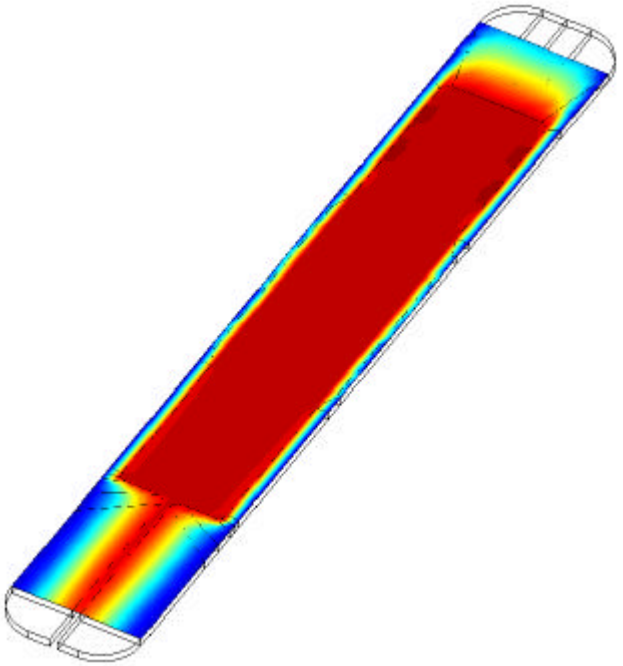

***Fig. 2:*** *B-field contour plot of the DC coil.*

### Science with MIRAs multi-MIEZE option

A multi-MIEZE setup is capable of producing very short, well separated pulses from a constant, polarised neutron beam [1]. A four-stage setup with frequency doubling between two subsequent levels produces the beam structure shown in Fig. 3 (compared to a single MIEZE signal).

If an additional spin flipper coil is placed directly behind the last MIEZE level, a macroscopic spatial splitting of the spin-up (?) and spin-down (?) states of the neutron pulses can be achieved (Fig. 4) [3].
This "longitudinal Stern-Gerlach effect" demonstrates the predictions of quantum mechanics in contrast to classical physics. Besides the demonstration of this basic quantum-mechanical effect, the so prepared beam may serve as an experimental basis for studying interference and coherence phenomena using cold neutrons.

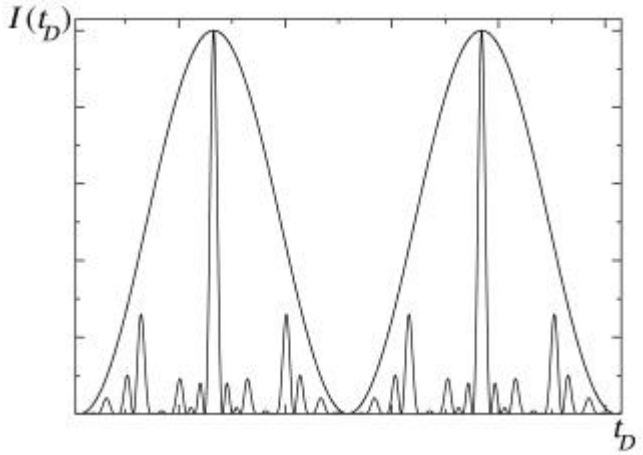


***Fig. 3:*** *Peaks produced by a four level multi-MIEZE (compared to single MIEZE signal).*

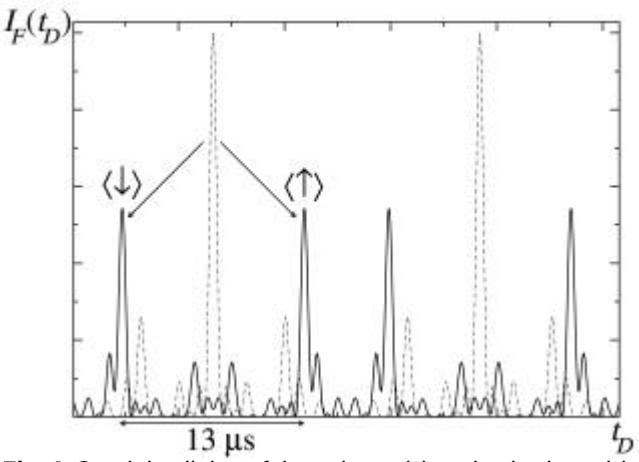


***Fig. 4:*** *Spatial splitting of the spin-up (?) and spin-down (?) states.*

References:

[1] Keller, T., Golub, R., Gähler, R. In Pike, R., Sabatier, P., editors, Scattering and Inverse Scattering in Pure and Applied Science, 126486 (Academic Press, San Diego, CA, 2002).

[2] Wahl, M. Aufbau einer Messanordnung zur Neutronenreflektometrie. Masters thesis, Max-Planck-Institut für Metall-forschung, Stuttgart, Germany/Institut für Theoretische und Angewandte Physik, Universität Stuttgart, Germany (2003).

[3] Arend, N., Gähler, R., Keller, T., Georgii, R.,Hils, T., Böni, P. Classical and quantum-mechanical picture of NRSE - Measuring the longitudinal Stern-Gerlach effect by means of TOF methods (2003). Submitted to Physics Letters A.

## 1.17 RESEDA Spectrometer: Annual Report 1.1.-31.12.03

project team: TU München, E21
project leaders: R. Gähler and P. Böni
instrument responsible: M. Bleuel

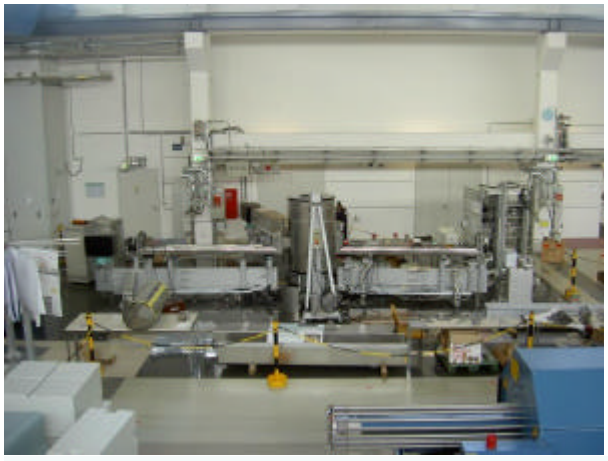

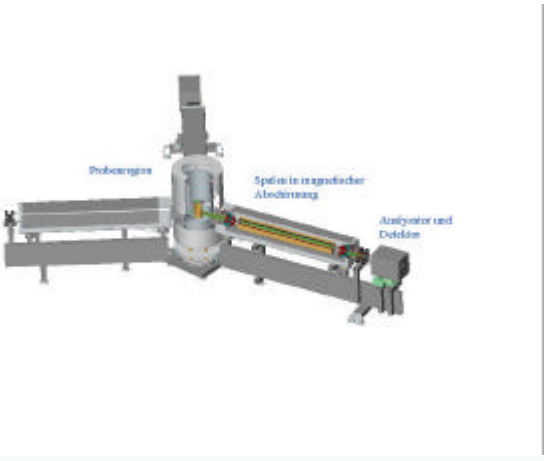

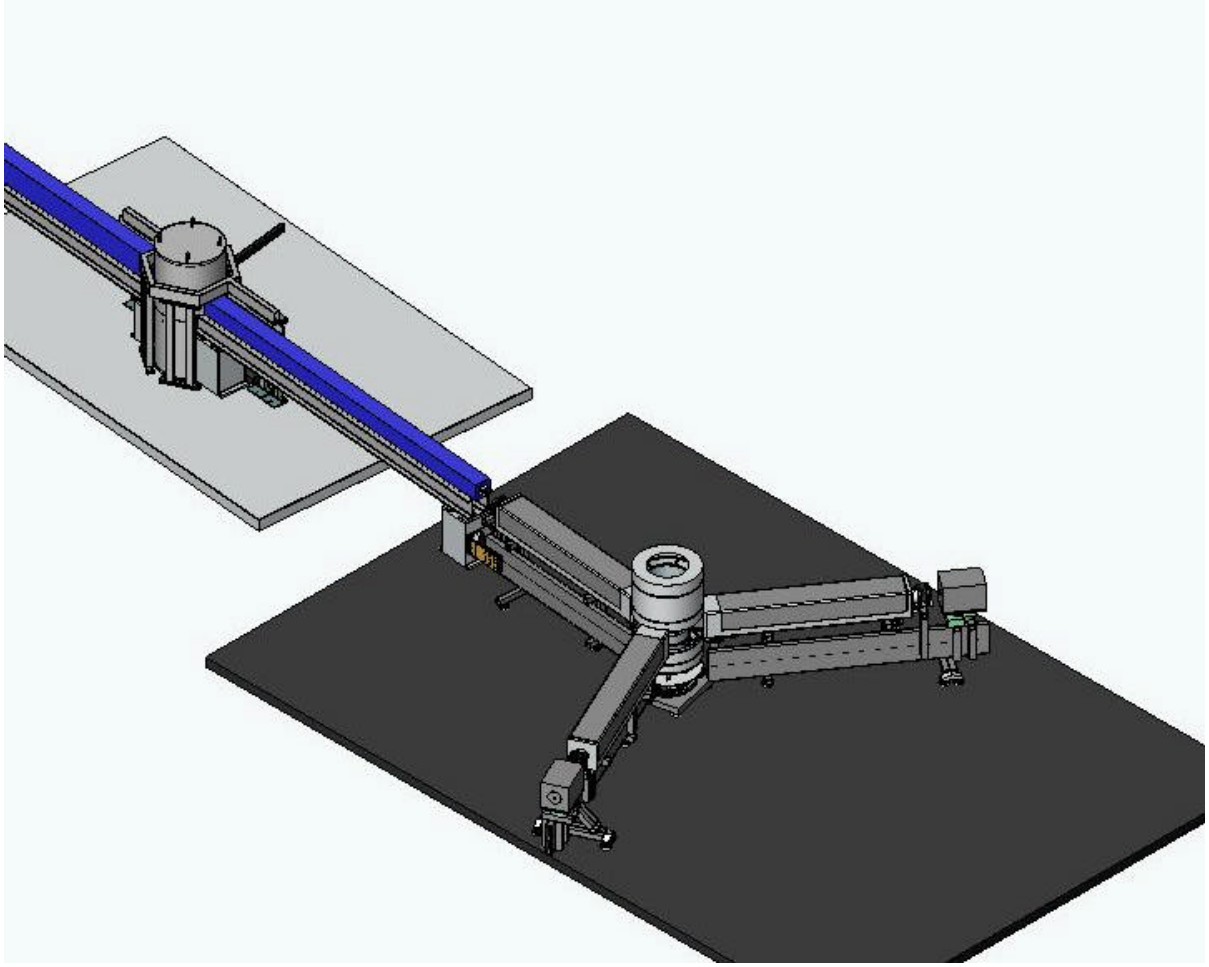

**Activities in 2003:**

RESEDA, the quasielastic neutron resonance spinecho (NRSE)-spectrometer at the FRM-II is located in the neutron guide hall. The neutron guide (5b) leading to the instrument was accomplished in 2003 and is the longest polarising neutron guide in the world. Because of its length the bending radius is big (r=1640m), so that even short wave neutrons ($\lambda$ =2Å) are transmitted to RESEDA. The polarisation is better than 96% over the whole wavelength range. The main activities in year 2003 at RESEDA were concentrated on the electric components of the instrument. The RF-circuits and the detector electronics were tested in their final position, the encoder, which determines the position of the spectrometer arms, and the NSE coils for the low resolution mode were mounted. Also the cabling of the instrument (motors, air cushions, air sensors, water, DC- and HF-supply for the bootstrapcoils) was continued and the instrument-control-programme was continuously improved.

In 2003 the three-dimensional model of RESEDA and surrounding installations became very helpful again, because the selector shielding has to be changed. A new reflectometer joins the polarising guide and so the selector shielding had to be changed to accommodate a monochromator as well.

**Actual project state (12.03):**

The estimated start of the FRM-II will not be before spring of 2004. Because of this delay of at least 3 years compared to the early time table, all RESEDA activities are stretched. It is important to keep the know how and avoid a further splitting of the team.

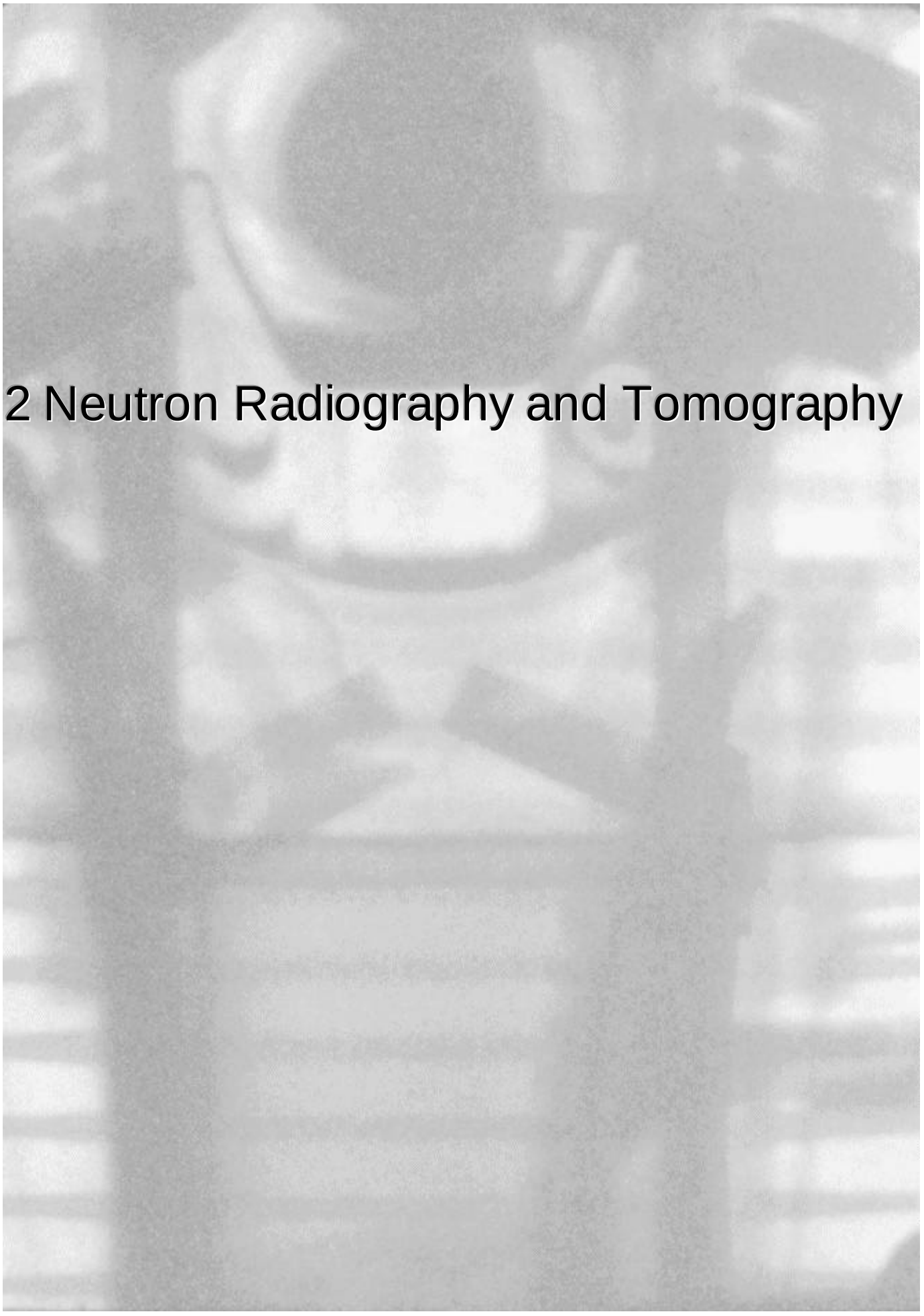

# 2 Neutron Radiography and Tomography

## 2.1 Construction of the Neutron Radiography and Tomography Facility ANTARES

B. Schillinger[a,b], E. Calzada[a], F. Grünauer[b]

[a)] *Technische Universität München, FRM-II, 85747 Garching, Germany*
[b)] *Technische Universität München, Physik Department E21, 85747 Garching, Germany*

### Overview

In 2003, the components for the neutron radiography and tomography facility ANTARES were constructed and assembled at beam line SR4b in the northeast corner of the experimental hall. The design of ANTARES has been explained in much detail in the previous annual report, so only a short overview is given here before details of the assembly are described. ANTARES consists of an external beam shutter, flight tube and block house. The external beam shutter is necessary because the UCN experiment at SR4a will insert a nozzle through the drum shutter in the biological shielding, rendering it unusable for ANTARES. Fig. 1 shows an overview of the facility, fig. 2 shows a 3D view.

### Construction of the wall elements

The shielding elements and block house walls were constructed as steel casings filled with heavy concrete. The secondary shutter housing and the block house elements were filled with concrete of density 4.5 tons/m3. As the collimated beam inside the flight tube does not touch the walls, a density of 3.5 tons/m3 was sufficient for the walls of the flight tube housing. As the crane in the experimental hall has a nominal capacity of 10 tons only, all elements were designed for a maximum weight of about 9.5 tons. For some elements of the blockhouse wall near the beam entrance, this weight constraint could not be met, so additional removable concrete filled cylinders were constructed inside the wall volume (Fig.3), which were mounted after the assembly of the wall elements.
Additional problems arose because the concrete company guaranteed only for the minimum density of the concrete, but not for the nominal density. In reality, the density became higher than the calculated values, leading to a component weight of more than ten tons. Fortunately, the reactor hall crane has a special 10% overload range (of which the use is restricted to a few hours per year), which was capable of handling all elements.

### Mounting of the wall elements

The blockhouse walls were mounted from five horizontal segments each, weighing more than 50 tons each. The assembled walls were fitted with mounting frames for up to six air cushions (fig.4) . An external compressor was used to lift the walls and to move them into place, as the capacity of the house installations was not sufficient.
Unfortunately, several cable channels in the hall floor were only roughly covered with uneven steel plates, rendering an uneven surface and an escape path for the compressed air. They had to be covered with thin steel plates, but still, the walls could only transit the uneven regions with the aid of two steel cable tackles affixed to the reactor hall walls (fig.5).

### The flight tube

As described in the last report, the flight tube consists of individual segments connected by rubber sealant rings, mounted on C-shaped brackets. The original design was taken from the vacuum housings for the neutron guides leading to the guide hall. No space was available top mount circular flanges, so the original square shape with rounded corners was altered by rounding the straight sections to a convex shape (fig.6).
Each segment has an individual vacuum connector, so single segments can be removed for experimental installations, the remaining segments can be closed off by covers.
Vacuum pump and vacuum control system were salvaged from the old reactor.
For the final neutron window at the end of the flight tube, a massive aluminium cover with a thin-milled window was foreseen. Static calculations predicted a material failure at the edge of the milled area, so the cover was constructed as a sandwich of a 3 mm aluminium plate, rubber seals and flange rings.
The cover stones for the flight tube housing have retractable ball casters on which they can slide from the middle, crane-accessible position to their final position under the platforms.

### Mounting of the blockhouse roof

The area of the blockhouse is not accessible by the hall crane. To be able to mount the roof at all, it was constructed from small two-ton bars. The original intention had been to use a balance bar and counterweight with the hall crane, which is able to telescope towards the corner of the hall just to the beginning of the block house. Later on, a special compact truck-mounted crane was found which was just able to drive into the reactor hall in the time when the other experiments at SR-2 and SR-3 were not yet assembled, with 5 cm space left next to the already mounted measuring cabins. The roof elements were deposited on the platform for the positron experiment with the hall crane, the truck-mounted crane took over from there and deposited them in position on the blockhouse roof (fig.7).

### The external beam shutter

The external shutter was constructed as a vertical concrete block containing two different collimators, driven by a hydraulic piston (fig.8) . A servo system with a position encoder and a control valve can position the shutter block to the accuracy of a tenth of a millimeter to a collimator position or to the closed position. When the position is reached, two hydraulic clamps hold the block in position, the hydraulic pump shuts off.
A hydraulic pressure tank holds sufficient pressure to open the hydraulic clamps and close the shutter within one third of a second when magnetic valves are opened in case of power failure.

### Outlook

In December 2003, The electric installation for the blockhouse was completed, so we had “first light” in the blockhouse even without neutrons. In 2004, The walls will be covered with B4C rubber mats to reduce the activation of the steel walls, the sample manipulator will be transported to the blockhouse and the detector box will be completed. The fast experimental pneumatic shutter and the filter wheel for phase contrast tomography will be mounted as the final installations, expecting the first measurements soon after commissioning of FRM-II.

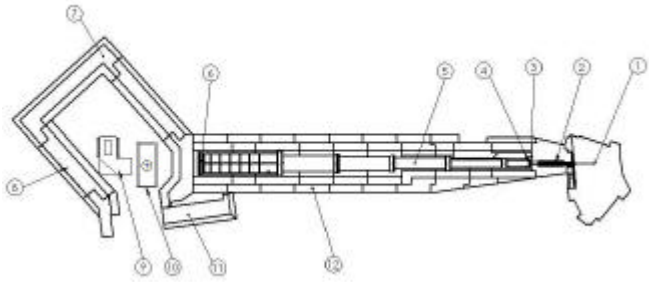

***Fig. 1:*** *Complete layout of the facility*

1. Collimator inside of the biological shielding
2. External vertical beam shutter
3. Iris diaphragm
4. Pneumatic shutter
5. Flight tube
6. Variable beam size limiter
7. Measurement cabin
8. Wall and beam stop
9. Detector and camera system
10. Sample manipulator
11. Sliding door
12. Flight tube shielding

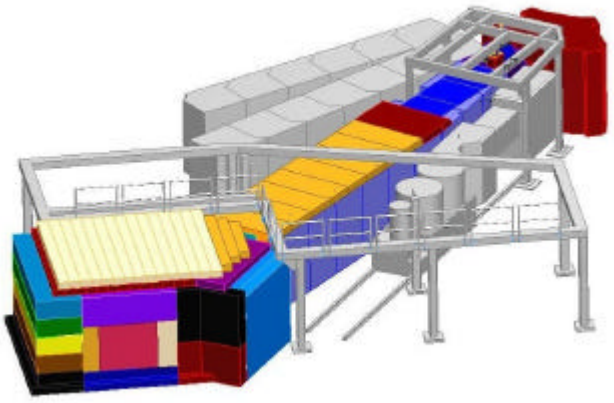

***Fig. 2:*** *Tomography facility surrounded by other experiments*


***Fig. 3:*** *Separately mounted concrete cylinder inside a wall to reduce weight for the crane*

***Fig. 4:*** *Assembly of the block house walls*

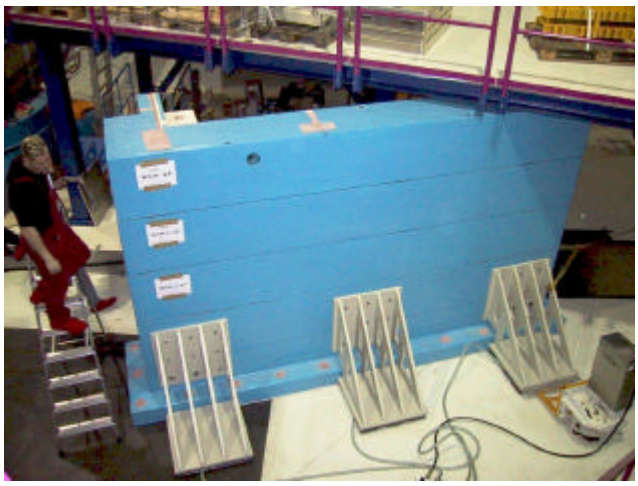

***Fig. 5:*** *Moving the wall with air cushions*

***Fig. 6:*** *The flight tube with convex flanges*

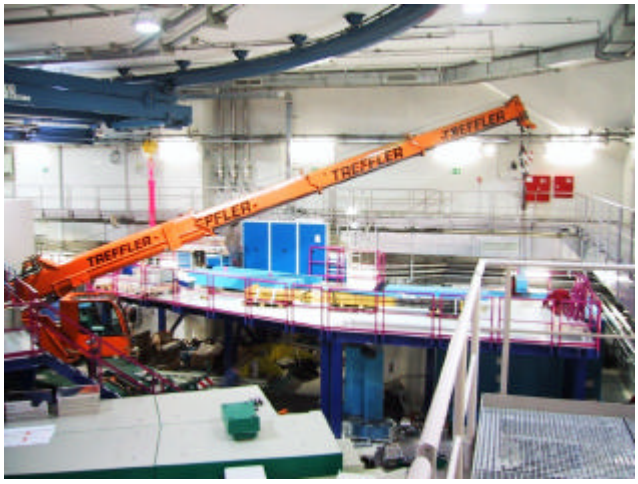


***Fig. 7:*** *Mounting the blockhouse roof elements with a truck-mounted crane*

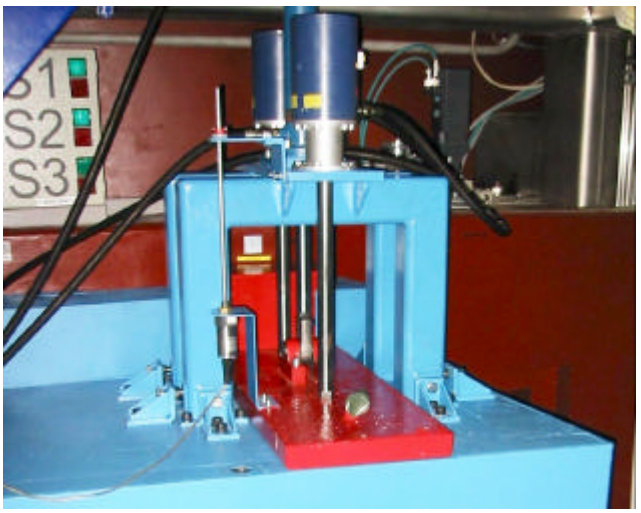


***Fig. 8:*** *The hydraulic servo system for the beam shutter*

***Fig. 9:*** *"First Light" in the block house, with part of the ANTARES team*

## 2.2 Short-time stroboscopic neutron imaging on a rotating engine

B. Schillinger[1], H. Abele[3], J. Brunner[1], G. Frei[2], R. Gähler[4], A. Gildemeister[3], A. Hillenbach[3], E. Lehmann[2], P. Vontobel[2]

[1]*Technische Universität München, FRM-II and Faculty for Physics, Germany*
[2]*Paul-Scherrer-Institut, Villigen PSI, Switzerland*
[3]*Universität Heidelberg, Faculty for Physics, Germany*
[4]*Institut Laue-Langevin, Grenoble, France*

*Todays neutron sources do not deliver sufficient flux to examine singular short-time events in the millisecond range by neutron radiography. However, periodic processes can be examined if a triggered accumulating detector collects information of identical time windows and positions over several cycles of the process. At the intense neutron beam H9 of ILL Grenoble, an electrically driven BMW engine was examined at 1000 rpm with time resolution of 200 microseconds.*

### Detection systems

So far, the only feasible detection systems found are interline frame transfer CCDs or CCD cameras with gated image intensifiers, in combination with a neutron sensitive scintillation screen and mirror.
For interline frame transfer CCD cameras, the CCD chip area consists of alternate light sensitive pixel columns and masked vertical shift registers. Image information from the light sensitive pixels can be transferred into the masked, light-insensitive shift register with a single clock cycle, enabling for exposure times in the range of ten microseconds. This process can be repeated several times (with flushing the image pixels between exposures) before the whole image information is read out via the shift registers. The advantage of this method is that no additional noise is introduced by an image intensifier, the disadvantage is that the number of on-chip accumulations is limited. Additional frame accumulations can be done off-line in the computer, but their statistics is limited by the digitization process of the individual frames.
With gated image intensifiers, theoretical gating times of down to 3 ns can be achieved, however the decay time to 10% of the employed scintillator is 85 microseconds, limiting the achievable time resolution. The advantage of intensified CCDs is their higher pixel capacity which enables for the accumulation of several hundred gating periods before readout. They are limited by the additional quantum noise generated by the electron multiplication in the intensifier. Up to now, there is no clear superiority of one system visible.
For both systems, less than one percent of the total neutron fluence is used for imaging, resulting in very high activation of the sample. A different approach is being tried with a chopper wheel in Japan, which drastically reduces activation, but is rather inflexible in adjusting the time window.

### Measurements

The beam line H9 behind the Lohengrin experiment at ILL Grenoble is the most intense neutron radiography beam in the world, with a flux of $2*10^9$ n/cm$^2$s and a collimation of L/D=110. ILL, Universität Heidelberg, Paul-Scherrer-Institut and TU München collaborated on the measurement of an electrically driven four-piston BMW engine. The engine was driven by a 2kW electro motor, mounted on a vertical translation stage. Since water cooling was not possible, the spark plugs were removed to reduce drag and heat production.
The detection system was a MCP intensified CCD camera PImax [1] with a Peltier cooled chip (1300 * 1024 pixels) with 16 bit digitization. The usable dynamic range is limited by the inherent noise of the intensifier.
The full cycle of this four-stroke engine running at 1000 rpm was split into 120 individual frames over 2 rotations, 150 individual images were recorded as an on-chip accumulation of a 200 microseconds exposure each. In this way, the total exposure time for the full run was in the order of 18 minutes only. The field of view was 24 cm * 24 cm. The observation area could be varied by displacement of the full set-up.
Figure 1 shows one frame of the recorded movie, showing valves, pistons, piston rods, piston pins and piston rings. Of special interest is the visualization of the oil cooling of the piston bottoms. Since the pistons are only connected to the engine body via the piston rings with very low heat dissipation, a continuous oil jet is directed from below at the piston bottoms, lowering the piston temperature by more than 200 degrees C. In the movie, the oil jet of 1-2 mm diameter is clearly visible. Around the upper turning point of the piston, the dome-like spread of the oil at the underside of the piston can be observed.

### Outlook

Further measurements will be done in 2004, using a single-piston diesel engine to examine the injection process. As soon as FRM-II is operational, measurements will commence in Garching as well, trading beam intensity for better collimation. Future measurements will focus especially on the oil cycle for the lubrication of the bearings of cam shaft and crank shaft. To overcome the limitation in time resolution given by the scintillator, new scintillation materials must be examined for feasibility for short-

time neutron radiography. The neutron quantum statistics and the quantum noise of the image intensifier will be the final limitation of achievable time resolution, though it is by far not met yet.

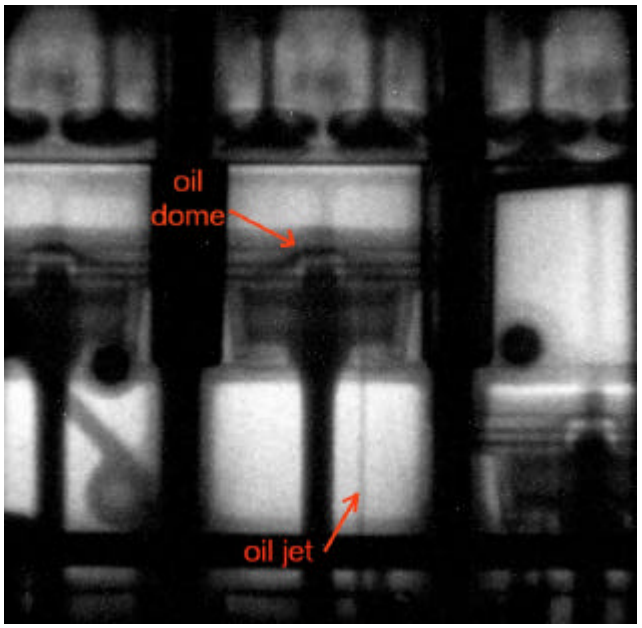


***Fig. 1:*** *Single frame of a sequence of images of a running car engine, rotated at 1000 rpm. All components are clearly visible (valves, cylinder head, connecting rod, piston, piston pin, piston ring). Of highest interest in this run was the oil injection from below for cooling the piston.*

References:

[1] http://www.roperscientific.com/ pdfs/datasheets/pimax/1024sb.pdf

## 2.3 Steps towards dynamic neutron radiography of a combustion engine

J. Brunner[a], G. Frei[b], R. Gähler[d], A. Gildemeister[c],
E. Lehmann[b],A. Hillenbach[c], B. Schillinger[a]

*a) Technische Universität München, Physik Department E21, 85747 Garching, Germany*
*b) Paul Scherrer Institut, 5232 Villigen, Switzerland*
*c) Universität Heidelberg, Physikalisches Institut, 69120 Heidelberg, Germany*
*d) Institute Laue Langevin, 38042 Grenoble, France*

*The Dynamic NR is a new technique, which is applied successfully for non-destructive testing for time dependent phenomena with a similar resolution and a similar contrast as in conventional NR. Of special interest is the investigation of the injection process in a running combustion engine under real conditions.*

For obtaining a 16-bit conventional radiography image at a typical flux of $10^6$ n/cm$^2$s one has to integrate scintillator light on the CCD chip typically for some seconds. Of course the sample thickness, the sample material as well as the detector efficiency determine the exact time. Additionally the readout time, depending on the dynamic range and the pixel number of the CCD, puts a lower limit to the highest achievable frame rate.
The observation of objects in the millisecond time scale is impossible with standard methods. A possible solution for repetitive processes can be stroboscopic imaging. That means a synchronization of the detector with the repetitive process and an integration of 1000 images taken at the same millisecond time window of the cycle. That way a virtual opening time of some seconds can be realized as long as the noise is constant within time (i.e. negligible readout noise) and not determined by the system.
With this method two combustion engines of aluminium towed by a electric motor were observed at ILL. The achieved spatial resolution was 1 mm because of the beam unsharpness.

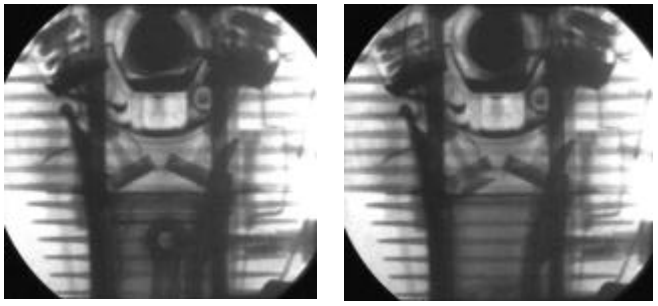

***Fig. 1:*** *Two images of the running cycle of a motorbike at 800 rpm, 250ms with 60 image accumulations*

***Fig. 2:*** *Piston cooling of a four stroke car combustion engine can be observed well by neutron radiography, t=200ms with 120 accumulations, image size is 24cm x 24cm*

This dynamic neutron investigations were performed with an detector system from PSI at a very high flux test beam line at ILL.
The PSI detector consisted of a peltier cooled CCD camera using a multi channel plate as an image intensifier coupled on the CCD-chip with fiber optics.
With this equipment and the high flux thermal neutron beam of $10^9$ n/cm$^2$s at ILL extremely high detection sensitivity was possible. The necessary fast triggering is done by the image intensifier. Since the scintillator decay time to 10% is 85 µs, that is the order of magnitude for the limit of the time resolution.

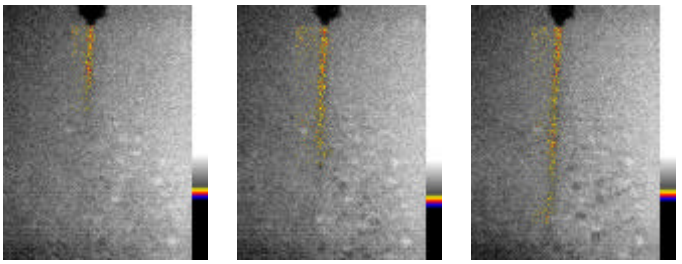

***Fig. 3:*** *Common Rail Diesel injection nozzle (500 bar) in action, 5000 neutron radiography frames of 100ms added by software, delay to the trigger, 600µs, 700µs, 800 µs, image size is 6.2cm x 8.2cm*

In the false color image **Fig. 3** the small attenuation of the injection liquid cloud is clearly visible. The next step will be such an observation in a running engine under real conditions.
The obtained results should be a starting point to fit the different requirements of car producers in respect to fuel injection, lubricant distribution, mechanical stability and operation control. Similar inspections will be possible for all devices with repetitive operation principle. At the FRM II the ANTARES tomography station with a high neutron flux of $10^8$ n/cm$^2$s and a high spatial resolution will allow such measurements soon.

References:

[**1**] B. Schilllinger, “Neue Entwicklungen zu Radiographie and Tomographie mit thermischen Neutronen“, Doktorarbeit an der technischen Universität München

[**2**] M. Balasko, “Neutron radiography visualization of internal processes in refrigerators”, Physica B: Condensed Matter, Volumes 234-236,2 June 1997, Pages 1033-1034

## 2.4 Nondestructive Testing with Phase Contrast Radiography

K. Lorenz[1], E. Steichele[1], E. Lehmann[2], P. Vontobel[2]

*1 Technische Universität München, 85747 Garching, Germany*
*2 Paul Scherrer Institut, 5232 Villigen, Switzerland*

*Phase contrast radiography allows the visualization of structures, which cannot be seen in conventional radiographies. In this technique, the wave characteristics of the neutron is exploited to get additional contrast besides the absorption contrast.*

### Theory

The refractive index of a material is given by the complex expression $n=1-\delta-i\beta$.. The imaginary part of this value is responsible for the mass attenuation coefficient $\mu$ of the material which creates absorption contrast. The real part $\delta$ causes a phase shift, which leads to a deviation of the wave front. If the incoming wave is approximately a plane wave (neutrons with a high transversal spatial coherence), you get in certain object-detector-distances interference effects. Fresnel's theory for diffraction, explains the increase in contrast at edges and interfaces in the object [1] (where the gradient of the phase shift perpendicular to the neutron beam is very high; fig. 1). This additional contrast to the absorption contrast is called phase contrast.

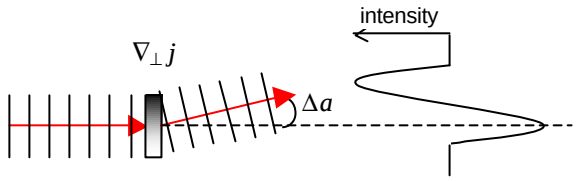


***Fig. 1:*** *Principle of phase contrast*

### Applications

Prof. Wellnitz, holder of the chair of conceptional lightweight construction at the FH Ingolstadt, provided us with probes of aluminum foams. In spite of the very small attenuation coefficient of aluminum, it is possible to visualize the inner structure of these foams with the help of phase contrast (fig. 2).
If during the casting process the outer region of a cast component solidifies quicker than the inner, the shrinking during solidification can create little hollows inside the cast material. The UTG in Garching lent us cast components with such defects inside. The size of those defects is often far too small to get enough absorption contrast to visualize them in a conventional radiography.
In association with Dr. Mollenhauer, director of the research department of the orthopedic surgery of the

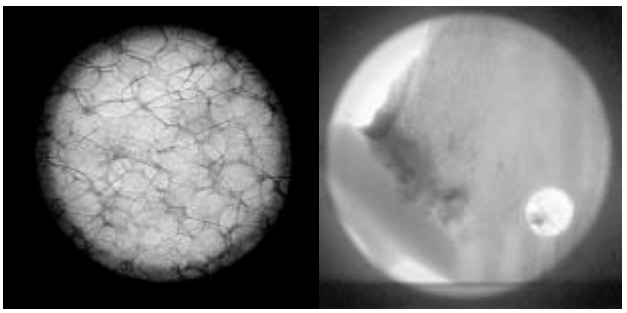

***Fig. 2,3:*** *Phase contrast radiographies of an aluminum foam and a bone-covered hip prosthesis (both made at the PSI in Switzerland; the diameter of the visible area is 42 mm)*

Friedrich-Schiller-University Jena, we use phase contrast neutron radiography to visualize the interface between an implant and the bone (fig. 3). By looking at this interface at different times after the implantation of the prosthesis, it is possible to study the dependence of the healing process on the surface material and the surface structure of the prosthesis.

### Recent Topics of Research

A disadvantage of phase contrast radiography are the long exposure times compared to conventional radiography. This is because of the need for a neutron beam with a high transversal coherence, which is achieved by the application of small pinholes and large distances between this pinhole and the probe. This leads to a strong reduction of the beams intensity and thus to long exposure times (90min and more). A possible solution for this problem is the utilization of coded apertures [2], which replace the single pinhole.
The small diameter of the pinhole (<1mm) allows the application of neutron lenses with very small radii. Like this it is possible to create lens systems with a focal length in the order of meter. With such a device, the resolution in the object plane can be improved by a factor of two or more by a given detector resolution.
By making a phase contrast radiography of an object in three different object-detector-distances, it is possible to use the transport of intensity equation (TIE) to calculate the phase shift of the neutrons on their different ways through the object [3]. Doing this phase retrieval for every single projection of a tomography makes it possible to assign every voxel of the tomography a phase shift and an attenuation coefficient.

Like this, it becomes possible to use the imaginary and the real part of the refractive index to separate materials.

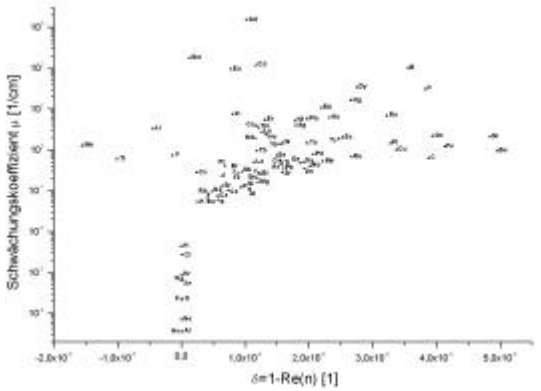


***Fig. 4:*** *Attenuation coefficient and phase shift of the elements*

References:

[1] Cowley, J. M. “Diffraction Physics”, NHPL, 1995
[2] Skinner, G. K. “Imaging with Coded Aperuture Masks”, Nuclear Instruments and Methods in Physics Research 221 (1984) 33-40)
[3] Gureyev, T. E.; Optics Communications 147 (1998) 229-232

## 2.5 Image Deconvolution in Neutron Radiography

F. Grünauer

*Institute for Experimental Physics E21*
*TU München, Garching*

Nearly all neutron radiography facilities use a setup similar to a pinhole camera. Lens systems afford a very high construction effort. Generic pinhole systems provide high resolution at big L/D ratios, where L is the distance between aperture and specimen and D the diameter of a circular aperture. As the neutron fluence decreases proportional to $(D/L)^2$ a high resolution means long exposure time and a bad signal to noise ratio. It would be desirable to record images with high intensity and low resolution and to correct the resulting blur by an appropriate algorithm. Deblurring of images was tested with a L/D=50 projection (fig. 1 B) of a test specimen (fig. 1 A), that was simulated by Monte Carlo Method. The projection is the convolution of the point spread function by the 'ideal image' (in this context, the ideal image is the projection, produced by a point source). Convolution in the spatial domain corresponds to a multiplication in the fourier domain. In principle the ideal image can be reconstructed by dividing the fourier transform of the projection by the fourier transform of the point spread function and back transforming the result to the spatial domain. However this 'invers filtering' is not successful if the image contains noise: Division by small absolute values of the point spread function in the fourier domain causes a big damage in the reconstructed image. This effect can be reduced by a Wiener filter [1], that gives a certain weight to each point in the fourier domain during the filtering process. The reconstruction by a Wiener filter, is shown in fig. 1 C. An other approach to solve the problem of noise are iterative algorithms. The idea is to guess the 'ideal' image, to convolute it with the point spread function and to compare the result with the real image. After an appropriate adjustment of the guessed image, the procedure is started again. Fig. 1 D shows the result of 18 iterations of the van Cittert algorithm and fig. 1 E shows the reconstruction by the Richardson-Lucy maximum likelihood algorithm. Best results are obtained by the Richardson-Lucy method. However none of the algorithms are able to recover details like the screw thread. Further improvements in the image quality can be achieved by a modification of the point spread function (see 'Coded apertures in neutron radiography' in the same report).

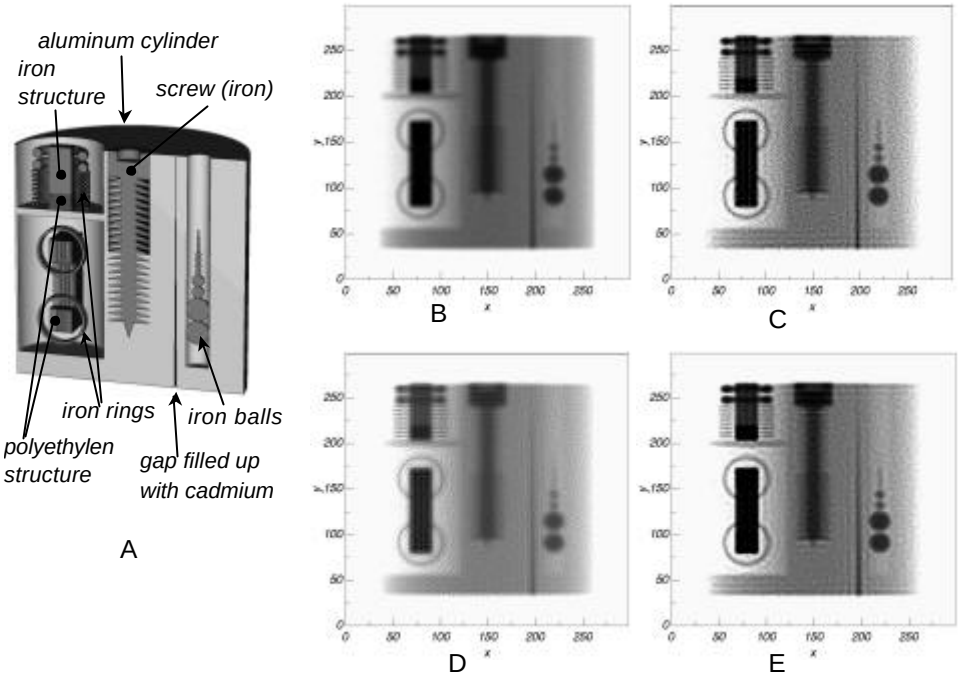


***Fig. 1:*** *A) test specimen B) unprocessed projection C) Reconstruction by a Wiener filter D) Reconstruction by van Cittert algorithm E) Reconstruction by Richardson-Lucy Method*

References:

[1] J.C. Russ, „The image processing handbook", CRC Press, Boca Raton Ann Arbor London Tokyo, 1995

## 2.6 Coded Apertures in Neutron Radiography

F. Grünauer

*Institute for Experimental Physics E21*
*TU München, Garching*

Most neutron radiography facilities use circular single hole apertures. Such apertures provide a so called pillbox point spread function. As the point spread function has a crucial impact on the quality of reconstructed images, investigations were carried out with regard to an optimal aperture design. Many different configurations were simulated by Monte Carlo method. The test specimen is presented in 'image deconvolution in neutron radiography' in the same report. A comparison of a multiple hole aperture (fig. 1 E) to the 'classic' single hole aperture (fig. 1 A) is shown below. Both apertures have the same transmission area. The overlap of information in the projection with the multiple hole aperture was reduced by minimization of the autocorrelation function of the point spread function. The resulting image is a superposition of six images (fig. 1G). For both aperture configurations the image was reconstructed by a Wiener filter. The reconstructed image, obtained with the multiple hole aperture (fig. 1 H), shows more details (e.g. the screw thread) and is less noisy than the reconstructed image, which stems from the single hole arrangement (fig. 1 D).

The quality of optical systems is usually defined by the modulation transfer function [1]. Fig. 1 B and fig. 1 F show, that the modulation transfer function has considerably less near zero zones in case of the multiple hole aperture.

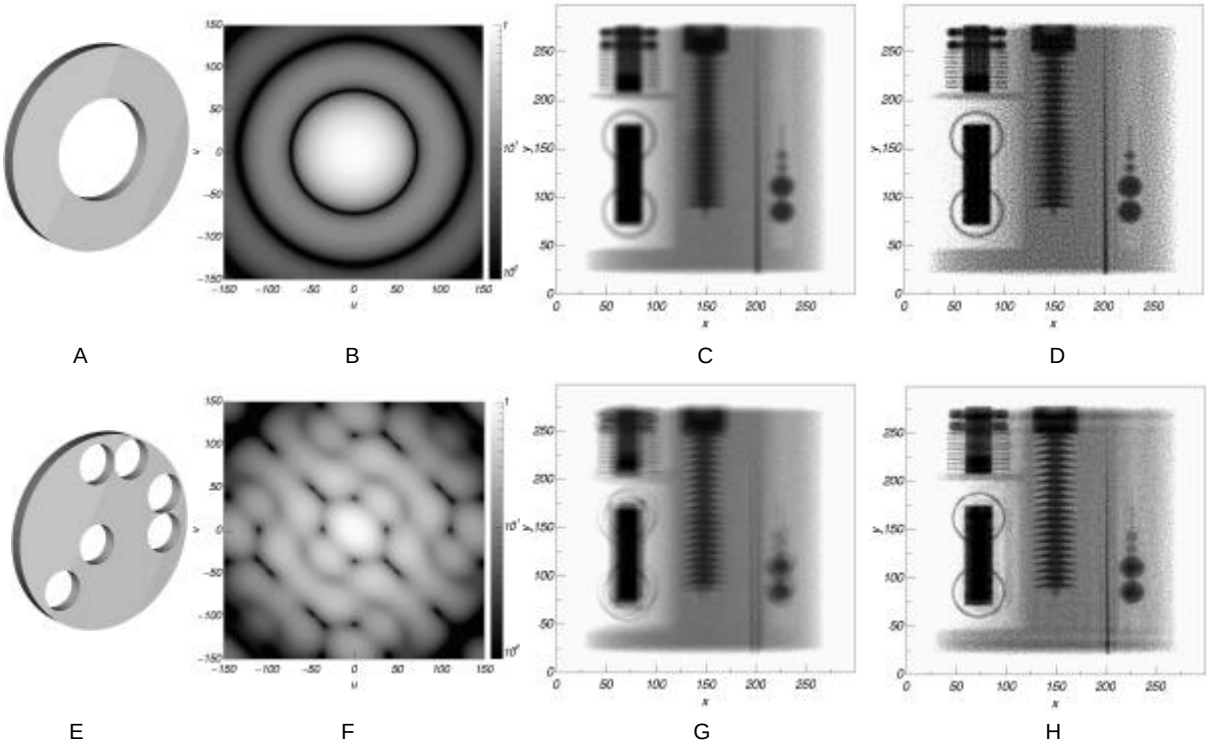


***Fig 1:*** *A) single hole aperture B) modulation transfer function for the single hole aperture*
*C) unprocessed projection from the single hole aperture D) reconstructed image for the single hole aperture*
*E) multiple hole aperture F) modulation transfer function for the multiple hole aperture*
*G) unprocessed projection from the multiple hole aperture H) reconstructed image for the multiple hole aperture*

References:

[1] E. Hecht, "Optik", Addison-Wesley, Bonn München,1989

# 3 Neutron Detectors

## 3.1 Response Function of a Neutron Detector for Radiation Protection Purposes

F. Grünauer

*Institute for Experimental Physics E21*
*TU München, Garching*

At FRM-II commercially available neutron detectors will be used for radiation monitoring and protection. These detectors are approved in the energy range of thermal to fast neutrons. In contrary to usual applications of neutron dosimetry (e.g. reactor halls), there has to be expected a major contribution of cold neutrons in the neutron-guide hall of FRM-II. It had to be examined whether this detector is suitable for cold spectra and if so, what calibration and security factors have to be applied under these special conditions. Monte Carlo calculations were carried out in order to assess the response function with respect to neutron energy and angle of incidence. It was shown, that the response function below thermal energies is rather flat. Therefore the detector can be used even in the subthermal energy range. The response of the detector is very depentent on the angle of incidence of radiation.

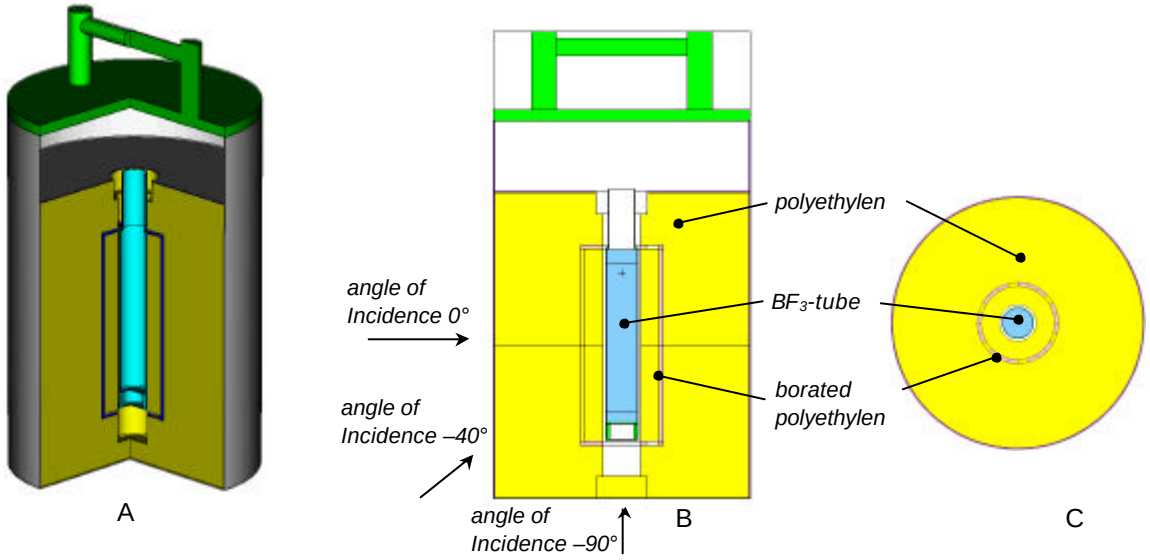


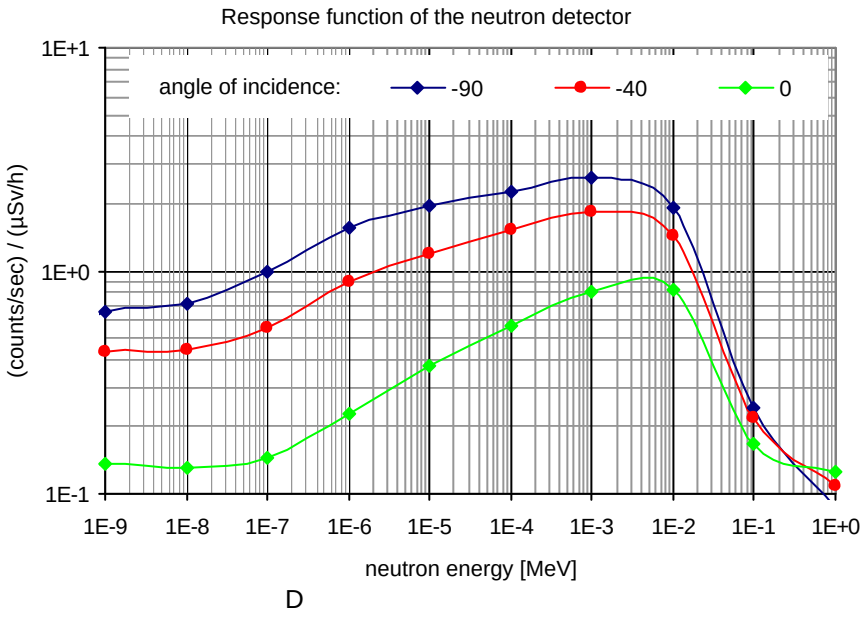


D

***Fig. 1:*** *A) Monte Carlo model of the neutron detector* *B) vertical cut through the detector*
*C) horizontal cut through the detector* *D) response function of the detector*

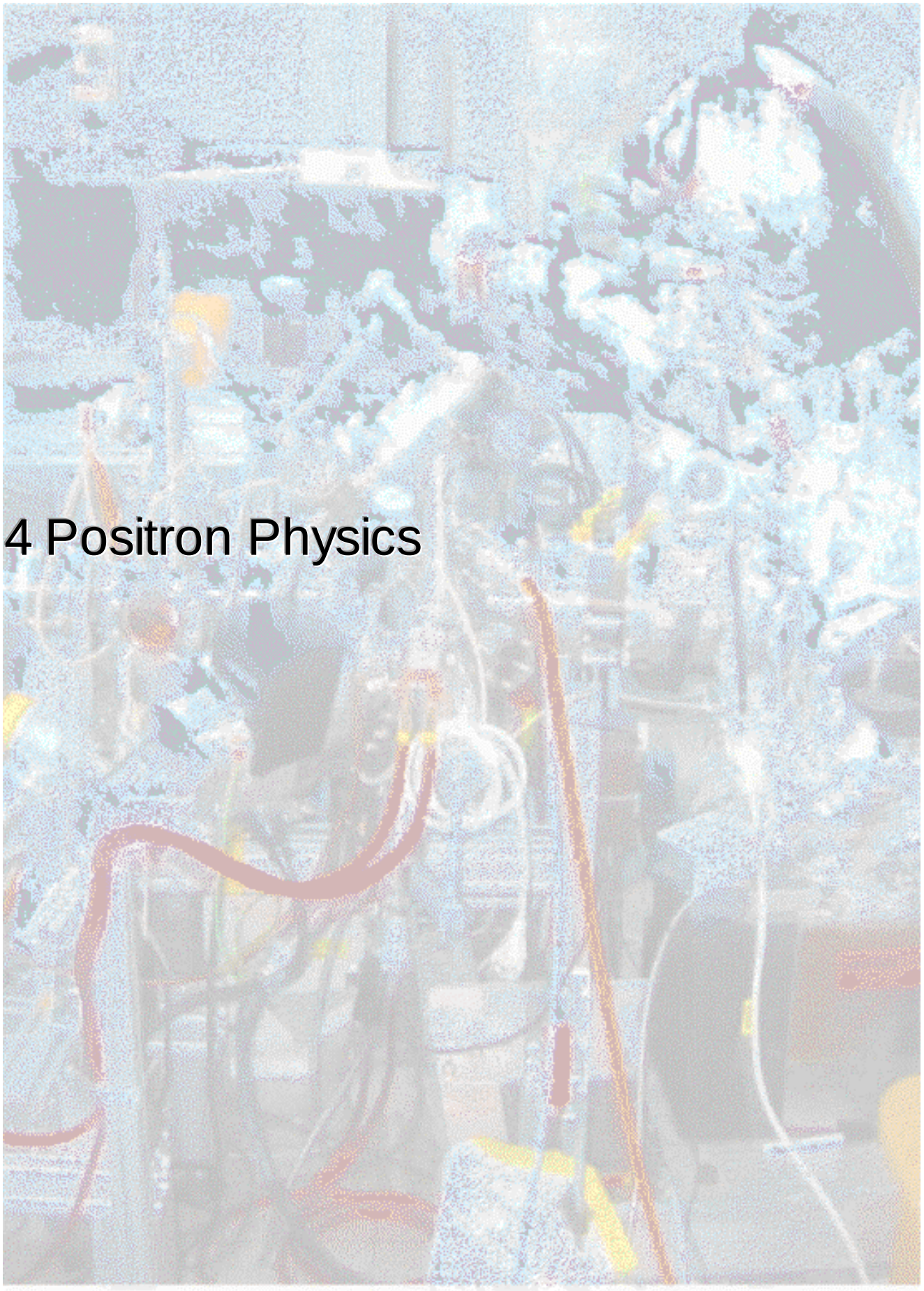

# 4 Positron Physics

## 4.1 NEPOMUC – Neutron Induced Positron Source Munich and its Instrumentation

C. Hugenschmidt[1], G. Kögel[2], R. Repper[1], K. Schreckenbach[1], P. Sperr[2], B. Straßer[1], W. Triftshäuser[2]

[1] *ZWE FRM II, Fakultät für Physik E21, Technische Universität München, 85747 Garching*
[2] *Institut für Nukleare Festkörperphysik, Universität der Bundeswehr München, 85577 Neubiberg*

### NEPOMUC

The intense positron source is installed as an in-pile component in the tip of the declined beam tube SR11 at the new research reactor FRM-II at the Technical University of Munich. After thermal neutron capture in cadmium the absorption of the released high-energy γ-radiation in platinum generates positrons by pair production. At NEPOMUC the world highest intensity of the order of $10^{10}$ slow positrons per second in the primary beam is expected. The moderated positrons are extracted by electrical lenses and magnetically guided to the outside of the biological shielding of the reactor. There, an aperture, gamma-detectors and a movable beam monitor are installed in order to measure the positron intensity as well as the beam profile. The following beam line guides the positrons to a beam splitter on the experimental platform.

### Instrumentation at NEPOMUC

In the first arrangement, the positron beam is connected to three experiments on the platform in the experimental hall of FRM II (see figure). Within our collaboration a **p**ulsed **l**ow **e**nergy **p**ositron beam **s**ystem (PLEPS) and a **s**canning **p**ositron **m**icroscope (SPM) will be transferred to NEPOMUC (see annual report 2003 of FRM II). Both, PLEPS and SPM were constructed at the University of the Bundeswehr in Munich (UniBW). The third instrument is a facility for **p**ositron annihilation induced **A**uger **e**lectron **s**pectroscopy (PAES). The PAES facility was built up at E21 at TUM and is designed for extremely sensitive studies in surface science (see contribution in this issue).

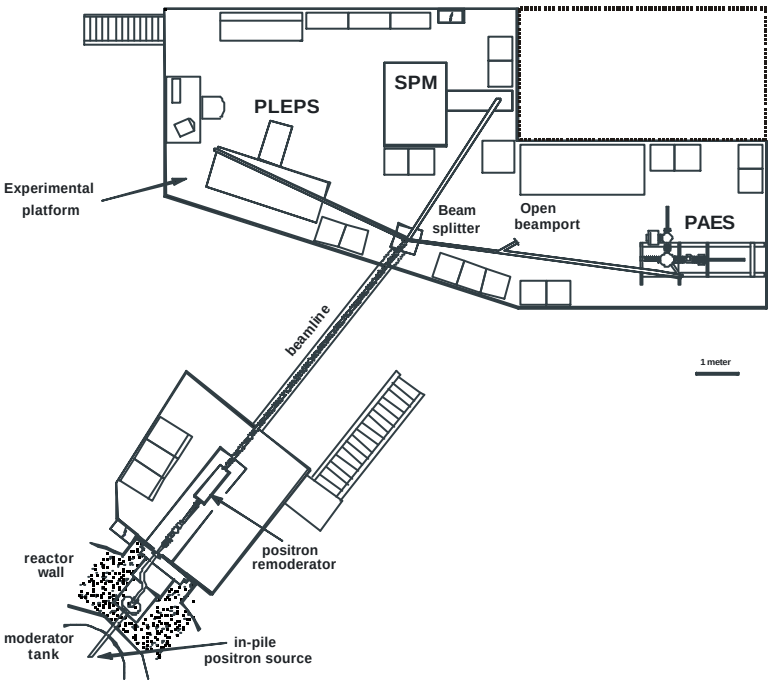


***Fig. 1:*** *Overview of NEPOMUC and its instrumentation*

## 4.2 Extension of the Munich Facility for Positron Induced Auger Electron Spectroscopy (PAES)

C. Hugenschmidt, B. Straßer and K. Schreckenbach

*Fakultät für Physik E21, ZWE FRM II, Technische Universität München, D-85748 Garching*

In contrast to common Auger electron spectroscopy, positron-induced Auger electron spectroscopy (PAES) uses the annihilation of slow energy positrons with core electrons of sample atoms to initiate the Auger process. Due to the low energy of the implanted positrons (some 10 eV), no secondary electron background is produced in the higher energy range of released Auger electrons. Thus, PAES possesses a considerably higher signal-to-noise-ratio compared to conventional AES. Moreover, PAES is more surface-sensitive since most of the implanted positrons annihilate with electrons of the topmost atomic layer.

The existing PAES facility is presently connected to the slow positron beam in our lab at E 21. The positron Auger electron spectrometer was extended by several components for sample surface preparation (see figure), before it will be transferred to the intense positron beam (NEPOMUC) at the new reactor FRM II in 2004.
This year, we installed a separate sample lock and a sample preparation chamber. In order to prepare clean and well-defined surfaces, it is equipped with an argon sputter source and an adapted sample heater for in-situ annealing of defects particularly in the near surface region. An effusion cell was installed which consists of a tungsten foil boat with tunable sample distance. In addition, an electron beam evaporator was mounted for evaporation of low vapor pressure materials. Both, the effusion cell as well as the electron beam evaporator, allow accurate deposition of adsorbates in the sub-monolayer range. The exact layer thickness of deposited material is determined by a piezo oscillator crystal. After preparation, the sample is transferred through a gate valve into the analysis chamber by a magnetic coupled rod. There, it is handed to the sample manipulator by a special transfer device. The capability of the experimental set-up was successfully demonstrated by electron induced AES on gold-coated copper samples. Presently, surface sensitivity of conventional and positron induced AES are investigated.

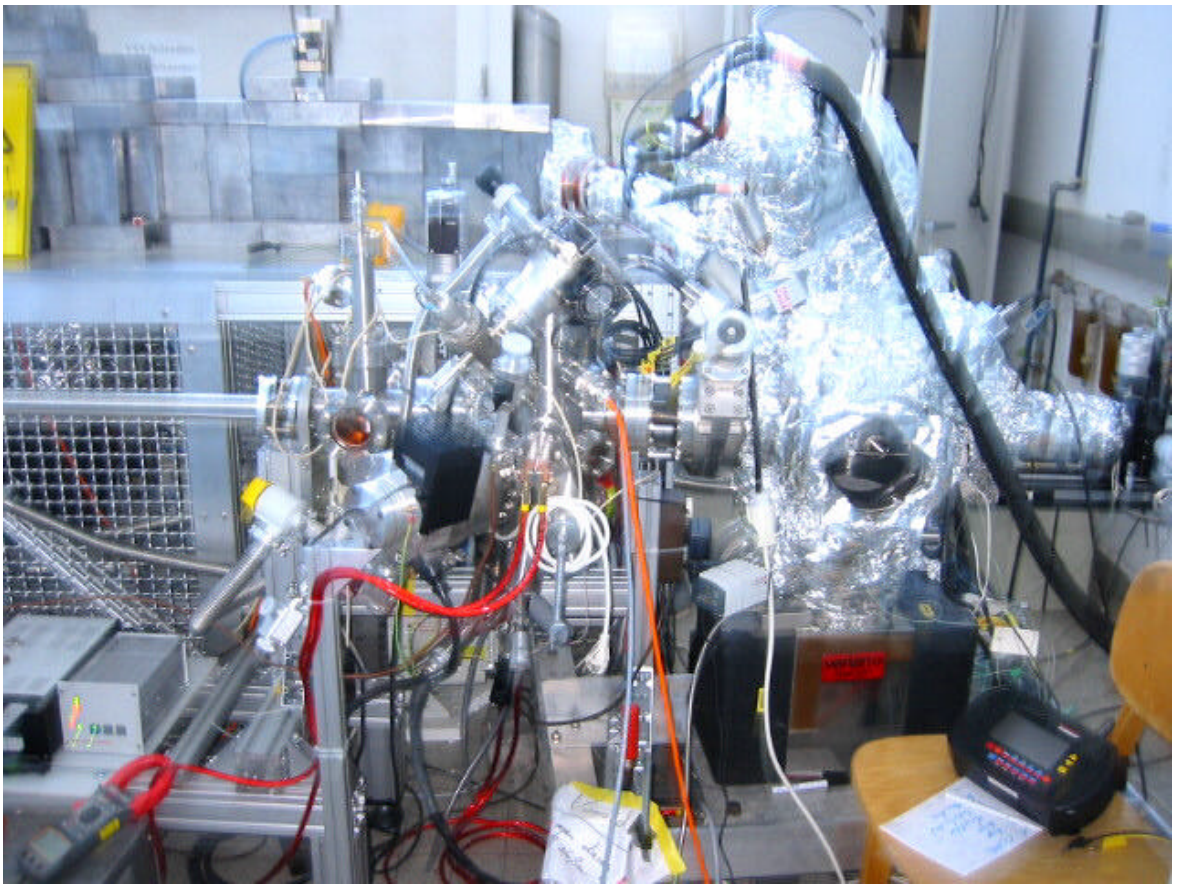

***Fig. 1:*** *The PAES-facility: PAES-chamber covered by Al-Foil (right) with sample preparation chamber and sample lock on the left. Background: Lead shielded positron beam.*

## 4.3 Measurement of Electron Momenta by Coincident Doppler Broadening Measurements of the 511 keV Positron Annihilation Line

C. Hugenschmidt[1,2], M. Stadlbauer[1] and K. Schreckenbach[1,2]

*[1]Fakultät für Physik E21, [2]ZWE FRM II*
*Technische Universität München, D-85748 Garching*

In solid state physics positron annihilation is applied as a high sensitive and non-destructive technique for defect spectroscopy and the investigation of the electron momentum distribution. After implantation in matter a positron thermalizes within a few picoseconds and diffuses through the sample material (typical diffusion length 0,1 µm). Together with an electron it annihilates into two 511 keV gamma quanta, which are emitted at an angle of 180° in the centre-of-mass-system. In the laboratory system, a Doppler shift occurs which reflects the momentum of the electron-positron-system before annihilation. Since the momentum of the thermalized positron is negligible, electron momenta of the sample atoms can be investigated by measuring the Doppler broadening of the 511 keV annihilation line.

### Experimental Setup

The coincident Doppler spectrometer consists of two facing germanium detectors with the sample in between. In our present experiment, a positron source ($^{22}$Na, 2.0 MBq) is sandwiched between two identical metallic samples in order to use almost the whole solid angle of the emitted positrons. The 180°-geometry of the germanium detectors allows the coincident detection of both annihilation photons. Hence, this technique leads to an improved energy resolution of about 0.9 keV at E = 511 keV and reduces the background of several orders of magnitude. Consequently, measurements in the high momentum region become feasible.

### Measurements and Results

Annealed samples of copper (>99.99%), zinc (>99.99%) and brass ($Cu_{63}Zn_{37}$) were studied. Each spectrum comprehended about 8 million counts. The resulting Doppler broadened annihilation lines were normalized. The recorded intensity is plotted with respect to pure zinc in Figure 1. Up to 514.5 keV gamma energy the lines of copper, brass and zinc are clearly distinguishable since the errors are sufficient small in this region. According to the different electron states in copper and zinc, i.e. different atomic number and hence unequal momenta of the electrons, a varying shape of the Doppler broadened annihilation line is observed. Since the probability of annihilation with core electrons in copper prevails that of zinc, the high momentum part in the spectrum of pure copper is larger.
With this coincident Doppler spectrometer it is possible to distinguish between different materials. Since positrons are very sensitive on crystal defects in alloys it should become feasible to study dedicated elements, which are related to open volume defects.

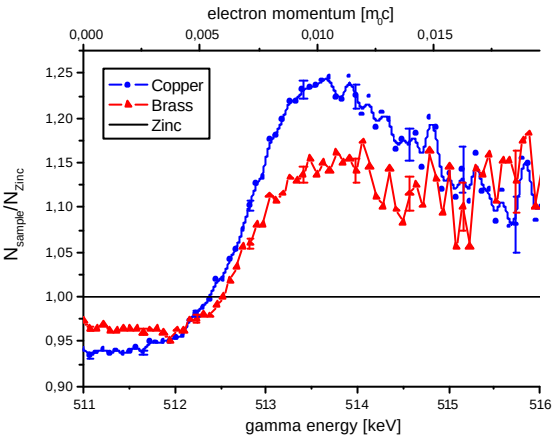


***Fig. 1:*** *Normalized Doppler broadening spectra of copper, brass and zinc*

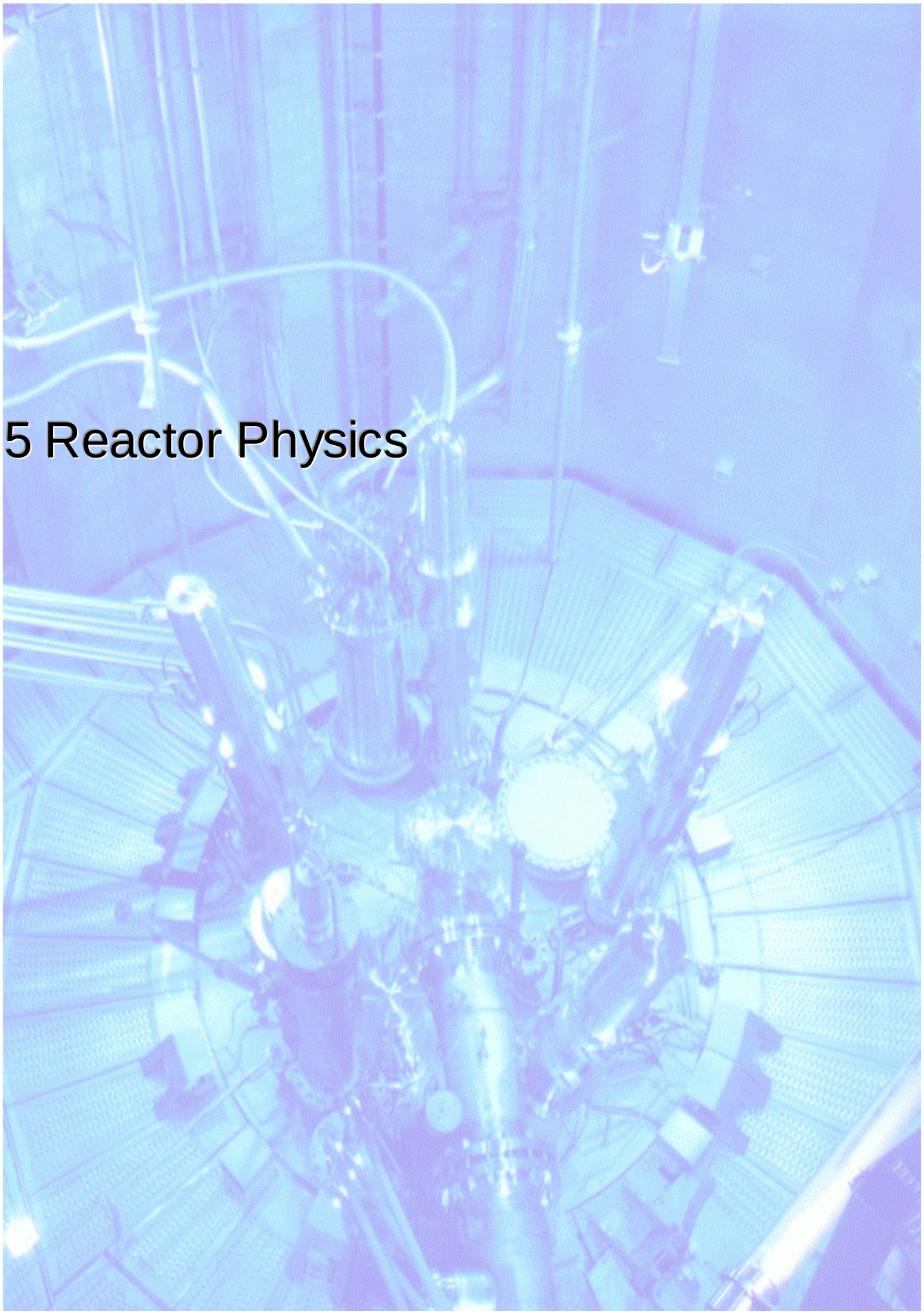

# 5 Reactor Physics

## 5.1 Development of a Fuel Element with Reduced Enrichment for the FRM-II

K. Böning, FRM-II, TUM

On May 12, 2003, the Bavarian State Ministry of Environment (StMLU) - on instructions received from the Federal Ministry of Environment (BMU) - awarded the FRM-II its 3rd partial nuclear license permitting nuclear startup and full power routine operation of the reactor. However, this long awaited and most welcome final license also involved the condition that the FRM-II should develop, until the end of the year 2010, a new fuel element allowing the FRM-II to continue its operation with medium enriched uranium (MEU, with a maximum of 50 % U235) instead of the present highly enriched uranium (HEU, with 93 % U235). This means that – as a first step towards this goal – an advanced fuel with a much higher density of uranium than presently available must be developed so that the reduction of enrichment could be compensated by an increase in density. Only in this way the dimensions of the fuel element can be kept unchanged, the replacement of the central part of the reactor facility can be avoided and the condition of "any penalty to the FRM-II being marginal only" can be obeyed.

After the issue of the 3rd nuclear permit an agreement between the Bavarian State Ministry of Science (StMWFK) and the Federal Ministry of Science (BMBF), which has been negotiated already two years ago and which also settled the budget requirements, has been signed on May 30, 2003. In consequence an international working group has been established at the Technische Universität München (TUM) comprising representatives of the FRM-II, of the fuel element manufacturer CERCA (France) and of the research reactor planning company Siemens/Framatome-ANP. The first meeting of this "MEU Working Group" was performed in Garching on July 29, 2003, where the break down of the project into three phases of 2 ½ years each has been agreed upon:

Phase I: 07.2003 – 12.2005: Fuel development and basic questions
Phase II: 01.2006 – 06.2008: Fuel specification and design of fuel element
Phase III: 07.2008 – 12.2010: Fuel element fabrication and licensing

Being well aware that this schedule is extremely tough the working group will do everything to render this project a success. In September 2003 the BMBF issued the official notification of having allocated its share of the budget for the project phase I.

The second meeting of the MEU working group was held in Garching on October 17, 2003. The FRM-II reported on neutronics calculations which showed that an uranium density in the MEU fuel of 8.0 – 8.5 g/cm$^3$ will be required for a fuel element with 50 % enrichment (the present density for HEU is 3.0 g/cm$^3$); the maximum obtained fission density in the fuel meat will be of the order of $2.3 \times 10^{21}$ fissions/cm$^3$. It was decided to ask CERCA to submit an offer concerning the supply of 2 kg of MEU and the fabrication of 2 test irradiation plates each with 8.0 and 8.5 g/cm$^3$ density and of 2 spare plates with 7.0 g/cm$^3$ for the case that some of the test irradiations should fail. The test irradiations will be performed at the OSIRIS materials testing reactor in Saclay which is operated by the French "Commissariat a l'Energie Atomique" (CEA) and which has already been used for the irradiation of HEU fuel plates of the FRM-II some years ago. On November 24, 2003, TUM and CERCA met with CEA at Saclay to negotiate the details of a contract concerning the irradiation of a total of 4 test plates (2 of each density) in the IRIS facility of OSIRIS, post irradiation examinations (PIEs) of probably 2 plates in a hot cell at Cadarache, and the final disposal of the plates which have become highly radioactive under irradiation. The final offers and updated draft contracts of CERCA and CEA are expected shortly. In order not to loose time and anticipating these contracts we have sent, on December 12, 2003, a letter of confirmation calling on CERCA to begin immediately with the production of the 50 % enriched MEU (as to be obtained from mixing 93 % and 20 % enriched uranium) and with the first steps to fabricate the irradiation test plates.

# 6 Activities 2002

## 6.1 Lectures, Courses and Seminars

| | |
|---|---|
| N. Arend | Tutorial „Anfängerpraktikum“ |
| M. Bleuel: | Tutorial "Introduction to Solid State Physics I"<br>Tutorial "Introduction to Solid State Physics II" |
| P. Böni: | Lectures " Introduction to Solid State Physics I "<br>Exercises “Introduction to Solid State Physics I<br>Lectures " Introduction to Solid State Physics II"<br>Exercises “Introduction to Solid State Physics II<br>Lectures “Magnetic Excitations: Theory and Experiment”<br>Exercises “Magnetic Excitations: Theory and Experiment”<br>Seminar "Neutrons in Research and Industry", together with Profs. Böning, Petry, and Schreckenbach<br>Seminar "Experimentelle Methoden der Festkörperphysik“, together with Ch. Hugenschmidt |
| K. Böning: | Lectures "Reactor physics I“<br>Tutorial "Reactor physics I“<br>Lectures "Reactor physics II“<br>Tutorial "Reactor physics II“<br>Seminar "Neutrons in Research and Industry" |
| J. Brunner: | Tutorial "Elektronikpraktikum" |
| R. Georgii: | Organisation Exercises Magnetic Excitations: Theory and Experiment<br>Organisation Seminar “Neutrons in Research and Industry”<br>Organisation Workshop “1st FRM-II Workshop on Neutron Scattering”, Burg Rothenfels |
| F. Grünauer: | Tutorial "Introduction to Solid State Physics I"<br>Tutorial "Introduction to Solid State Physics II" |
| C. Hugenschmidt | Seminar "Experimentelle Methoden der Festkörperphysik“ |
| V. Kargl: | Tutorial "Introduction to Solid State Physics II" |
| T. Keller: | Tutorial "Elektronikpraktikum" |
| D. Lamago | Tutorial „Magnetic Excitations I“<br>Tutorial „Elektronikpraktikum“<br>Tutorial „Anfängerpraktikum“ |
| K. Lorenz | Tutorial "Introduction to Solid State Physics II"<br>Tutorial "Elektronikpraktikum" |
| C. Schanzer | Tutorial “Demonstrationspraktikum für Lehramt Physik” |
| B. Schillinger: | Tutorial "Elektronikpraktikum" |
| K. Schreckenbach | Seminar "Neutrons in Research and Industry" |
| S. Valloppilly | Examination evaluation “Semestralklausur – Experimental Physik für Machinenbauer, Sommersemester 2003” |

## 6.2 Seminar: „Neutronen in Forschung und Industrie“ Sommersemester 2003

Physik-Department, HS 3, 15:15

| Datum | Sprecher | Titel |
|---|---|---|
| 7.4.2003 | W. Doster (E13, TUM) | Biomolekulare Dynamik mit Neutronenstreuung: ERS statt ESS |
| 14.4.2003 | O. Zimmer (E18, TUM) | Spin-off spin-abhängiger Wechselwirkungen von Neutronen mit polarisierten Atomkernen |
| 28.4.2003 | H.-C. Bartscherer (ProLehre, TUM) | Lehren mit Folien, Tafel, Beamer. (ca. 90 min !) |
| 5.5.2003 | A. Wiedenmann (HMI) | Magnetic nanostructures analysed by Small Angle Scattering of polarised neutrons |
| 12.5.2003 | | |
| 19.5.2003 | N. V. Abrosimov (Institut für Kristallzüchtung,Berlin) | Züchtung von $Si_{1-x}Ge_x$-Mischkristallen für Röntgen-, $\gamma$- and Neutronenoptik |
| 26.5.2003 | | |
| 2.6.2003 | J. Kohlbrecher (PSI) | Polarized Proton Domains in Matter - a combined NMR and polarised SANS study |
| 16.6.2003 | W. Kob (Univ. Montpellier) | Computer Simulationen von silikatischen Schmelzen und Gläsern |
| 23.6.2003 | Th. Proffen (LANSCE, Los Alamos) | Totale Neutronenstreuung als Schlüssel zur atomaren Struktur fehlgeordneter Materialien |
| 30.6.2003 | D. Williams (LANCE, Los Alamos) | The Synthesis and structural analysis of binary and tertiary group 2, 11, 12 and 13 cyanides |
| 7.7.2003 | J. Beckmann (FRM-II, TUM) | Bestimmung von Proteinpositionen im Ribosom mittels polarisierter SANS Messungen |
| 14.7.2003 | Ch. Carbogno (Stud. 8.Sem., TUM) | Ray-Tracing Methoden zur Optimierung von Instrumenten |
| 28.7.2003 | R. Knobel (Wacker-Chemie Burghausen) | Neutronendotiertes Silizium Herstellung – Eigenschaften - Anwendungen |
| 4.8.2003 | Adrian Rühm (MPI Stuttgart) | How to handle and use the spin in polarized neutron reflectometry |
| 25.8.2003 | Z. Tamer (Stud. 8.Sem, TUM) | Messung von Verzwilligung mit Neutronen |
| 12.9.2003 | B. Fultz (Caltech) | Instrumentation at SNS |

## 6.3 Seminar: „Neutronen in Forschung und Industrie“ Wintersemester 2003/2004

Physik-Department, HS 3, 15:15

| Datum | Sprecher | Titel |
|---|---|---|
| 29.9.03 | U. Keiderling (HMI) | Zeitaufgelöste Insitu SANS-Messungen am Instrument "V4" des HMI Berlin |
| 6.10.03 | | |
| 10.10.03 | Verabschiedung: Dr. E. Steichele | R. Gähler (ILL) Die Kohärenzeigenschaften des Neutrons |
| 20.10.03 | Vorbesprechung | |
| 27.10.03 | T. Hicks (Monash Uni., Australia) | Evidence for a truly 2D Ising antiferromagnet |
| 10.11.03 | F. Demmel (ILL) | A Multiplexing Three Axis Spectrometer: Performance and applications |
| 17.11.03 | A. Ioffe (FZ Jülich) | Neutron speed echo |
| 24.11.03 | O. Moze (INFM Modena) | Magnetic ordering and structural phase transitions in RNi10Si2 compounds |
| 1.12.03 | Festvortrag zum 60.ten Geburtstag von Prof. G. Borchert | -Dr. Hans Börner ( ILL) Strolling through applications of high-resolution gamma ray spectroscopy<br>-Dr. Leopold Simons ( PSI) High resolution spectroscopy of exotic atoms<br>-Prof. Dr. Otto Schult ( FZJ) |
| 8.12.03 | T. Soldner (ILL) | Ein perfekt polarisierter Neutronenstrahl für die Teilchenphysik |
| 15.12.03 | S. Grigoriev (PNPI) | Neutron multiwave interference experiments with many resonance coils |
| 12.1.04 | | |
| 19.1.04 | S. Campbell (TUM) | Neutron Science in Australia – ANSTO; AINSE; ANBUG and the RRR |
| 26.1.04 | A. Hiess (ILL) | Wechselspiel zwischen Magnetismus und Supraleitung in $UPd_2Al_3$ |
| 2.2.04 | | |
| 9.2.04 | W. Treimer (FH Berlin) | Alte und neue bildgebende Signale für die Tomographie |
| 16.2.04 | S. Janssen (PSI) | FOCUS: a versatile TOF spectrometer at SINQ/PSI |

## 6.4 1st FRM-II Workshop on Neutron Scattering -Advanced Materials-

21.7-24.7 Burg Rothenfels am Main

| | Monday<br>21.7.03 | Tuesday<br>22.7.03 | Wednesday<br>23.7.03 | Thursday<br>24.7.03 |
|---|---|---|---|---|
| 8:00 | 7:30 Departure | Breakfast | Breakfast | Breakfast |
| 8:45– 10:45 | | *Magnetism 1 (9:00)*<br>P. Böni (30+10)<br>R. Georgii (15+5)<br>P. Link (15+5)<br>S. Valloppilly (15+5) | *Applied Science*<br>C. Hugenschmidt (15+5)<br>J. Kornmeier (15+5)<br>B. Pedersen (15+5)<br>K. Lorenz (15+5)<br>M. Schlapp (15+5) | *Soft Matter*<br>P. Müller-Buschbaum(30+10)<br>T. Titz<br>P. Panagiotou (all 3 together (30+10))<br>S. Loi + E. Maurer<br>M. Bleuel (15+5)<br>A. Ostermann (15+5) |
| 10:45 –11:15 | | Break | Break | Break |
| 11:15 –13:00 | 12:00 Arrival | *Structure*<br>R. Kampmann/E. Sackmann (15+5)<br>R. Gilles (15+5)<br>M. Hölzel (15+5)<br>M. Meven (15+5)<br>K. Hradil (15+5) | *Magnetism 3*<br>S. Chambell (30+10)<br>M. Hofmann (15+5)<br>A. Mirmelstein (15+5)<br>E. Clementyev (15+5) | *Methods*<br>U. van Bürck (30+10)<br>J. Brunner (15+5)<br>N. Arend (15+5) |
| 13:00 –14:30 | Lunch (12:30) | Lunch | Lunch | Lunch in Rothenfels |
| 14:30 –16:15 | *Lattice Dynamics*<br>W. Petry (15+5)<br>J. Neuhaus (15+5)<br>T. Keller (15+5)<br>W. Schirmacher (30+10) | *Nuclear Physics*<br>K. Schreckenbach (30+5)<br>O. Zimmer (30+5)<br>A. Türler (30+5) | Excursion | 15:00 Departure |
| 16:15 –16:45 | Coffee | Coffee | | |
| 16:45 –18:30 | *Viscous Melts*<br>A. Meyer (30+10)<br>S. M. Chathoth (15+5)<br>M. Pöhlmann (15+5)<br>A. R. Müller (15+5) | *Magnetism 2*<br>R. Röhlsberger (30+10)<br>E. Steichele (15+5)<br>J. Mayor (15+5)<br>C. Schanzer (15+5) | | 19:30 Return |
| 18:30 | Dinner | Dinner | Dinner | |

| | |
|---|---|
| W.Schirmacher | Anomalous Vibrational Properties of Disordered Solids |
| P. Link | Antiferroquadrupolar order of TmTe, neutron diffraction under high magnetic field |
| A. Meyer | Atomic transport in multicomponent melts -- From bulk glass forming alloys to volcanic rock |
| N. Arend | Comparison of the classical and quantum mechanical description of MIEZE |
| C. Schanzer | Dependence of magnetic properties of multilayers from structural parameters |
| T. Unruh | Development of nanostructured drug delivery systems |
| M. Meven | Disorder of the [PO4H2]- groups in the paraelctric phase of RDP |
| M. Hölzel | Elastic and inelastic neutron scattering on hydrogen charged austenitic stainless steels |
| B. Pedersen | Experimental electron density determination on catalysts |
| K. Schreckenbach | Experimente zu fundamentalen Wechselwirkungen und Symmetrien von freien Neutronen |
| C. Hugenschmidt | First Positron Induced Auger Electron Spectrum of Annealed Polycrystalline Cu |
| T. Titz | Gradient samples: heterogeneous polymer films |
| R. Röhslberger | Imaging of magntic depth profiles in thin films |
| M. Bleuel | Inelastische Messungen mit Spin-echo Spektrometern |
| S. Loi | In-situ USAX and GISAXS adhesive polymers film properties |
| E. Clementyev | Interplay of major interactions in the rare-earth based intermetallic compounds |
| R. Gilles | Investigations of Ni-base superalloys by SANS |
| J. Kornmeier | Keramische Faserverbundwerkstoffe für Hochleistungsantriebe in der Raum fahrt |
| T. Keller | Larmor labelling based on NRSE for high resolution spectroscopy and diffraction |
| J. Mayor | Magnetic structures of thin film systems as studied by full spin-resolved neutron grazing angle scattering |
| W. Petry | Martensitic Phase Transitions |
| P. Müller-Buschbaum | Micro-beam grazing incidence small angle x-ray scattering - new technique, new possibilities |
| A. Mirmelstein | Neutron diffraction, specific heat and muSR study of the spin-chain compounds Ca2+xY2-xCu5O10 |
| M. Schlapp | Neutron Image Plates with low gamma-sensitivity for SANS |
| E. Steichle | Neutronenstreu-Experimente an Ferrofluiden - ein Überblick |
| A. Ostermann | Neutronenstrukturanalyse von Proteinen |
| R. Kampmann | Novel Perspectives for Investigations on Biological Surface Structures using REFSANS |
| K. Lorenz | Phase contrast neutron radiography |
| J. Neuhaus | Phonons and Martensitic Phase Transitions in Shape-Memory Alloys |
| R. Georgii | Polarizied magnetic small angle scattering on MnSi |
| K. Hradil | Probing the local structure of a decagonal quasicrystal using the analysis of the pair distribution function |
| A. R. Müller | Proton dynamics in water bearing silicates |

| | |
|---|---|
| S. Campbell | Rare Earth Magnetism - 1-2-2 Intermetallic Compounds |
| F. Grünauer | Simulations for the new neutron radiography facility |
| P. Böni | Spin Excitations in Correlated Magnets |
| U. van Bürck | SRPAC: Synchrotron Radiation based Perturbed Angular Correlation |
| A. Türler | Stand und Aussichten der PGA |
| J. Brunner | Steps toward dynamic neutron radiography of a running combustion engine |
| S. Valloppilly | Structural and magnetic characterization of some spin-valve multilayers |
| S. M. Chathoth | Structural relaxation in Nickel and Aluminium based melts |
| P. Panagiotou | Surface morphology of thin immiscible ternary polymer blend films investigated with GISAXS |
| O.Zimmer | Teilchenphysik mit langsamen Neutronen |
| M. Hofmann | Valence and Magnetic transitions in EuMn2Si2-xGex |
| M. Pöhlmann | Water bearing silicates -- Neutron scattering and Car Parinello Computer simulations |

## 6.5 Publications 2003


1. D. Attié, B. Cordier, M. Gros, Ph. Laurent, S. Schanne, G. Tauzin, P. von Ballmoos, L. Bouchet, P. Jean, J. Knödlseder, P. Mandrou, Ph. Paul, J.-P. Roques, G. Skinner, G. Vedrenne, R. Georgii, A. von Kienlin, G. Lichti, V. Schönfelder, A. Strong, C. Wunderer, C. Shrader, S. Sturner, B. Teegarden, G. Weidenspointner, J. Kiener, M.-G. Porquet, V. Tatischeff, S. Crespin, S. Joly, Y. André, F. Sanchez and P. Leleux, "INTEGRAL/SPI ground calibration", Astronomy and Astrophysics A&A **411**, L71-L79 (2003).

2. R. Georgii, P. Böni, N. Pleshanov, "Polarised reflectometry with MIRA at the FRM-II", Physica B **335**, 250-254 (2003).

3. R. Georgii, P. Böni, N. Pleshanov, "The VCN reflectometer for MIRA at the FRM-II", Langumir **19**, 7794-7795 (2003).

4 H. Hiraka, Y. Endoh, P. Böni, M. Fujita, K. Yamada, and G. Shirane, "Reinvestigation of Magnetic Excitations in the Spin-Density-Wave of Chromium", Phys. Rev. B **67,** 064423 (2003).

5. C. Hugenschmidt, B. Straßer, and K. Schreckenbach, "Investigation of the Annealed Copper Surface by Positron Annihilation Induced Auger Electron Spectroscopy", Phys. Chem. **68**, 3-4, 627-629 (2003).

6. C. Hugenschmidt, G. Kögel, R. Repper, K. Schreckenbach, P. Sperr, and W. Triftshäuser, Radiat. „Positron Source Based on Neutron Capture", Phys. Chem. **68**, 3-4, 669-671(2003).

7. C. Hugenschmidt, L. Liszkay, W. Egger, "Investigation of Laser Treated AlN by Positron Lifetime Measurements", Proceedings of the 3rd International Workshop on Positron Studies of Semiconductor Defects PSSD-2002, Sendai, Japan

8. Kardjilov N, Baechler S, Basturk M, Schillinger B, et al., "New features in cold neutron radiography and tomography - Part II: applied energy-selective neutron radiography and tomography", Nucl. Instrum. Meth. A **501** (2-3), 536-546 (2003).

9. S. Klimko, C. Stadler, P. Böni, R. Currat, F. Demmel, B. Fåk, R. Gähler, F. Mezei, and B. Toperverg, "Implementation of a Zero Field Spin-Echo Option at the Three-Axis Spectrometer IN3 and First Application for Measurements of Phonon Linewidths in Superfluid $^4$He", Physica B **335**, 188-192 (2003).

10. D. Lamago, M. Dameris, C. Schnadt, V. Eyring and C. Brühl, "Impact of large solar zenith angles on lower stratospheric dynamical and chemical processes in a coupled chemistry-climate model", Atmos. Chem. Phys. **3**, 1981-1990 (2003).

11. C. Reich, P. Böni, B. Roessli, and E. Rastelli, "Upward Renormalization of Fluctuations in $CsMnBr_3$ with Increasing Temperature", Phys. Rev. Lett. **91**, 157203 (2003).

12. B. Roessli, P. Böni, W. E. Fischer, and Y. Endoh, "Chiral Fluctuations in MnSi above the Curie Temperature Measured with Polarized Inelastic Neutron Scattering", Acta Phys. Pol. B **34**, 1557 (2003).

13. M. Senthil, P. Böni, and M. Horisberger, "Perpendicular Magnetic Anisotropy, Hysteresis and Structural Properties of Nanostructured FeCoV/Ti Multilayers", Physica **B 325**, 401-409 (2003).

14. A. Schebetov, A. Serebrov, V. Pusenkov, M. Lasakov, P. Böni, M. Lüthy, and J. Sromicky, "New Facility for Fundamental Research in Nuclear Physics with Polarized Cold Neutrons at PSI", Nucl. Instr. Meth. A **497**, 479-491 (2003).

15. B. Schillinger: "Neutronen sehen, was Röntgenstrahlen verborgen bleibt", Technik in Bayern **4**/2003 pp.14-15.

16. V.R. Shah, G. Markandeyulu, K. V .S. Rma Rao, M. Q. Huang, K. Sirisha and M. E. McHenry, Structural and Magnetic Properties of $(Sm_{1-x}Pr_x)_3Fe_{27.5}Tl_{1.5}$[x=0.2, 0.5, 0.8, 1.0] and Their Nitrides", J. Alloys. Comp **352**, 6 (2003).

17. S. Verkhovskii, K. Mikhalev, A. Gerashenko, Yu. Piskunov, V. Kazantsev, V. Bobrovskii, E. Mitberg, A. Podlesnyak, and A. Mirmelstein, “Electronic inhomogeneity and possible pseudogap behavior of spin susceptibility in the electron-doped superconductor $Sr_{0.93}La_{0.07}$ $CuO_2$: $^{63}$Cu NMR study”, Journal of Superconductivity: Incorporating Novel Magnetism **16**, 543-554 (2003).

### 6.6 Conference, Workshop and Seminar Contributions

1. P. Böni, B. Roessli, D. Görlitz, and J. Kötzler, "Damping of Spin Waves and Singularity of the Longitudinal Modes in the Dipolar Critical Regime of the Heisenberg Ferromagnet EuS", Frühjahrstagung der Deutschen Physikalischen Gesellschaft, March 24-28 2003, Dresden.

2. P. Böni, C. Reich, B. Roessli, and E. Rastelli, "Upward-Renormalization of Fluctuations in $CsMnBr_3$", Workshop "Magnetismus und Streumethoden", July 14 2003, Stuttgart.

3. P. Böni, "Spin Excitations", 1. FRM-II Workshop on Neutron Scattering and Advanced Materials, Burg Rothenfels, July 21 - 24 2003, Rothenfels am Main, Germany.

4. P. Böni, "Neutrons, Muons, Low Temperatures", Sept. 8 2003, Paul Scherrer Institute, Villigen, Switzerland.

5. P. Böni, "Neutronen in der Grundlagenforschung: Magnetismus", Schülertag: Schwerpunkt Neutronenphysik, Oct. 15 2003, Garching.

6. P. Böni, "Austausch und DM-Wechselwirkung: Spindynamik und kritisches Verhalten", Schwerpunktinitiative: Wechselwirkungen und komplexe lokale Topologie, Nov. 4 2003, IFW Dresden.

7. P. Böni, "Neutron Scattering from Magnetic Materials", Seminar E18, Nov. 20 2003, Technical University of Munich.

8. K. Böning, W. Waschkowski, K. Schreckenbach:“Konzept und Sicherheit des FRM-II“. Technik in Bayern 4/2003, page 12 – 13.

9. K. Böning, Technical Meeting on Purpose-Designed Research Reactor Fatures, International Atomic Energy Agency IAEA, Vienna, 30 June – 02 July 2003.

10. J. Brunner,"Neutron imaging and other non destructive testing techniques at KFKI“, Workshop, KFKI, Atomic Institut of Hungary, Budapest 01.03.-31.04.2003.

11. J.Brunner,"Status of dynamic neutron radiography “, European Neutron Radiography Association ENRA, 2$^{nd}$ Meeting, 04.04.2003 Ladenburg.

12. J. Brunner,"Dynamic Neutron Radiography of a combustion engine “, 1$^{st}$ FRM-II Workshop on Neutron Scattering, Burg Rothenfels am Main, 21.7.-24.7.2003.

13. E.S.Clementyev, P.Böni, F.Demmel, and G.Shirane, “Mapping of magnetic excitations in single-Q Chromium”, 3$^{rd}$ European Conference on Neutron Scattering, Montpellier, 3.9.-6.9.2003.

14. E.S.Clementyev, P. A. Alekseev, P. Allenspach, G. Lapertot, and V. N. Lazukov, “Single ion anisotropy and soft-mode-driven magnetic ordering in PrNi”, 3$^{rd}$ European Conference on Neutron Scattering, Montpellier, 3.9.-6.9.2003.

15. R. Georgii, 1$^{st}$ FRM-II Workshop on Neutron Scattering, “Critical small angle scattering of MnSi”, Burg Rothenfels am Main, 21.7.-24.7.2003.

16. R. Georgii, “Critical exponents in small angle scattering of MnSi”, 3$^{rd}$ European conference on Neutron Scattering, Montpellier, 3.9.-6.9.2003.

17. N. Golosova, A. Mirmelstein, V. Bobrovskii, E. Mitberg, A. Podlesnyak, K. Conder, and A. Furrer, "Influence of Th substitution on the crystal structure and the crystal field spectrum of the high-$T_c$ superconductor $HoBa_2Cu_3O_{6.95}$", European Conference on Neutron Scattering ECNS 2003, 3 - 6 September, Montpellier, France.

18. T. Hils, P. Böni, J. Stahn, "Focusing parabilic guide for very small samples", 3rd European Conference on Neutron Scattering, Montpellier, 3.9.-6.9.2003.

19. C. Hugenschmidt, L. Liszkay, and W. Egger, "Untersuchung von laserbestrahltem Aluminiumnitrid und Quarzglas durch Positronenlebensdauermessungen", Frühjahrstagung der Deutschen Physikalischen Gesellschaft, Dresden, March 2003.

20. C. Hugenschmidt, "Theoretical Aspects for the Improvement of Positron Transmission moderators", 13th International Conference on Positron Annihilation, Kyoto, Japan, September 2003.

21. V. Kargl, A. Mirmelstein, P. Böni, D. Sheptyakov, A. Amato, S. Kazakov, J. Karpinski, A. Erb, "Neutron diffraction, specific heat and μSR study of the spin-chain compounds $Ca_{2+x}Y_{2-x}Cu_5O_1$", European Conference on Neutron Scattering ECNS 2003, 3 - 6 September, Montpellier, France.

22. V. Kargl, "Static and dynamical behaviour of $Ca_{2+x}Y_{2-x}Cu_5O_{10}$", Seminar, NIST, Gaithersburg, USA, 16.12.2003.

23. K. Lorenz, "Phase Contrast Radiography and Tomography",1st FRM-II Workshop on Neutron Scattering -Advanced Materials-, Burg Rothenfels am Main, 21.7.-24.7.2003.

24. L. Liszkay, G. Kögel, P. Sperr, W. Egger, C. Hugenschmidt, and W. Triftshäuser, "Positron Beam Splitter at the High Intensity Positron Beam in Munich", 13th International Conference on Positron Annihilation, Kyoto, Japan, September 2003.

25. A. Mirmelstein, "Magnetic susceptibility: from static magnetization to neutron scattering invited lecture", Project Workshop (Swiss National Science Foundation, Scientific Co-Operation between Eastern Europe and Switzerland, Project SCOPES 7IP 65598 "Education, research, application around the metamagnetic Laves phase compounds"), 27 October - 3 November 2003, Tashkent, Uzbek Republic.

26. C. Schanzer, "Neutron guides at Forschungsreaktor München II (FRM-II)", Seminar, Argonne National Laboratory, January 17 2003.

27. C. Schanzer, "Installation of neutron guides at Forschungsreaktor FRM-II in Munich", Workshop 'Beamline 4 Alignment Planning Workshop', Oak Ridge National Laboratory, Jan. 21 2003.

28. C. Schanzer, "Probing of magnetic nanostructures by specular and off-specular reflectometry with polarized neutrons", 1st MagneTUM workshop 'Nanoscale magnetism as seen by X-rays and neutrons, Technische Universität München, 13.3.2003.

29. C. Schanzer, "Dependence of magnetic properties of multilayers from structural parameters: FeCoV/Ti multilayer", 1st FRM-II Workshop on Neutron Scattering -Advanced Materials-, Burg Rothenfels am Main, 21.7.-24.7.2003.

30. C. Schanzer, V.R. Shah, P. Böni, T. Gutberlet and M. Gupta, "Investigation of magnetisation reversal in FeCoV/Ti multilayers", 3rd European Conference on Neutron Scattering, Montpellier, 3.9.-6.9.2003.

31. Shah Valloppilly,"Interface magnetism of neutron polarizer multilayers", 1st MagneTUM workshop "Nanoscale magnetism as seen by x-rays and neutrons", Technische Universität München, 13.3.2003.

32. Shah Valloppilly, "Structural and magnetic characterization of some spin-valve multilayers", 1st FRM-II Workshop on Neutron Scattering -Advanced Materials-, Burg Rothenfels am Main, 21.7.-24.7.2003.

33. Shah Valloppilly, ''Magnetic nanostructures'' invited – at Union Christian College Alwaye, Mahatma Gandhi University, Kerala, India, Óctober 30 2003.

34. M. Senthil Kumar, V.R. Shah, C. Schanzer, P. Böni, T. Krist and M. Horisberger, "Polarized neutron reflectivity of FeCoV/Ti multilayers", 3rd European Conference on Neutron Scattering, Montpellier, 3.9.-6.9.2003.

35. C. Hugenschmidt, LEPPP-03, "Positron Beams and the New Reactor Based Positron Source at Munich", 12th International Workshop on Low Energy Positron and Positronium Physics, Sønderborg, Denmark, July 2003.

## 6.7 Committee Memberships

**P. Böni:**

- Nutzerausschuss deutsches Kontingent, Institut Laue Langevin, Grenoble
- Instrument Subcommittee, Institut Laue Langevin, Grenoble
- SINQ Scientific Committee
- Projektbegleitender Beirat FRM-II
- Instrumentierungsausschuss FRM-III
- TUM-Beirat für den FRM-II
- Coordinator of Work Package on Neutron Optics, Joint Research Projects in EU: NMI3 FP6
- International Conference on Neutron Optics NOP2004, Tokyo: Scientific Advisory Committee
- Conference on Polarized Neutrons in Condensed Matter Research PNCMI 2004, Washington: Scientific Advisory Committee

**K. Böning**

- Chairman (President) of the International Group on Research Reactors IGORR (until April 2003)

**R. Georgii:**

- Local Coordinator of Work Package on Polarised Neutron Techniques, joint research projects in EU: NMI3 FP6 JRA7.

## 6.8 Accomplished PhD Theses

- N. Kardjilov: Further Developments and Applications of Radiography and Tomography with Thermal and Cold Neutrons
- M. Bleuel: Aufbau des Neutronen-Resonanz-Spinecho-Spektrometers RESEDA am FRM-II
- T. Soldner: Test der Zeitumkehrinvarianz am D-Koeffizienten des freien Neutronen-Zerfalls mit Trine

## 6.9 Accomplished Diploma Theses

- J. Brunner: Aufbau eines Teststands für dynamische Neutronenradiographie eines Verbrennungsmotors
- Ch. Reich: A Neutron Spectroscopic Study of Paramagnetic Excitations in $CsMnBr_3$
- N. Wieschalla: Optimierung von Messinstrumenten mit der Monte Carlo Methode am FRM-II

## 6.10 E21 Members

Phone: +49-89-289-

| Name | Phone | Fax | Room | email |
|---|---|---|---|---|
| Arend Nikolas, Dipl. Phys. | -12180 | -13776 | RS, 124a | Nikolas.Arend@frm2.tum.de |
| Axtner Markus | -12125 | -13776 | RS, 140 | maxtner@frm2.tum.de |
| Böni Peter, Prof. Dr. | -14711 | -14713 | PH 1, 2215 | peter.boeni@frm2.tum.de |
| Böning Klaus, Prof. Dr. | -12150 | -12191 | FRM-II UBA 0325 | klaus.boening@frm2.tum.de |
| Brunner Johannes, Dipl. Phys. | -12106 | -13776 | RS, 146b | johannes.brunner@frm2.tum.de |
| Clementyev Evgeni, Dr. | -14722 | -14713 | PH 1, 2207 | eclement@frm2.tum.de |
| Gläser Wolfgang, Prof. emerit. | -12476 | -12474 | PH 1, 2227 | wglaeser@ph.tum.de |
| Grünauer Florian, Dipl. Phys. | -12115 | -13776 | RS, 140 | florian.gruenauer@frm2.tum.de |
| Hils Thomas, Dr. | -14721 | - | Flachbau, 17 | thomas.hils@hils-consult.de |
| Jones Sylvia, Secretary | -14712 | -14713 | PH 1, 2217 | Sylvia.Jones@frm2.tum.de |
| Kahle Eberhard | -14742 | -14989 | RS 118 | eberhard.kahle@frm2.tum.de |
| Kargl Verena, Dipl. Phys. | -12515 | -14713 | PH 1, 2373 | vkargl@frm2.tum.de |
| Lamago Daniel, Dipl. Phys. | -14740 | -13776 | RS, 146b | daniel.lamago@frm2.tum.de |
| Lorenz Klaus, Dipl. Phys. | -14741 | -13776 | RS, 146b | klaus.lorenz@frm2.tum.de |
| Plonka Christian, Dipl. Phys. | -12299<br>-12199 | -13776 | Flachbau, 13 | cplonka@frm2.tum.de |
| Reingen Gabriel, | -12656 | - | PH 1, 1321 | - |
| Russ Barbara, Dipl. Ing. | -14717 | -14713 | PH 1, 2207 | barbara.russ@frm2.tum.de |
| Schanzer Christian, Dipl. Phys. | -14725 | - | PH 1, 2214 | christian.schanzer@frm2.tum.de |
| Schreckenbach Klaus, Prof. Dr. | -12183 | -12191 | RS | Klaus.Schreckenbach@frm2.tum.de |
| Stadlbauer Martin | -14739 | -13776 | RS 124 | Martin.Stadlbauer@frm2.tum.de |
| Steichele Erich, Dr. | -12141 | -12112 | RS | esteich@frm2.tum.de |
| Strasser Benno, Dr. | -12137 | -13776 | RS Flachbau 16 | benno.strasser@frm2.tum.de |
| Valloppilly Shah, Dr. | -14723 | -14713 | PH 1, 2205 | shah@frm2.tum.de |
| Wieschalla Nico, Dipl. Phys. | -12111 | -13776 | RS 146b | Nico.Wieschalla@frm2.tum.de |

PH: Physics Department
RS: Reactor Station

## 6.11 Associated Members at FRM-II

Phone: +49-89-289-

| Name | Phone | Fax | Room | email |
|---|---|---|---|---|
| Calzada Elbio, Dipl. Ing. | -14611 | -13776 | RS 126 | elbio.calzada@frm2.tum.de |
| Georgii Robert, Dr. | -14986 | -14989 | NL-Halle RSUYH 0336 | robert.georgii@frm2.tum.de |
| Hugenschmidt Christoph, Dr. | -14609 | -13776 | RS 103 | christoph.hugenschmidt@frm2.tum.de |
| Schillinger Burkhard, Dr. | -12185 | -13776 | RS 127 | burkhard.schillinger@frm2.tum.de |
| Wagensonner Heinz, Dipl. Ing. | -14915 | -14995 | NL-Halle UYH 0336 | heinz.wagensonner@frm2.tum.de |

PH: Physics Department
RS: Reactor Station

## 6.12 Guests

| Name | Phone | Fax | Room | email |
|---|---|---|---|---|
| Gähler Roland, Dr. | +33 4 7620 7189 | +33 4 7648 3906 | - | gahler@ill.fr |
| Keller Thomas, Dr. | +49/89/289-12164 | +49/89/289-13776 | RS 106 | thomas.keller@frm2.tum.de |

PH: Physics Department
RS: Reactor Station

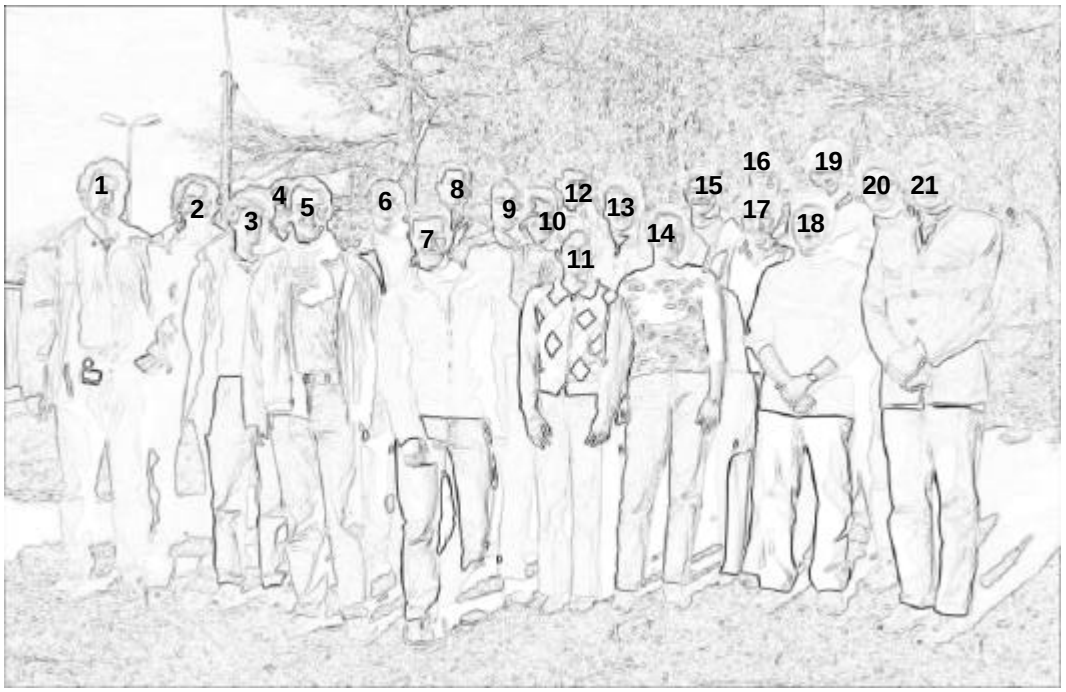


1 B. Schillinger
2 J. Brunner
3 R. Georgii
4 M. Mühlbauer
5 H. Wagensonner
6 D. Lamago
7 B. Gohla-Neudecker
8 T. Keller
9 P. Böni
10 M. Stadlbauer
11 V. Kargl
12 K. Lorenz
13 C. Hugenschmidt
14 S. Jones
15 E. Calzada
16 C. Schanzer
17 B. Russ
18 S. Valloppilly
19 E. Clementyev
20 F. Grünauer
21 K. Böning